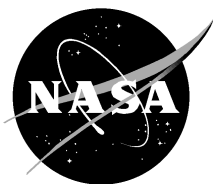# SeaWiFS Technical Report Series

Stanford B. Hooker and Elaine R. Firestone, Editors

Volume 40, SeaWiFS Calibration Topics, Part 2

Robert A. Barnes, Robert E. Eplee, Jr., Eueng-nan Yeh, and Wayne E. Esaias

NASA Technical Memorandum 104566, Vol. 40

SeaWiFS Technical Report Series

Stanford B. Hooker, Editor
NASA Goddard Space Flight Center
Greenbelt, Maryland

Elaine R. Firestone, Technical Editor
General Sciences Corporation
Laurel, Maryland

Volume 40, SeaWiFS Calibration Topics, Part 2

Robert A. Barnes, Robert E. Eplee, Jr., Eueng-nan Yeh
General Sciences Corporation
Laurel, Maryland

Wayne E. Esaias
NASA Goddard Space Flight Center
Greenbelt, Maryland
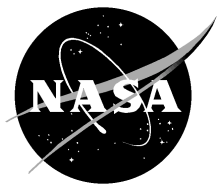
PREFACE

The SeaWiFS Calibration and Validation Program consists of four primary components (see the Prologue of Volume 38), that is, the SeaWiFS Instrument, Field Program, SeaBASS, and Calibration and Validation Element Software. Several volumes of the *SeaWiFS Technical Report Series* provided detailed analyses of prelaunch SeaWiFS sensor performance data, e.g., Volumes 22 (prelaunch acceptance), 23 (prelaunch calibration) 31 (stray light), and 39 (sensor calibration). This volume continues our efforts to identify and address issues associated with the SeaWiFS sensor calibration and characterization. The considerations described herein also apply to the calibration of other instruments with finite bandwidths including most *in situ* radiometers to be used in the vicarious calibration and algorithm development for SeaWiFS.

The chapters in this volume present discussions of:

  a) A nominal top-of-the-atmosphere spectrum for SeaWiFS;

  b) SeaWiFS measurements in orbit: spectral radiances at the nominal center wavelengths;

  c) The effect of atmospheric absorption on the output of SeaWiFS band 7;

  d) The 1993 SeaWiFS calibration using band-averaged spectral radiances;

  e) SeaWiFS measurements in orbit: band-averaged spectral radiances; and

  f) The SeaWiFS revised temperature calibration.

Greenbelt, Maryland
May 1997

—C.R.M.
Project Scientist

R.A. Barnes, R.E. Eplee, Jr., E-n. Yeh, and W.E. Esaias

Table of Contents

R.A. Barnes, R.E. Eplee, Jr., E-n. Yeh, and W.E. Esaias

ABSTRACT

For Earth-observing satellite instruments, it was standard to consider each instrument band to have a spectral response that is infinitely narrow, i.e., to have a response from a single wavelength. The SeaWiFS bands, however, have nominal spectral bandwidths of 20 and 40 nm. These bandwidths effect the SeaWiFS measurements on orbit. The effects are also linked to the manner in which the instrument was calibrated and to the spectral shape of the radiance that SeaWiFS views. The spectral shape of that radiance will not be well known on orbit. In this technical memorandum, two source spectra are examined. The first is a 12,000 K Planck function, and the second is based on the modeling results of H. Gordon at the University of Miami. By comparing these spectra, the best available corrections to the SeaWiFS measurements for source spectral shape, plus estimates of the uncertainties in these corrections, can be tabulated.

PROLOGUE

The Sea-viewing Wide Field-of-view Sensor (SeaWiFS) measures the Earth's upwelling radiance at eight wavelengths. These bands have finite spectral bandwidths, ranging from 20–40 nm. As a result, there is a dependence of the SeaWiFS measurements on the spectral shape of the Earth-exiting radiance that it measures. The manner in which this dependence manifests itself in the SeaWiFS data derives from the radiometric calibration of the instrument before launch.

There are two methods of interpreting the SeaWiFS calibration data. In the first method, the digital counts from each band of the instrument are related to the spectral radiance at the nominal center wavelength for that band. By definition, the center wavelengths for the bands are fixed. For this method, the relationship between the counts and the radiance varies with the spectral shape of the source that is measured. Since the laboratory calibration source has a spectral shape that is markedly different from the upwelling Earth radiance, there must be a correction factor to convert the laboratory calibration to the calibration on orbit.

In the second method, the digital counts from each band of the instrument are related to the band-averaged spectral radiance. Since the band-averaged spectral radiance is taken over the full spectral response of the band, there is no source shape dependence in the counts to radiance relationship for the band. However, the wavelength for the band-averaged center wavelength will change with different source spectral shapes. Fundamentally, it is not possible to determine both the radiance responses of the SeaWiFS bands and their center wavelengths during the laboratory calibration. Depending on the type of laboratory calibration, one of them will vary on-orbit with the spectral shape of the Earth-exiting radiance.

A previous volume in this technical memoranda series (Barnes et al. 1996) included several sensitivity studies to examine the effects of different source spectral shapes on the output of the SeaWiFS bands. These studies used Planck function curves with a wide range of color temperatures (2,000–38,000 K) covering the full range of laboratory and ocean scenes that SeaWiFS is expected to view. Using these Planck curves and the typical SeaWiFS spectral radiances from the sensor's specifications, it was determined that a 12,000 K Planck function curve best represented the Earth-exiting radiance spectrum for ocean scenes (Barnes et al. 1996).

In this technical memorandum, a model from H. Gordon (at the University of Miami) of the upwelling Earth radiance for an ocean scene and a clear atmosphere is adapted to provide a prelaunch top-of-the-atmosphere (TOA) radiance spectrum for SeaWiFS. Comparisons of the responses of the SeaWiFS bands, using this model TOA spectrum to those for the 12,000 K Planck function, give an estimate of the uncertainty in the SeaWiFS measurements that comes from a lack of knowledge of the actual spectral shape of the upwelling Earth radiance on-orbit. These differences are investigated for the two types of instrument calibrations described above.

In addition, the `LOWTRAN` and `MODTRAN7` atmospheric radiative transfer codes were modified and combined with the Gordon model to allow estimates of the effects of atmospheric water vapor and oxygen A-band absorption on the SeaWiFS measurements. Again, these effects are investigated for the two types of instrument calibrations described above. The laboratory measurements from November 1993 calibration were also used to provide a calibration in terms of band-averaged spectral radiances. These results were used for comparison with the postthermal-vacuum calibration of the SeaWiFS instrument and spacecraft at the conclusion of environmental testing. This took place at the spacecraft manufacturer—Orbital Sciences Corporation (OSC)—on 23–24 January 1997. The results of the second SeaWiFS radiometric calibration will be published in a future volume in this series. Preliminary calculations suggest a consistency between the two SeaWiFS calibrations at the 3% level.

A short synopsis of each chapter in this volume is given below.

1. A Nominal Top-of-the-Atmosphere Spectrum for SeaWiFS

This chapter presents a TOA radiance spectrum to be used in modeling studies of the interaction of the SeaWiFS relative spectral responses with the radiance spectrum that they view. The TOA spectrum presented here was developed from previous modeling work by H. Gordon at the University of Miami. It covers the full wavelength range of the relative spectral responses for the SeaWiFS bands (380–1,150 nm), and it can be modified using `LOWTRAN` absorption spectra for atmospheric water vapor and oxygen to account for the effects of these absorbers. In addition, it includes the `MODTRAN7` spectrum for atmospheric oxygen A-band absorption, which occurs in the band pass of SeaWiFS band 7 (765 nm). These spectra are available on the SeaWiFS Web site (Barnes 1997a).

2. SeaWiFS Measurements in Orbit: Spectral Radiances at the Nominal Center Wavelengths

In November 1993, SeaWiFS was calibrated using a technique in which the digital counts from the instrument were paired with the spectral radiances from a laboratory integrating sphere at the nominal center wavelengths for the SeaWiFS bands. The conversion of this type of laboratory calibration to orbit requires three factors linked to the spectral shape of the source that SeaWiFS views. First, the total band response to the laboratory source must be converted to that for the source viewed in orbit. In this case, the nominal TOA spectrum of Barnes and Esaias (1997) is used. Second, the effects of water vapor and oxygen A-band absorption on the upwelling atmospheric radiance must be removed; and third, the out-of-band response of the SeaWiFS bands to the upwelling radiance must also be removed. These factors are presented in a tabular form as the basis for an efficient correction algorithm for on-orbit measurements.

3. Atmospheric Oxygen Absorption and SeaWiFS Band 7

Oxygen A-band absorption in SeaWiFS band 7 (765 nm) has been investigated twice previously. Fraser (1995) calculated the ozone equivalent bandwidth for two pathlengths through the atmosphere, and Ding and Gordon (1995) provided an analysis in which ozone absorption was imbedded in their radiative transfer model. Here, ozone absorption is presented using the relative spectral responses from Barnes (1994), the nominal TOA spectrum from Barnes and Esaias (1997), and the ozone absorption spectrum from `MODTRAN7`. The study presented here is compared with the previous studies. The `MODTRAN7` spectrum has a much higher wavelength resolution than the `LOWTRAN` spectrum used by Barnes et al. (1997), and Table 5 in this paper completes Table 11 in Barnes et al.

(1997). The uncertainty in the correction for oxygen absorption in SeaWiFS band 7 is estimated to be 0.8%.

4. The 1993 SeaWiFS Calibration Using Band-Averaged Spectral Radiances

The radiometric calibration of SeaWiFS in November 1993 used a calibration technique that paired the digital counts from the instrument bands, with the spectral radiances from the laboratory's spherical integrating source (SIS) at the nominal center wavelengths for those bands. Using the spectral shape of the output of the laboratory radiance source, as provided by the manufacturer, it is possible to provide a radiometric calibration of SeaWiFS in terms of band-averaged spectral radiances. That calibration is presented here. It is given for three wavelength ranges, 380–940 nm, 380–1,150 nm, and for the in-band response ranges of the SeaWiFS bands.

5. SeaWiFS Measurements in Orbit: Band-Averaged Spectral Radiances

This paper presents the culmination of the source spectra shape studies in Barnes et al. (1996) and in this technical memorandum. The SeaWiFS band-averaged spectral radiances are independent of the spectral shape of the source that the instrument measures; however, the band-averaged center wavelengths associated with them do have such a dependence. The current radiometric calibration (Barnes et al. 1994b) does not use band-averaged measurements. The adoption of band-averaged spectral radiances awaits analysis of the radiometric recalibration of SeaWiFS at the spacecraft manufacturer, which was done during the first quarter of 1997. For measurements of on-orbit band-averaged spectral radiances, it is recommended that the in-band results be used. A modification of the technique of Barnes and Yeh (1996), for use with band-averaged measurements, is presented. Since band-averaged center wavelengths are not part of the SeaWiFS level-1b processing, the best estimates for these wavelengths are given here. In addition, estimates are provided of the uncertainties in the on-orbit band-averaged spectral radiances and center wavelengths that derive from the lack of information on the spectral shape of the Earth-exiting radiance.

6. SeaWiFS Revised Temperature Calibration

The radiometric calibration of SeaWiFS data includes a correction for the temperature dependence of the individual detector sensitivities. The detector temperatures are measured by temperature sensors mounted on the instrument focal planes. Processing of the temperature sensor output by an onboard instrument computer introduces a nonlinear response into the temperature data. This chapter describes the calibration of the temperature sensor output and the computation of the temperature corrections for the radiometric calibration of the instrument.

Chapter 1

A Nominal Top-of-the-Atmosphere Spectrum for SeaWiFS

Robert A. Barnes
General Sciences Corporation
Laurel, Maryland

Wayne E. Esaias
Goddard Space Flight Center
Greenbelt, Maryland

Abstract

This chapter presents a TOA radiance spectrum to be used in modeling studies of the interaction of the SeaWiFS relative spectral responses with the radiance spectrum that they view. The TOA spectrum presented here was developed from previous modeling work by H. Gordon at the University of Miami. It covers the full wavelength range of the relative spectral responses for the SeaWiFS bands (380–1,150 nm), and it can be modified using `LOWTRAN` absorption spectra for atmospheric water vapor and oxygen to account for the effects of these absorbers. In addition, it includes the `MODTRAN7` spectrum for atmospheric oxygen A-band absorption, which occurs in the band pass of SeaWiFS band 7 (765 nm). These spectra are available on the SeaWiFS Web site (Barnes 1997a).

1.1 INTRODUCTION

For filter radiometers with finite bandpasses, there is a fundamental interaction between the spectral responses of the instrument bands and the spectral shape of the radiance spectrum that they measure. For instruments with narrow bandpasses of 10 nm or less, such as the SeaWiFS Transfer Radiometer (SXR), the effects of source spectral shape are negligibly small. For SeaWiFS, which has bandwidths of 20 and 40 nm, different source spectral shapes lead to different output from the instrument.

The effects of source spectral shape were studied in Barnes et al. (1996), using normalized Planck function (i.e., blackbody) curves to provide TOA radiance spectra. These were combined with the published spectral response curves for the SeaWiFS bands from Barnes (1994) to examine changes to the in-band and out-of-band responses of the instrument, as well as to the total band responses. For those studies, it was assumed that the TOA spectrum for SeaWiFS measurements was best approximated by a 12,000 K Planck function curve. In addition, the Planck function curves in those studies did not include any accommodation for absorption features in the TOA spectrum.

Using models of atmospheric radiative transfer, it is possible to provide more realistic TOA spectra. The model results of H. Gordon from the University of Miami (Hooker et al. 1992) are the basis for the refinement presented here.

They are used to create a baseline TOA spectrum, that is, a TOA spectrum with no absorption features. This base spectrum covers the wavelength range from 380–1,150 nm at 1 nm intervals covering the range for the measured spectral responses of the SeaWiFS bands. In addition, the `LOWTRAN` tropical model has been adapted to provide spectra for atmospheric water vapor and oxygen A-band absorption features over the wavelength range of the base spectrum.

A high resolution (`MODTRAN7`) oxygen A-band absorption spectrum has also been created to examine the effects of oxygen absorption on the output of SeaWiFS band 7. A more detailed spectrum is required, since oxygen absorption occurs at the peak of the spectral response for band 7 (as shown in the Prologue to Barnes et al. 1996). The absorption spectrum presented here is provided at 0.1 nm intervals. To use this spectrum, the base radiance profile and the spectral response values for SeaWiFS band 7 have been set to the same wavelength interval via interpolation.

1.2 BASELINE SPECTRUM

This nominal spectrum is based on the model results of H. Gordon as given in Fig. 3 of Hooker et al. (1992). Those results cover wavelengths from 400–890 nm for a nadir view with a 60° solar zenith angle. The model includes absorption by oxygen, ozone, and water vapor, plus scattering by

aerosols. It also includes extremely low and high oceanic chlorophyll concentrations (0.01 and 10.0 mg m^{-3}, respectively).

As shown in Fig. 3 of Hooker et al. (1992), oceanic chlorophyll provides a small contribution to the TOA radiance. This leads to requirements for a highly stable and sensitive satellite instrument and for precise corrections for the radiance generated by the atmosphere. For the nominal TOA radiance spectrum developed here, the low and high chlorophyll concentrations lead to TOA spectra that are nearly identical for the entire range of oceanic chlorophyll concentrations. As a result, the low chlorophyll model in Hooker et al. (1992) is used here (Fig. 1).

Figure 1a shows the model radiance spectrum using a linear ordinate. It has been normalized to a value of 9.1 mW cm^{-2} μm^{-1} sr^{-1} at 412 nm to assure approximate agreement with the typical radiances in the SeaWiFS performance specifications (Barnes et al. 1994a). The feature near 760 nm comes from oxygen A-band absorption in the atmosphere, and the features near 720 nm and 820 nm come from absorption by water vapor. Figure 1b shows the radiance spectrum using a logarithmic ordinate.

The ordinates for Figs. 1a and 1b are given in terms of spectral radiances (mW cm^{-2} μm^{-1} sr^{-1}). The spectral radiances in this figure cover a portion of the total radiance that exits the Earth at the TOA. Radiance is the integral over wavelength of spectral radiance; radiance does not include the unit, μm^{-1}. The nominal radiance spectrum presented here includes the portion of the Earth-exiting radiance from 380–1,150 nm. This is the wavelength region over which the spectral responses of the SeaWiFS bands have been measured.

This region includes wavelengths beyond those for the model results in Fig. 1 (400–890 nm). These model results cover the bandwidths (full-widths at half-maximum [FWHM]) of the eight SeaWiFS bands. For SeaWiFS band 1, the bandwidth extends from 403–423 nm (Barnes et al. 1994a), and for SeaWiFS band 8, it extends from 846–887 nm. For wavelengths outside of the range from 400–890 nm there is only a small response from the SeaWiFS bands, so the extensions to the original model that are provided here have been made primarily for completeness.

The extensions were made based on the spectra of TOA and sea level solar radiation found in Brasseur and Solomon (1986). In these spectra, spectral radiance decreases rapidly and linearly with decreasing wavelength from 400 nm down to 380 nm. For the nominal TOA spectrum presented here, the slope of this decrease is an extension of the spectral radiance change from 400–405 nm in Fig. 1a. This extrapolation is shown in Fig. 2a. It is not a straight line in the figure, since the ordinate is logarithmic.

The extension from 890–1,150 nm was made using three pieces that are exponential functions of wavelength (Fig. 2a). Again, this extension follows the shape of the spectra in Brasseur and Solomon (1986). This extension

contains none of the water vapor absorption features that dominate the actual TOA spectrum in this spectral region.

Figure 2b shows the nominal TOA spectrum with the water vapor and oxygen A-band absorption features in the Gordon model removed. These features were replaced with exponential splices, which were made with a knowledge of the wavelengths at which the LOWTRAN model shows water vapor and oxygen absorption to be zero (see below). The TOA spectrum in Fig. 2b was developed to provide an improvement to the Planck function approximations in Barnes et al. (1996); it is the baseline for the nominal TOA spectrum for SeaWiFS. In addition, the TOA spectrum in Fig. 2b provides a backbone for studies of the effects of water vapor and oxygen absorptions for different pathlengths and for different water vapor column amounts.

1.3 LOWTRAN ABSORPTIONS

Figure 3a gives the transmission spectrum for water vapor and oxygen for two vertical passes through the atmosphere and a vertical water vapor column of 3.332 g cm^{-2} (or 1.12×10^{23} cm^{-2}). In this figure, absorption by oxygen causes the feature near 760 nm; absorption by water vapor causes the others. The data come from the LOWTRAN tropical model, as used by Gordon (1995); the data from the LOWTRAN model are not given at 1 nm intervals, as are the values in the baseline radiance spectrum. The intervals between the LOWTRAN data increase with increasing wavelength from less than 1 nm in the near ultraviolet region to more than 1 nm in the near infrared region. In order to provide the same wavelength spacing as the baseline TOA spectrum, the LOWTRAN data were placed on 1 nm centers by interpolation.

For a single vertical pass through the atmosphere, the atmosphere is said to have an airmass of unity. For an airmass of unity, there are 2.15×10^{25} molecules of air per square centimeter of surface area between the Earth's surface and the TOA (Chamberlain and Hunten 1987). The actual number of molecules in the atmospheric column will vary as a function of the surface pressure. Since oxygen is well mixed throughout the overwhelming bulk of the atmosphere, its column amount is a direct function of the airmass. However, since the water vapor content of the atmosphere varies with time and location, its column amount must be specified independently.

Atmospheric absorption by water vapor and oxygen in the LOWTRAN model is assumed to follow the Beer–Lambert law, at least to a very good approximation,

$$I(\lambda) = I_0(\lambda)e^{-a(\lambda)bc}, \tag{1}$$

where λ is the wavelength; $I_0(\lambda)$ is the intensity of light in the absence of absorption as a function of wavelength; $I(\lambda)$ is the intensity of light with absorption as a function of wavelength; $a(\lambda)$ is the absorption cross section as a function of wavelength (cm^2); b is the pathlength (cm); and c is the concentration of the absorber (cm^{-3}).
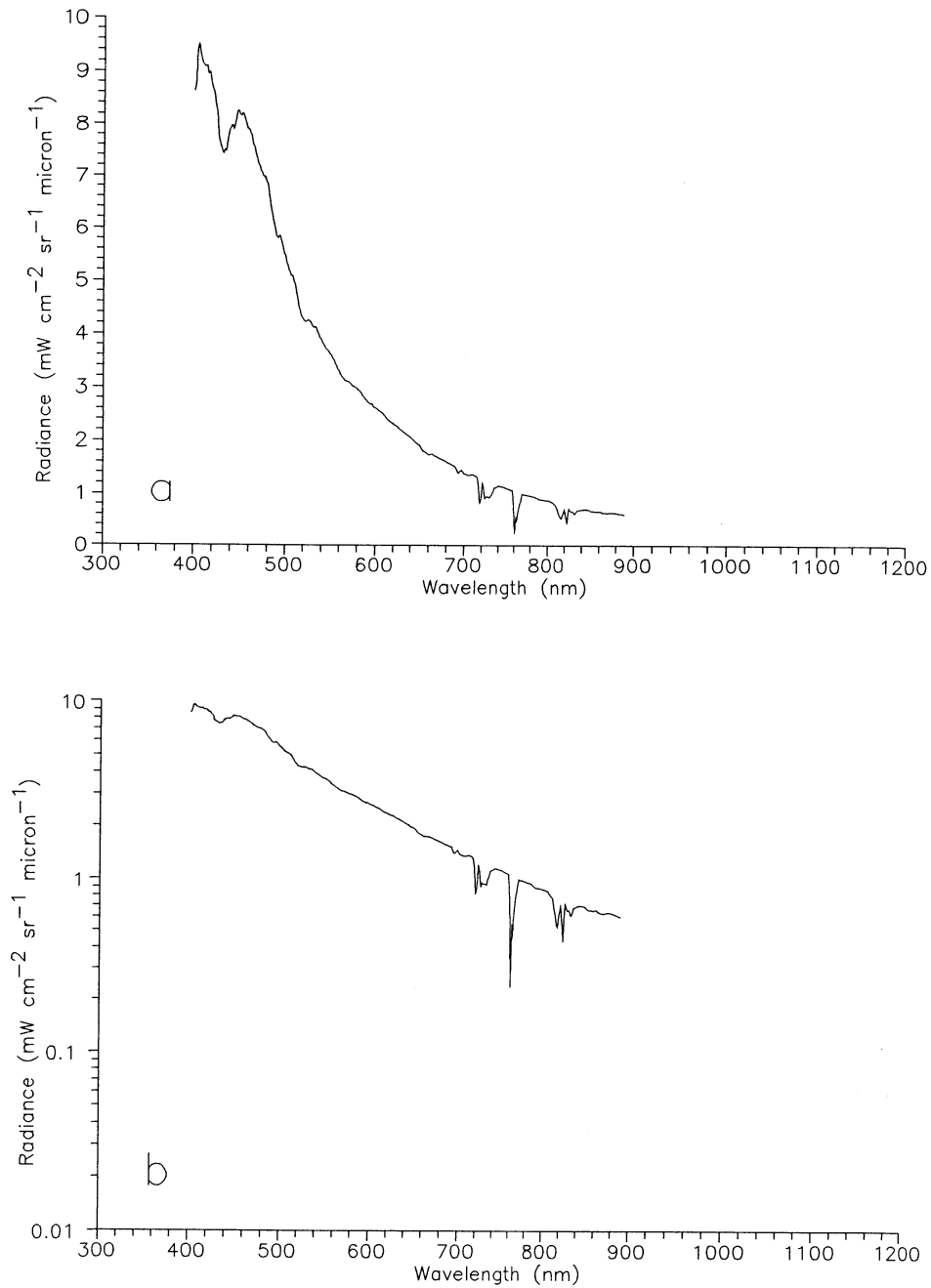
Fig. 1. The TOA radiance spectrum of Gordon, as given in Hooker et al. (1992) is presented here. The radiances have been normalized to bring them into approximate agreement with the SeaWiFS typical radiances. **a)** Spectral radiances are shown on a linear scale. **b)** Spectral radiances are shown on a logarithmic scale.
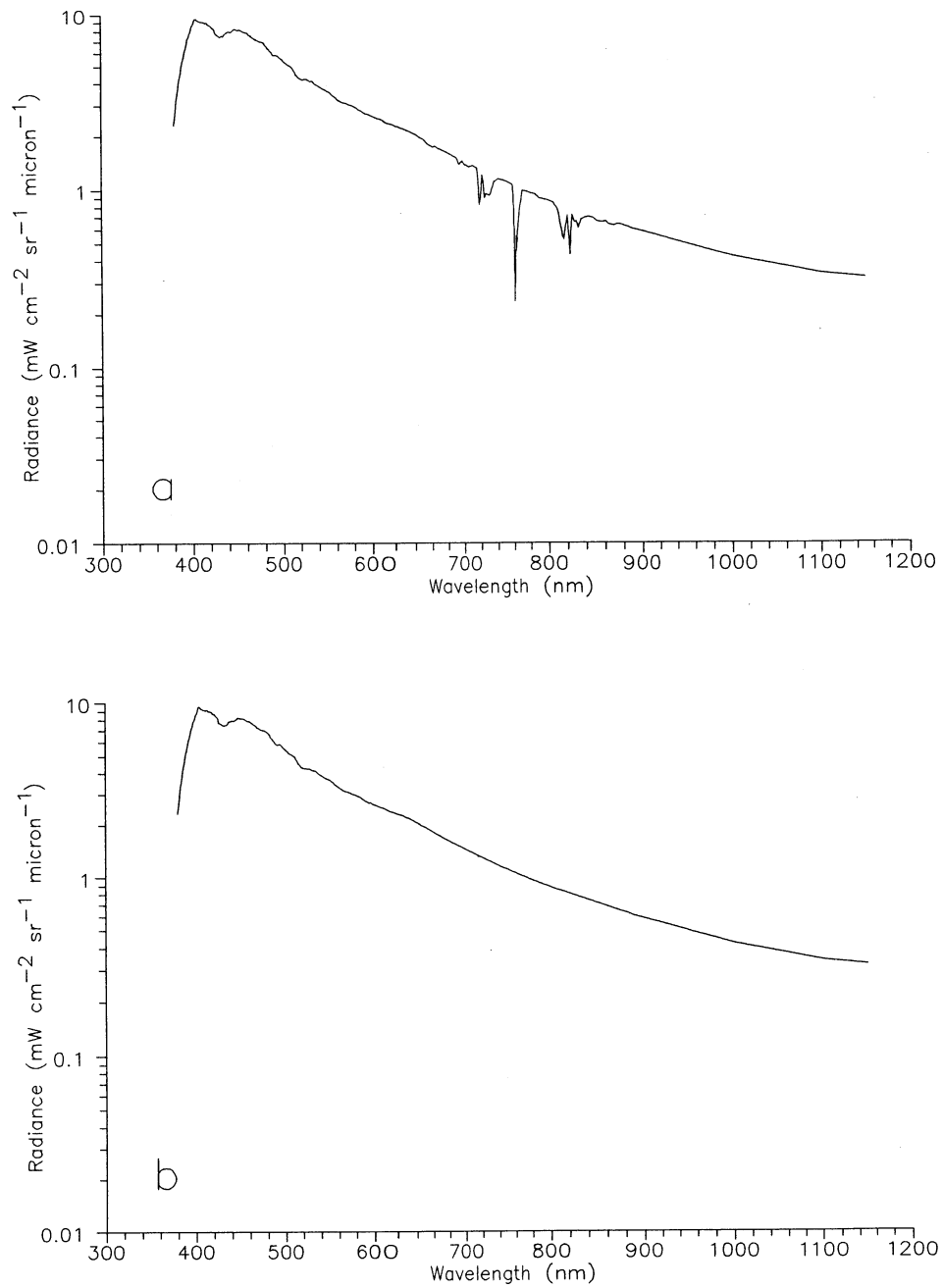
Fig. 2. Modifications to the radiance spectrum of Gordon are shown. **a)** This shows an update of Fig. 1b with extensions from 380–400 nm and from 890–1,150 nm. **b)** This shows an update of Fig. 2a with the water vapor and oxygen A-band absorption features removed. This is the baseline for the nominal TOA spectrum for SeaWiFS.
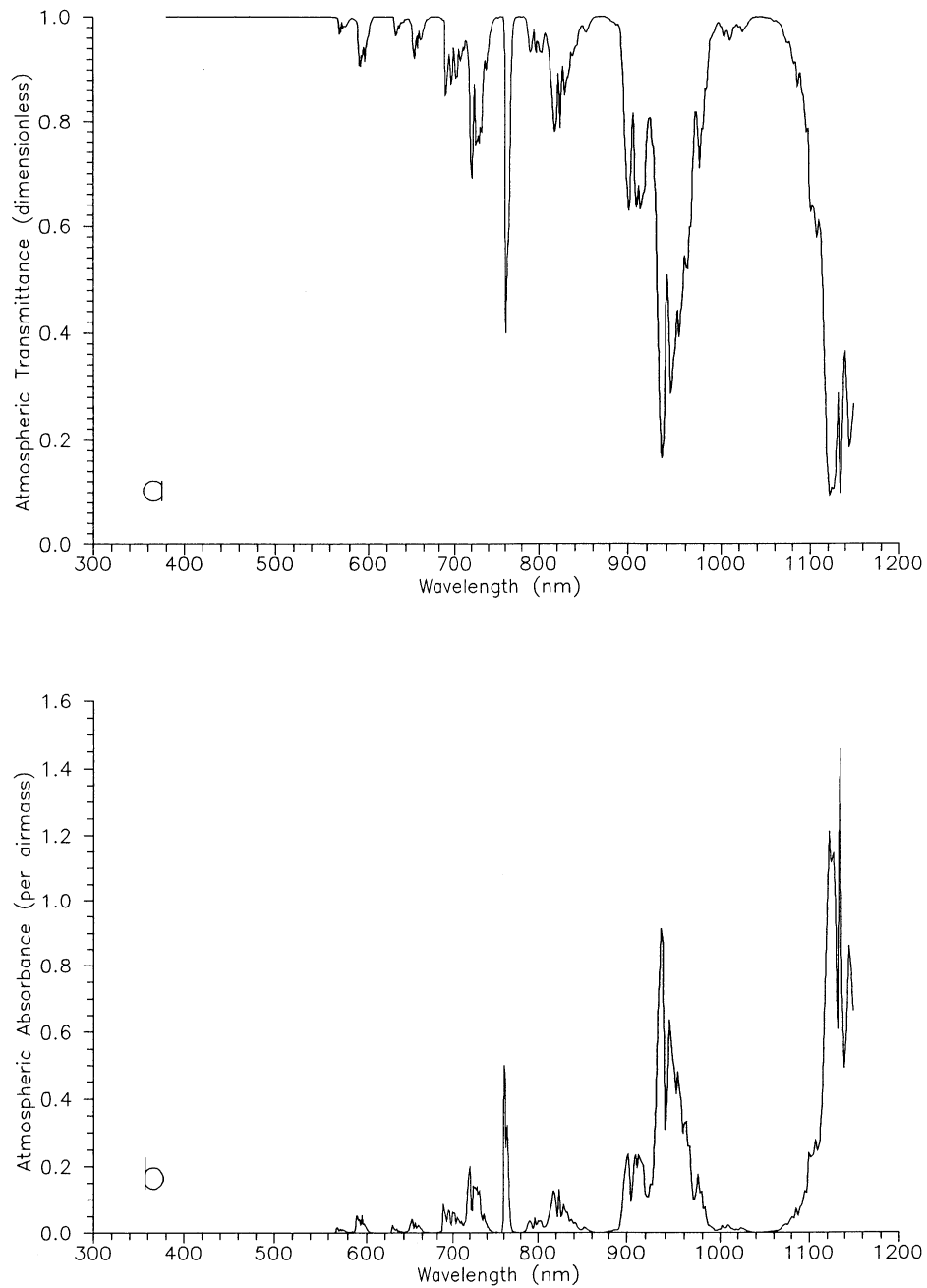
Fig. 3. The `LOWTRAN` tropical model is shown from 380–1,150 nm. The spectrum includes the effects of absorption in the atmosphere by water vapor and the A-band of oxygen. **a)** This is the atmospheric transmittance spectrum for an airmass of 2 and a water vapor column amount of $3.332\,\mathrm{g\,cm^{-2}}$ per unit airmass. The feature near 760 nm comes from oxygen A-band absorption. The other features come from absorption by water vapor. **b)** This is the corresponding absorbance spectrum. Absorbance is in terms of per unit airmass, with a water vapor column amount of $3.332\,\mathrm{g\,cm^{-2}}$ per unit airmass.

The absorption cross section, a, can also be defined as a mass scattering coefficient or a volume scattering coefficient (Kidder and Vonder Haar 1995). The atmospheric transmittance in Fig. 3a is defined as the ratio, $I(\lambda):I_0(\lambda)$, which is dimensionless and is the form in which light intensity will be used here. For this reason, light intensity has been described in (1) without units. When the absorption bands consist of fine rotational lines, the Beer–Lambert law is not obeyed, that is, the absorption coefficient is not constant at different pressures (Okabe 1978). For the nominal TOA spectrum presented here, deviations from the Beer–Lambert law are not a consideration.

In the laboratory, the term, b, is determined by the length of the absorption cell. For atmospheric measurements, it is the practice to combine the terms b and c to create a column amount, μ, which defines the amount of the absorber along a given pathlength (Barnes et al. 1986). Using the terms in (1), this column amount has units of molecule per square centimeter. The exponent in (1) must be kept dimensionless. This leads to an alternate form of the Beer–Lambert law

$$I(\lambda) = I_0(\lambda)e^{-\alpha(\lambda)\mu}, \qquad (2)$$

where the product of $\alpha(\lambda)$ and μ is dimensionless. For oxygen A-band absorption, μ can be defined in terms of airmass (where 1 airmass equals $2.15 \times 10^{25} \, \text{cm}^{-2}$). Since oxygen is well mixed in the atmosphere with a fractional amount of 0.2095 (Chamberlain and Hunten 1987), the column amount of oxygen in 1 airmass is $4.50 \times 10^{24} \, \text{cm}^{-2}$. Thus, an $\alpha(\lambda)$ of 1 per unit airmass in (2) corresponds to an $\alpha(\lambda)$ of $2.22 \times 10^{-24} \, \text{cm}^2$ in (1).

In Fig. 3a, the values of transmittance, $I(\lambda):I_0(\lambda)$, are given for two vertical passes through the atmosphere, that is, for an airmass of 2. Using these values, it is possible to use (2) to calculate $\alpha(\lambda)$ for oxygen (per unit airmass). Oxygen absorption in Fig. 3a covers the wavelength range from 758–770 nm.

For the other wavelengths, it is possible to use (2) to calculate $\alpha(\lambda)$ for water vapor, where 1 airmass of the `LOWTRAN` tropical model contains $3.332 \, \text{g cm}^{-2}$ (or $1.21 \times 10^{23} \, \text{cm}^{-2}$). This was done to create the absorption spectrum in Fig. 3b.

With the baseline radiance spectrum and the `LOWTRAN` absorption profile compiled at 1 nm intervals from 380–1,150 nm, it is possible to produce a combined radiance-absorption spectrum using point-by-point multiplication. Such a combined profile is shown in Fig. 4a. It is a spectrum for an airmass of 3 with a vertical water vapor column of $3.332 \, \text{g cm}^{-2}$ (or $3.332 \, \text{g cm}^{-2}$ per unit airmass). Figure 4b shows a comparison of the radiance spectrum in Fig. 4a with the original model spectrum from Fig. 1b. The comparison between the two spectra is reasonably close, with the new spectrum showing small water vapor absorption features that are not present in the original spectrum from Hooker et al. (1992).

1.4 AIRMASS AND PATHLENGTH

If one neglects the curvature of the Earth, it is possible to model a *plane parallel* atmosphere in which non-vertical pathlengths through the atmosphere can be linked to the vertical pathlength (airmass = 1) using plane geometry. In this model, the pathlength varies with the secant ($1/\cos$) of the angle from vertical. Such a formulation was used by Ding and Gordon (1994) and by Gordon (1995).

For large angles from vertical, the airmass can be determined using the Chapman function (Chapman 1931 and Swider and Gardner 1967), which accounts for the curvature of the Earth. The Chapman function is applied to atmospheric constituents that have concentrations which decrease exponentially with altitude at a known rate. The function is ideal for calculating the airmass of the atmosphere and of well-mixed constituents, such as oxygen. In other cases, it may be necessary to calculate airmass using a model in which the atmosphere is considered as a set of spherical shells.

For SeaWiFS measurements, radiation passes through the atmosphere twice. For incoming radiation, the pathlength is determined by the solar zenith angle. For outgoing radiation, the pathlength is determined by the nadir viewing angle of the instrument. With the sun at the zenith and the instrument viewing at nadir, the airmass for SeaWiFS measurements is 2. For a plane parallel atmosphere with a solar zenith angle of 60° and a nadir viewing angle of 60°, the airmass is twice the secant of 60°, that is, an airmass of 4. These are the lower and upper limits of the airmasses for SeaWiFS measurements.

The nominal TOA radiance spectrum presented here can be modified for different airmasses; however, the spectrum itself is not dependent on the manner in which airmass is calculated.

1.5 OXYGEN ABSORPTION

Figure 5a gives a high resolution transmission spectrum for oxygen for two vertical passes through the atmosphere. The data come from the `MODTRAN7` model and were provided by K. Thome of the University of Arizona. The original `MODTRAN7` values are given at $1 \, \text{cm}^{-1}$ intervals, and the values provided by Thome were interpolated to 0.1 nm intervals using a $10 \, \text{cm}^{-1}$ triangular slit function. These `MODTRAN7` results included attenuation from oxygen and ozone absorption and from molecular scattering. Molecular scattering, which accounted for a transmission reduction of about 3%, was removed from the spectrum. For wavelengths outside the region of oxygen A-band absorption (from 758–772 nm), the transmission in Fig. 5a is unity.

In addition, Fig. 5a shows the transmission spectrum from the `LOWTRAN` model from 745–785 nm. This wavelength region covers the bandwidth (FWHM) for SeaWiFS band 7 (Barnes et al. 1994b). The `LOWTRAN` values in
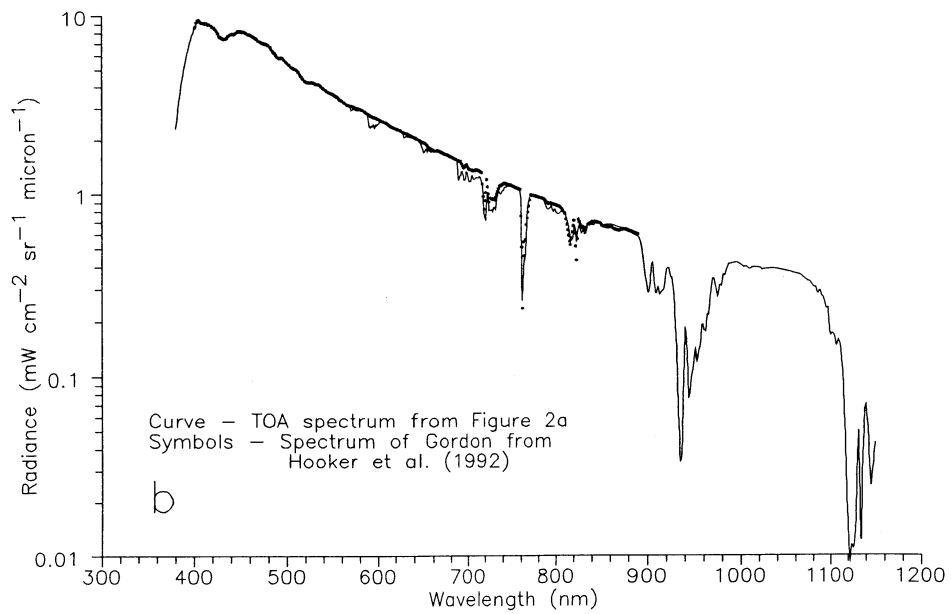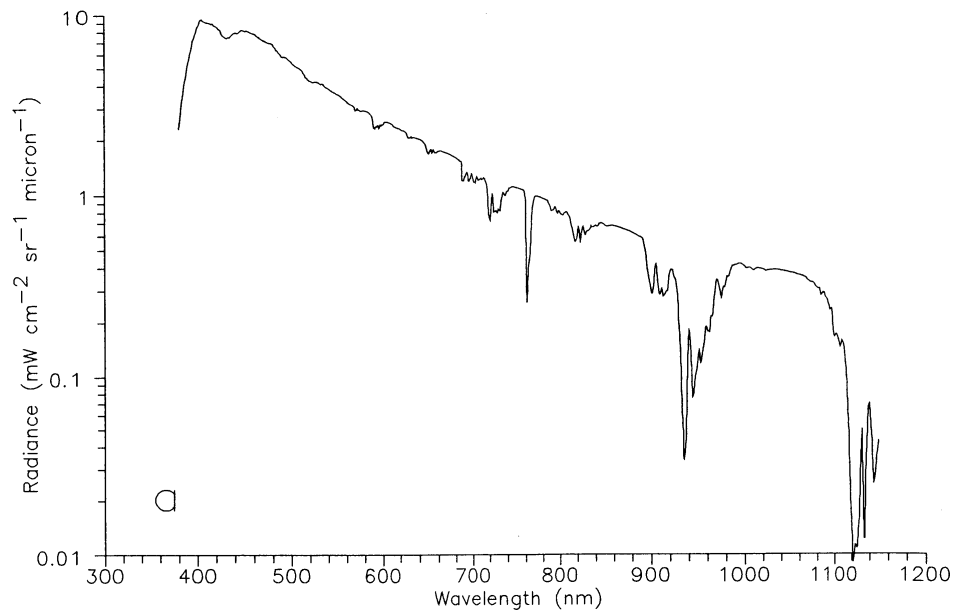
Fig. 4. The composite TOA radiance spectrum is compared with the model of Gordon. **a)** This part combines the baseline spectrum from Fig. 2b with the transmittance for an airmass of 3 and a water vapor column amount of $3.332\,\mathrm{g\,cm^{-2}}$ per unit airmass. **b)** This part is a comparison of the results in Fig. 4a with the model of Gordon from Fig. 1b.
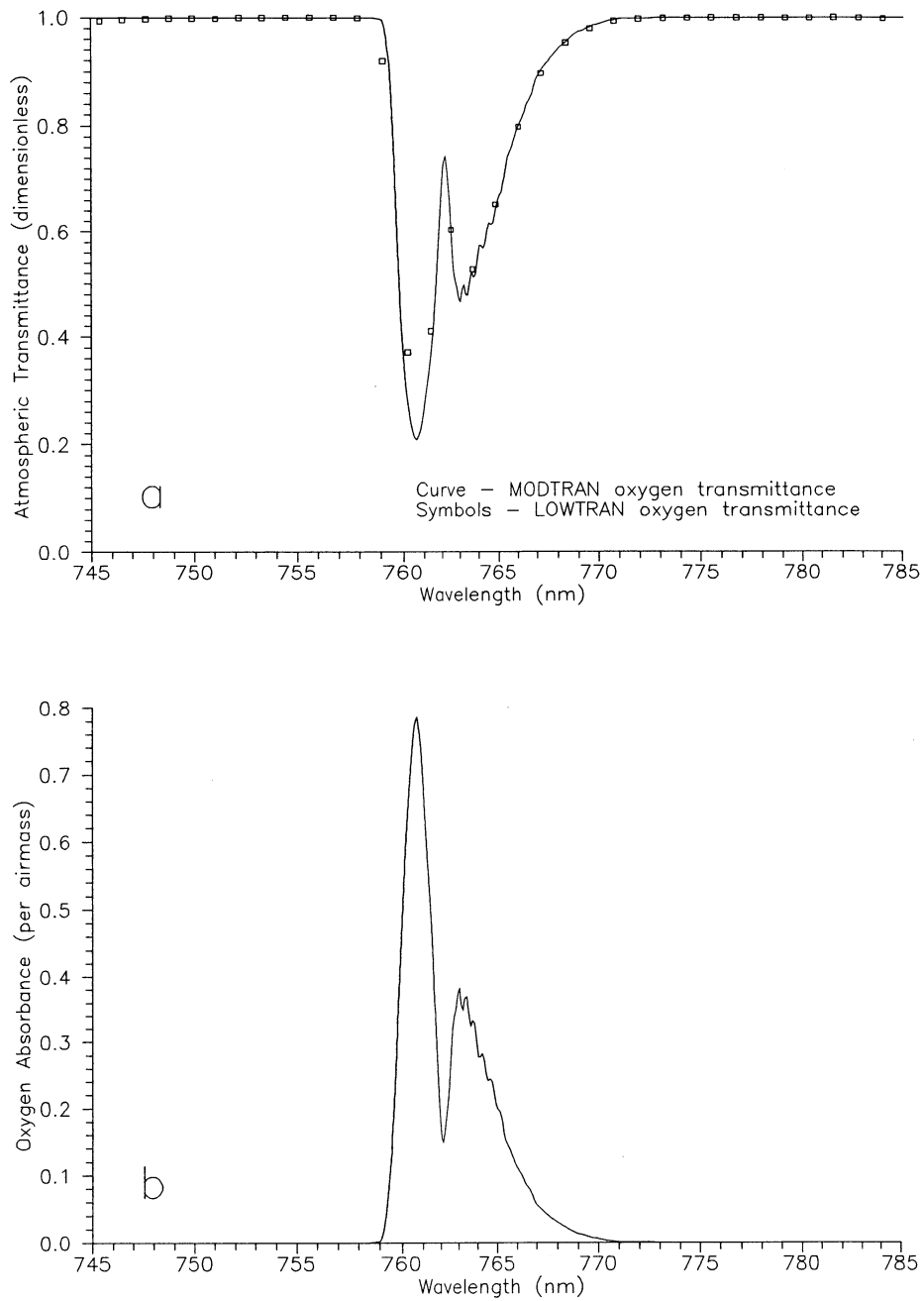
Fig. 5. The `MODTRAN7` model for oxygen A-band absorption is plotted here. The model results are given at 0.1 nm intervals. **a)** Here is the atmospheric transmittance spectrum for an airmass of 2. The symbols show the corresponding values from the `LOWTRAN` model. **b)** Here is the absorbance spectrum from the `MODTRAN7` model. Absorbance is in terms of per unit airmass.

Fig. 5a come directly from the model and have not been interpolated to 1 nm intervals. As shown in this figure, the `LOWTRAN` data do not fully reproduce the fine structure in the `MODTRAN7` results. This fine structure is important in the analysis of the effects of oxygen A-band absorption on the output of SeaWiFS band 7, since the absorption occurs at the peak of the spectral response of the band.

Figure 5b shows the oxygen A-band absorbance spectrum in per units of airmass. These values were calculated using (2), the transmittance spectrum in Fig. 5a, and an airmass (μ) of 2.

1.6 CONCLUDING REMARKS

In a series of modeling studies, Barnes et al. (1996) developed a set of TOA spectra using Planck function (blackbody) curves with temperatures from 2,000–38,000 K. These curves did not include a provision to examine the effects of atmospheric absorption. Of these curves, the 12,000 K Planck function was determined to best fit the spectral shape of the typical radiances from the SeaWiFS Performance Specifications (Barnes and Yeh 1996). As such, the 12,000 K Planck function was considered to give the best approximation to the TOA spectrum viewed by SeaWiFS during ocean color measurements.

Here, the authors developed a nominal TOA spectrum that is an incremental improvement to the Planck function in Barnes and Yeh (1996). This nominal TOA spectrum can also be modified to include atmospheric absorption features. When combined with the relative spectral responses of the SeaWiFS bands, the nominal TOA spectrum can be used to calculate the integrated output from the bands. When compared with the integrated output for bands and the 12,000 K Planck function curve, it should be possible to estimate the uncertainties in the band responses due to differences in the spectral shape of the source that they view.

Chapter 2

SeaWiFS Measurements in Orbit:
Spectral Radiances at the Nominal Center Wavelengths

Robert A. Barnes
Robert E. Eplee, Jr.
Eueng-nan Yeh
General Sciences Corporation, Laurel, Maryland

Abstract

In November 1993, SeaWiFS was calibrated using a technique in which the digital counts from the instrument were paired with the spectral radiances from a laboratory integrating sphere at the nominal center wavelengths for the SeaWiFS bands. The conversion of this type of laboratory calibration to orbit requires three factors linked to the spectral shape of the source that SeaWiFS views. First, the total band response to the laboratory source must be converted to that for the source viewed on orbit. In this case, the nominal TOA spectrum of Barnes and Esaias (1997) is used. Second, the effects of water vapor and the oxygen A-band on the upwelling atmospheric radiance must be removed; and third, the out-of-band response of the SeaWiFS bands to the upwelling radiance must also be removed. These factors are presented in a tabular form as the basis for an efficient correction algorithm for on-orbit measurements.

2.1 INTRODUCTION

The radiometric calibration of SeaWiFS in November 1993 was based on spectral radiances at eight wavelengths, i.e.,the nominal center wavelengths for the SeaWiFS bands (412, 443, 490, 510, 555, 670, 765, and 865 nm). The SIS in the laboratory was, itself, calibrated at these wavelengths. A calibration of this sort works well for radiometric instruments that measure at one (or several) individual wavelengths. The SeaWiFS bands, however, have nominal spectral bandwidths (FWHM response) of 20 and 40 nm. For instruments with finite spectral bandwidths such as these, this type of calibration creates a dependence of the instrument's response on the spectral shape of the source that is measured.

According to the manufacturer of SeaWiFS, the SIS used in calibrating the instrument has the spectral shape of a 2,850 K blackbody. The analysis behind this assumption was not a required part of the laboratory calibration data for SeaWiFS. For measurements of a similar SIS, however, the SeaWiFS output were equivalent to those for a Planck function with the same temperature (Barnes et al. 1996). For the current radiometric calibration of SeaWiFS (Barnes et al. 1994b), the manufacturer's calibration source is assumed to have the spectral shape of a 2,850 K blackbody.

The initial prelaunch calibration of SeaWiFS used the relative spectral responses (RSRs) of the eight SeaWiFS bands to convert the instrument's responses from a 2,850 K blackbody spectral shape in the laboratory, to an on-orbit response for a 5,900 K blackbody (Table 12 of Barnes et al. 1994b). This is the spectral shape for the solar output and is the spectral shape found in the SeaWiFS Performance Specifications (Barnes et al. 1994a). In a series of modelling studies (Barnes et al. 1995 and Barnes and Yeh 1996), it was determined that a 12,000 K Planck function (blackbody) curve is more representative of the spectral shape for the upwelling radiance from the ocean scenes that will be viewed by SeaWiFS. The factors to convert the output from the eight instrument bands for a 2,850 K laboratory source to those for a 12,000 K on-orbit source are listed in Table 17 of Barnes and Yeh (1996). Neither the 12,000 K nor the 5,900 K TOA spectra include the absorption features found in the upwelling Earth radiance.

More recently, Barnes and Esaias (1997) developed a TOA radiance spectrum based on the atmospheric radiative transfer model results of H. Gordon at the University of Miami (Hooker et al. 1992). The TOA spectrum includes a baseline component, extending from 380–1,150 nm in 1 nm increments, which has no absorption features. The `LOWTRAN` tropical model was also adapted by Barnes and Esaias (1997) to provide spectra for atmospheric water vapor and oxygen A-band absorption features. In addition, a higher resolution spectrum, based on `MODTRAN7`, was adapted to examine the effects of oxygen A-band absorption on the output of SeaWiFS band 7. The TOA

spectrum of Barnes and Esaias (1997) provides an incremental improvement to the previous 5,900 K and 12,000 K Planck function curves.

The application of the TOA spectra to the SeaWiFS measurements is performed in two steps. First, the baseline spectrum (without absorption features) is used to convert the instrument's responses for the laboratory spectrum, to those for the on-orbit spectrum. This is a one-step process that is part of the prelaunch radiometric calibration (Barnes et al. 1994b). Second, the effects of atmospheric absorption are calculated and corrections are applied to the measurements. These corrections require knowledge of both the column amount of the absorbing gas and the pathlength of the solar flux through the atmosphere, i.e., from the top of the atmosphere to the ground and then back to the top of the atmosphere. The correction for atmospheric absorption described below is designed for application to each SeaWiFS band for each measured pixel.

As part of the algorithm to produce calibrated on-orbit radiances from SeaWiFS, the out-of-band responses for the eight bands are removed following the correction for attenuating the upwelling Earth radiance by atmospheric absorption. A description of the out-of-band correction scheme is given in Barnes and Yeh (1996).

2.2 TOA BASELINE SPECTRUM

The spectral responses of the SeaWiFS bands (Barnes 1994) are tabulated as the system level response to a spectrally flat source having a radiance of $1\,\mathrm{mW\,cm^{-2}\,sr^{-1}}$ $\mu\mathrm{m}^{-1}$. The responses are listed at 1 nm intervals from 380–1,150 nm, covering the wavelength region over which the photodiodes in the instrument have a significant quantum efficiency (Fig. 11 of Barnes et al. 1994b). The responses are given in picoamperes of current from the photodiode over each interval. When these currents are multiplied by the radiance from the source at each wavelength and the result is summed, the calculation gives the total current from the photodiode for that source. This current is amplified and digitized by the instrument to give the output for each band in digital numbers (or counts). The digital numbers are proportional to the photodiode current.

The radiances in these comparisons were normalized to the typical SeaWiFS radiance for each SeaWiFS band at that band's nominal center wavelength (Table 1). They provide a normalization point for changes in the photodiode responses to different source spectral shapes. The calculated responses to the laboratory source (2,850 K) and to three approximations to the spectral shape of the upwelling radiances from ocean scenes (5,900 K, 12,000 K, and the nominal TOA spectrum) are listed in Table 2. The total band responses for the 2,850 K, 5,900 K, and 12,000 K sources were taken from Barnes and Yeh (1996). The ratios in Table 2 give the fractional differences in the photodiode currents for the three source spectral shapes. These fractional differences can be applied to the instrument's

calibration constants as part of the prelaunch radiometric calibration equations (Barnes et al. 1994b).

Table 1. This table shows the nominal center wavelengths and typical (L_{typical}) radiances in units of $\mathrm{mW\,cm^{-2}\,sr^{-1}\,\mu m^{-1}}$ for the SeaWiFS bands. These values come from the performance specifications for the instrument (see Barnes et al. 1994a).

Band Number	Nominal Center Wavelength [nm]	L_{typical}
1	412	9.10
2	443	8.41
3	490	6.56
4	510	5.64
5	555	4.57
6	670	2.46
7	765	1.61
8	865	1.09

A comparison of the photodiode responses to the 12,000 K Planck function and nominal TOA spectrum is given in Table 3. The table shows a comparison of the total band (R_T) and the in-band (R_{IB}) responses. The total band response covers the wavelength range from 380–1,150 nm. The in-band response covers the region over which the response of the band is 1% or more of the maximum response of the band. The 1% response points are also called the extended band edges. For the calculations here, the extended band edges are the wavelengths for a spectrally flat source in Table 13 of Barnes et al. (1994b).

For each SeaWiFS band, the in-band response is 93–99% of the total band response; the remainder is out-of-band. For bands 1, 2, 3, 4, and 7 in Table 3 (412, 443, 490, 510, and 765 nm nominal center wavelengths), the total band and in-band conversion ratios are the same at the 0.1% level. This indicates that the differences in the responses of these bands to the two source spectral shapes is dominated by the in-band portion of the band response. A plot of the radiance curves for the 12,000 K and the nominal TOA spectra, normalized to the typical radiance for SeaWiFS band 1, is shown in Fig. 6a. For band 1, the differences between the spectra in the wavelength region between 396–423 nm (the in-band region) cause a much greater change than the differences in the out-of-band region. This is due to the large out-of-band rejection for this band (Fig. 28 of Barnes et al. 1994b).

For bands 5 and 6 in Table 3 (555 and 670 nm nominal center wavelengths), the in-band ratios for the two sources are much closer to unity than the total band ratios. This indicates that more than half of the difference in the responses of these bands to the two spectra comes from the out-of-band regions. For band 8, the out-of-band regions contribute almost all of the difference in the correction ratios for the two source spectral shapes.

The cause of this out-of-band difference in band 8 is shown in Fig. 6b. In this figure, the two radiance spectral
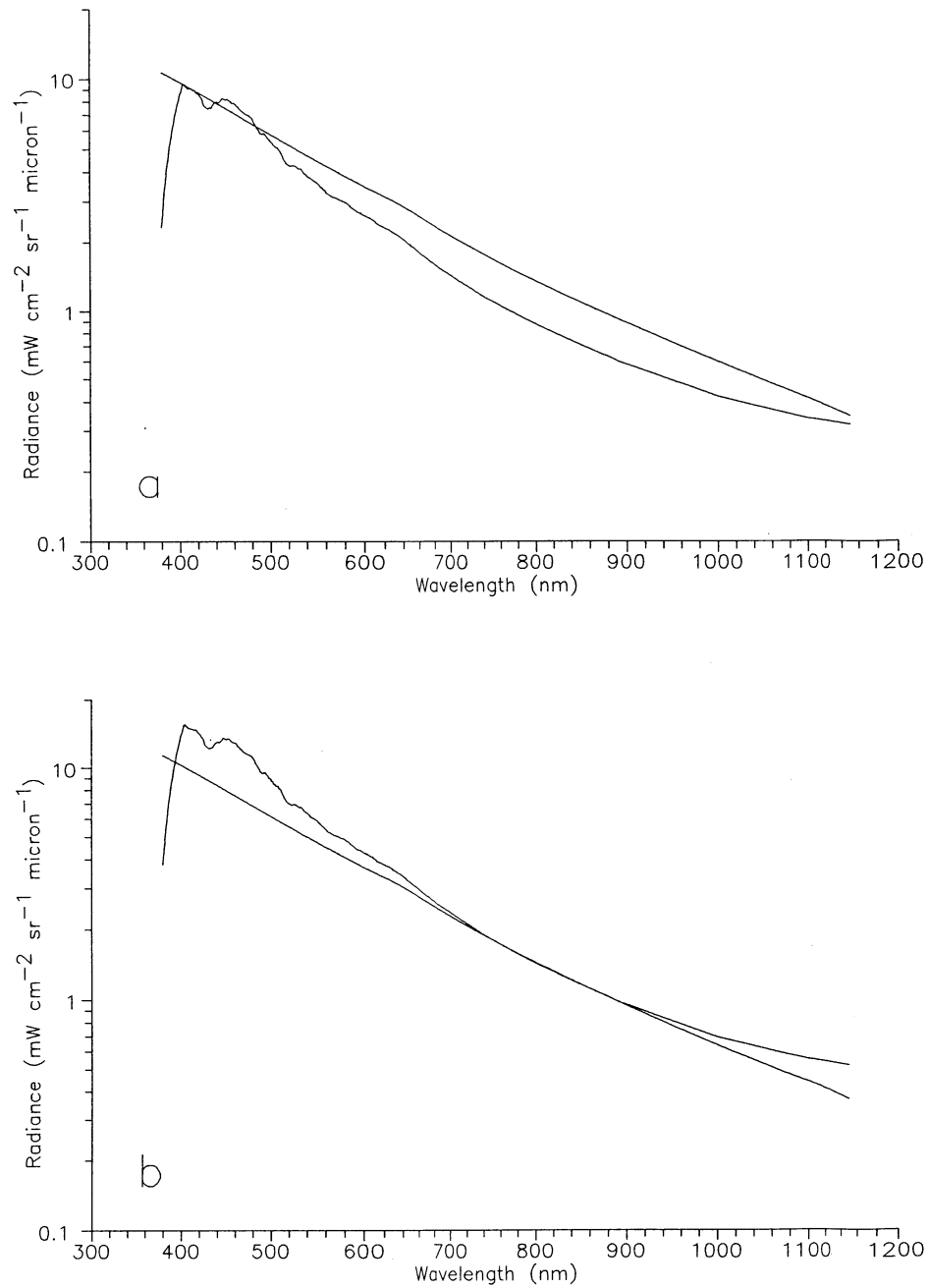
Fig. 6. These are plots of the radiance curves for the 12,000 K and the nominal TOA spectra. The plots have no absorption features. **a)** Normalized at 412 nm to the typical radiance for SeaWiFS band 1. **b)** Normalized at 865 nm to the typical radiance for SeaWiFS band 8.

Table 2. Listed here are the total band (R_T) responses for three on-orbit radiance spectra. These responses are compared with the responses to a 2,850 K spectrum which represents that for the laboratory integrating sphere. The 5,900 K spectrum was used in Barnes et al. (1994b). The 12,000 K spectrum was used in Barnes and Yeh (1996). The nominal TOA spectrum was developed by Barnes (1997a). The ratios give the relative differences between the band responses for the paired sources.

Band Number	R_T for 2,850 K Source [pA]	R_T for 5,900 K Source [pA]	Ratio to 2,850 K	R_T for 12,000 K Source [pA]	Ratio to 2,850 K	R_T for Nominal TOA Spec. [pA]	Ratio to 2,850 K
1	2274.304	2192.031	0.9638	2166.343	0.9525	2136.222	0.9393
2	3492.898	3434.870	0.9834	3419.122	0.9789	3452.778	0.9885
3	4315.636	4227.442	0.9796	4203.933	0.9741	4276.129	0.9908
4	4623.705	4612.427	0.9976	4621.536	0.9995	4540.688	0.9820
5	3900.117	3866.629	0.9914	3886.181	0.9964	3904.549	1.0011
6	2069.400	2092.267	1.0111	2111.836	1.0205	2125.703	1.0272
7	2874.331	2858.048	0.9943	2860.844	0.9953	2863.650	0.9963
8	2248.979	2275.286	1.0117	2325.586	1.0341	2348.277	1.0442

Table 3. Listed here are total band (R_T) and in-band (R_{IB}) responses for two on-orbit spectra. These spectra are approximations of the actual radiance spectrum that SeaWiFS will view on orbit. The ratios show the relative differences in the output for each source spectral shape. The ratios suggest an uncertainty in the on-orbit output of about 1% due to uncertainty in the spectral shape of ocean scenes.

Band Number	R_T for 12,000 K Source [pA]	R_T for Nominal TOA Spec. [pA]	Ratio	R_{IB} for 12,000 K Source [pA]	R_{IB} for Nominal TOA Spec. [pA]	Ratio
1	2166.343	2136.222	0.9861	2154.071	2125.825	0.9869
2	3419.122	3452.778	1.0098	3401.671	3438.153	1.0107
3	4203.933	4276.129	1.0172	4174.468	4250.652	1.0183
4	4621.536	4540.688	0.9825	4591.212	4509.905	0.9823
5	3886.181	3904.549	1.0047	3782.678	3788.240	1.0015
6	2111.836	2125.703	1.0066	2081.381	2087.479	1.0029
7	2860.844	2863.650	1.0010	2821.399	2820.899	0.9998
8	2325.586	2348.277	1.0098	2190.074	2190.479	1.0002
		Average	1.0022		*Average*	1.0003
		Standard deviation	0.0113		*Standard deviation*	0.0109

curves are normalized to the typical radiance for SeaWiFS band 8. The differences between these two spectra, combined with the out-of-band response of band 8 at shorter wavelengths (Fig. 31 of Barnes et al. 1994b) creates the 1% difference in the band's response to the 12,000 K and the nominal TOA spectrum.

For bands 5, 6, and 8, it is possible to apply the out-of-band correction in a manner that minimizes the effect in the conversion from the laboratory to the TOA source spectral shape. For bands 1, 2, 3, 4, and 7, however, there does not appear to be a means of bringing the conversion ratios for the two source spectral shapes into better agreement. It is estimated that, overall, the correction of the SeaWiFS radiances from the 2,850 K laboratory source spectral shape to the nominal TOA spectrum of Barnes and Esaias (1997) will add an uncertainty of about 1% to the on-orbit radiances measured by SeaWiFS band 2. For bands 1, 3, and 4, the conversion adds an estimated uncertainty of 1.5% to the on-orbit radiances. For bands

5, 6, 7, and 8, the estimated uncertainties (after the removal of the out-of-band response) are about 0.3% or less. Each of these uncertainties are less than the 5% maximum absolute uncertainty requirement for radiance or the 2% maximum relative (band-to-band) uncertainty for radiance in the SeaWiFS performance specifications (Barnes et al. 1994a).

2.3 ABSORPTION FEATURES

These calculations use the data of Barnes (1997a). The absorption values in this tabulation are given for an airmass of unity and a vertical water vapor column amount of $3.332 \, \text{g cm}^{-2}$. The tabulated data include oxygen A-band absorption (for wavelengths from 758–775 nm) and water vapor absorption (for all other wavelengths from 380–1,150 nm). In the calculations presented here, oxygen A-band and water vapor absorption are treated separately. For the water vapor absorption calculations, the values in

the oxygen A-band absorption region (from 758–775 nm) are set to zero. In the same manner for oxygen A-band absorption calculations, the values for wavelengths from 380–757 nm, and from 776–1,150 nm, are set to zero.

Figure 7a shows the TOA spectrum, including the atmospheric transmission feature for oxygen A-band absorption for an airmass of three. There are no absorption features for water vapor. The baseline portion of the spectrum has been normalized at 412 nm to the typical radiance for SeaWiFS band 1. Figure 7b shows a similar TOA spectrum, except that there is no oxygen absorption and there is a water vapor vertical column amount of $3.332 \, \text{g cm}^{-1}$ with an airmass of 3. This gives a slant path water vapor amount of $9.996 \, \text{g cm}^{-2}$.

Table 4 shows the integrated photodiode currents for SeaWiFS bands 1 and 2 for slant path water vapor amounts ranging from zero to $19.992 \, \text{g cm}^{-2}$. The increments of water vapor amount in this table have been calculated for a vertical column amount of $3.332 \, \text{g cm}^{-2}$ for airmasses from zero to 6 in increments of 0.5 airmass. The table gives the total band responses (R_T), in-band responses (R_{IB}), and the ratios of the in-band responses to the total band responses. In the same manner, Tables 5, 6, and 7 give the photodiode currents for the other SeaWiFS bands.

Figure 8a shows the band 8 (865 nm) total band response (R_T) from Table 7 normalized to unity at a slant path water vapor column amount of zero. The figure shows the relative decrease in the total current from the photodiode as the slant path water vapor amount increases. From these data it is possible to *restore* the instrument response that has been *attenuated* by water vapor absorption. Of the SeaWiFS bands, band 8 shows the greatest sensitivity to water vapor absorption. This includes a significant sensitivity in the in-band (R_{IB}) portion of the band's response. It is estimated that the uncertainty in the correction for water vapor absorption is around one-tenth of the correction value. This estimate is, itself, based on an estimate of the quality of the LOWTRAN absorption data and of the water vapor column amount obtained from the ancillary SeaWiFS data. In addition, it is assumed that the major portion of atmospheric water vapor lies in the planetary boundary layer and in the lower part of the free troposphere.

For water vapor in band 8, the decrease in band output is about 2.1% for a column amount of $3.332 \, \text{g cm}^{-2}$ and an airmass of 3 (a slant path amount of $9.996 \, \text{g cm}^{-2}$). This is a mid-range water vapor amount for SeaWiFS ocean measurements. For band 8, the uncertainty in the water vapor correction is estimated at 0.3%. The uncertainty is zero for the other bands.

Table 8 shows the integrated photodiode currents for SeaWiFS bands 1–6 for oxygen A-band absorption at air masses of zero and 6. Since oxygen is well mixed in the atmosphere, it is possible to define the effects of absorption in terms of the slant path length through the atmosphere only, that is, in terms of airmass. For bands 1 and 2, there

is no effect from oxygen A-band absorption. For bands 3, 4, 5, and 6, there is also no effect at the level of one part in 100,000.

For SeaWiFS band 7, oxygen A-band absorption effects the in-band response by 15% or more, depending on the slant path through the atmosphere (Ding and Gordon 1995 and Fraser 1995). The LOWTRAN absorption spectrum used in this analysis does not reproduce the details of the A-band absorption spectrum (Fig. 5a of Barnes and Esaias 1997) which is a significant effect. Because the details of the absorption spectrum are so important, the actual analysis of band 7 is discussed in Barnes (1997b), the next chapter of this technical memorandum. As such, the portion of Table 9 dealing with band 7 is incomplete; the completed, detailed version of this table is given in Table 16 of Barnes (1997b).

Figure 8b shows the band 8 total band response from Table 9 normalized to unity at an airmass of zero. The effect on the response of the band, all in the out-of-band spectral region, is less than 0.2% at an airmass of 6. The uncertainty in the oxygen absorption correction is zero, as are the uncertainties for bands 1–6.

2.4 OUT-OF-BAND RESPONSE

The out-of-band correction for SeaWiFS is applied using the ratio of the in-band response to the total band response (R_{IB}/R_T). This ratio is listed in Tables 4–9. For SeaWiFS band 8 and for atmospheric water vapor absorption, the change in the ratio can be 0.5%; however, the process that *restores* the effects of atmospheric absorption eliminates most of this effect. In addition, the out-of-band correction ratios for the nominal TOA spectrum (without atmospheric absorption) are different from those for the 12,000 K Planck function given in Barnes and Yeh (1996).

Table 10 gives the out-of-band correction factors, k_{b}, from Barnes and Yeh (1996) and the corresponding values from Tables 4–7. Those corresponding values are the ratios (with no atmospheric attenuation) in the tables. In Barnes and Yeh (1996), there are two correction factors for band 7—one with oxygen A-band absorption included in the calculation and one without. The value from Barnes and Yeh (1996) used here comes from band 7 without the oxygen notch.

The correction factors from the nominal TOA spectrum are an incremental improvement to the values from Barnes and Yeh (1996). For bands 1–4 and band 7, the correction factors in Table 10 are the final values. For bands 5, 6, and 8 the factors are input data to the calculation scheme of Barnes and Yeh (1996).

The correction factors in Table 10 are used as the basis for the uncertainties in the out-of-band corrections using the nominal TOA spectrum. For bands 1–4 and 7, the corrections for the 12,000 K and nominal TOA spectra disagree by about 0.1%. This is the estimated uncertainty in the correction for these bands. For bands 5 and 6, the
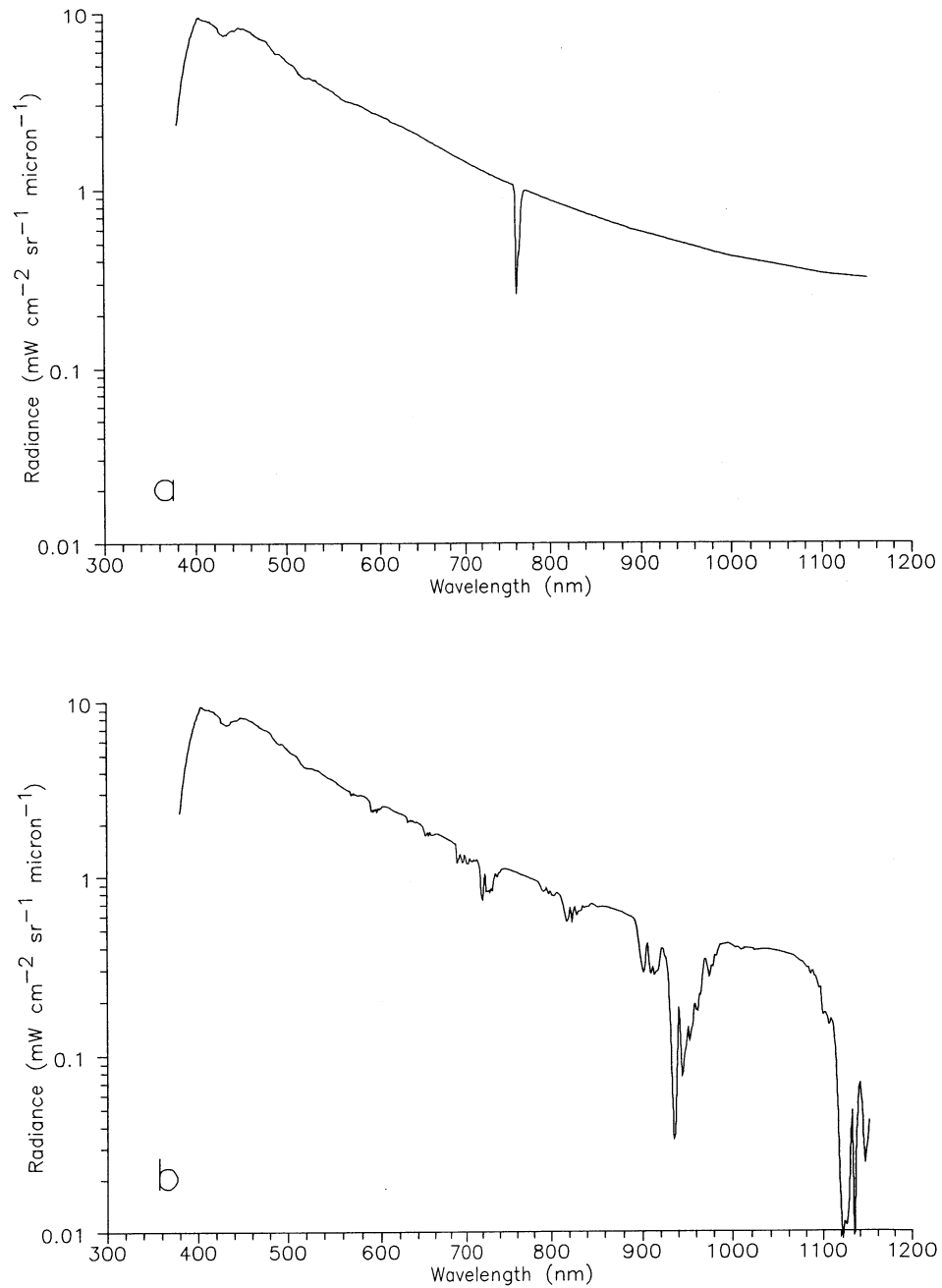
Fig. 7. This figure shows the nominal TOA spectra with atmospheric absorption features; **a)** with oxygen A-band absorption for an airmass of 3; and **b)** with water vapor absorption for a slant path column amount of $9.996\,\mathrm{g\,cm^{-2}}$.

Table 4. These are the total band (R_T) and in-band (R_{IB}) responses for SeaWiFS bands 1 and 2 for several slant path water vapor column amounts. The responses are the calculated currents from the band's photodiode for each column amount.

Slant Path Water	Band 1 (412 nm)			Band 2 (443 nm)		
Vapor Column	R_T	R_{IB}	Ratio	R_T	R_{IB}	Ratio
[g cm^{-2}]	[pA]	[pA]	(R_{IB}/R_T)	[pA]	[pA]	(R_{IB}/R_T)
0.000	2136.222	2125.825	0.99513	3452.778	3438.153	0.99576
1.666	2136.221	2125.825	0.99513	3452.777	3438.153	0.99576
3.332	2136.221	2125.825	0.99513	3452.777	3438.153	0.99576
4.998	2136.220	2125.825	0.99513	3452.777	3438.153	0.99576
6.664	2136.220	2125.825	0.99513	3452.777	3438.153	0.99576
8.330	2136.219	2125.825	0.99513	3452.777	3438.153	0.99576
9.996	2136.219	2125.825	0.99513	3452.777	3438.153	0.99576
11.662	2136.218	2125.825	0.99513	3452.776	3438.153	0.99576
13.328	2136.218	2125.825	0.99514	3452.776	3438.153	0.99576
14.994	2136.217	2125.825	0.99514	3452.776	3438.153	0.99576
16.660	2136.217	2125.825	0.99514	3452.776	3438.153	0.99576
18.326	2136.217	2125.825	0.99514	3452.776	3438.153	0.99577
19.992	2136.216	2125.825	0.99514	3452.776	3438.153	0.99577

Table 5. These are the total band (R_T) and in-band (R_{IB}) responses for SeaWiFS bands 3 and 4 for several slant path water vapor column amounts. The responses are the calculated currents from the band's photodiode for each column amount.

Slant Path Water	Band 3 (490 nm)			Band 4 (510 nm)		
Vapor Column	R_T	R_{IB}	Ratio	R_T	R_{IB}	Ratio
[g cm^{-2}]	[pA]	[pA]	(R_{IB}/R_T)	[pA]	[pA]	(R_{IB}/R_T)
0.000	4276.129	4250.652	0.99404	4540.688	4509.905	0.99322
1.666	4276.067	4250.652	0.99406	4540.666	4509.905	0.99323
3.332	4276.008	4250.652	0.99407	4540.647	4509.905	0.99323
4.998	4275.952	4250.652	0.99408	4540.629	4509.905	0.99323
6.664	4275.897	4250.652	0.99410	4540.612	4509.905	0.99324
8.330	4275.843	4250.652	0.99411	4540.596	4509.905	0.99324
9.996	4275.791	4250.652	0.99412	4540.582	4509.905	0.99324
11.662	4275.740	4250.652	0.99413	4540.567	4509.905	0.99325
13.328	4275.690	4250.652	0.99414	4540.554	4509.905	0.99325
14.994	4275.641	4250.652	0.99416	4540.540	4509.905	0.99325
16.660	4275.592	4250.652	0.99417	4540.528	4509.905	0.99326
18.326	4275.545	4250.652	0.99418	4540.515	4509.905	0.99326
19.992	4275.498	4250.652	0.99419	4540.503	4509.905	0.99326

Table 6. These are the total band (R_T) and in-band (R_{IB}) responses for SeaWiFS bands 5 and 6 for several slant path water vapor column amounts. The responses are the calculated currents from the band's photodiode for each column amount.

Slant Path Water Vapor Column [g cm^{-2}]	Band 5 (555 nm)			Band 6 (670 nm)		
	R_T [pA]	R_{IB} [pA]	Ratio (R_{IB}/R_T)	R_T [pA]	R_{IB} [pA]	Ratio (R_{IB}/R_T)
0.000	3904.549	3788.240	0.97021	2125.703	2087.479	0.98202
1.666	3903.711	3787.762	0.97030	2122.308	2084.286	0.98208
3.332	3902.891	3787.287	0.97038	2118.949	2081.122	0.98215
4.998	3902.087	3786.813	0.97046	2115.627	2077.989	0.98221
6.664	3901.297	3786.342	0.97053	2112.341	2074.885	0.98227
8.330	3900.519	3785.873	0.97061	2109.089	2071.810	0.98232
9.996	3899.753	3785.406	0.97068	2105.869	2068.760	0.98238
11.662	3898.998	3784.942	0.97075	2102.683	2065.739	0.98243
13.328	3898.254	3784.479	0.97081	2099.529	2062.745	0.98248
14.994	3897.519	3784.019	0.97088	2096.403	2059.776	0.98253
16.660	3896.794	3783.560	0.97094	2093.309	2056.833	0.98258
18.326	3896.078	3783.104	0.97100	2090.244	2053.915	0.98262
19.992	3895.371	3782.650	0.97106	2087.207	2051.021	0.98266

Table 7. These are the total band (R_T) and in-band (R_{IB}) responses for SeaWiFS bands 7 and 8 for several slant path water vapor column amounts. The responses are the calculated currents from the band's photodiode for each column amount.

| Slant Path Water Vapor Column [g cm^{-2}]	Band 7 (765 nm)			Band 8 (865 nm)		
	R_T [pA]	R_{IB} [pA]	Ratio (R_{IB}/R_T)	R_T [pA]	R_{IB} [pA]	Ratio (R_{IB}/R_T)
0.000	2863.650	2820.899	0.98507	2348.227	2190.749	0.93280
1.666	2857.073	2816.452	0.98578	2338.073	2182.628	0.93352
3.332	2850.941	2812.080	0.98637	2328.319	2174.941	0.93413
4.998	2845.161	2807.780	0.98686	2318.911	2167.408	0.93467
6.664	2839.664	2803.551	0.98728	2309.807	2160.020	0.93515
8.330	2834.402	2799.390	0.98765	2300.973	2152.769	0.93559
9.996	2829.337	2795.296	0.98797	2292.382	2145.644	0.93599
11.662	2824.444	2791.257	0.98825	2284.012	2138.641	0.93635
13.328	2819.700	2787.299	0.98851	2275.843	2131.751	0.93669
14.994	2815.089	2783.393	0.98874	2267.860	2124.968	0.93699
16.660	2810.599	2779.549	0.98895	2260.050	2118.288	0.93727
18.326	2806.218	2775.757	0.98915	2252.399	2111.704	0.93754
19.992	2801.939	2772.024	0.98932	2244.897	2105.211	0.93778
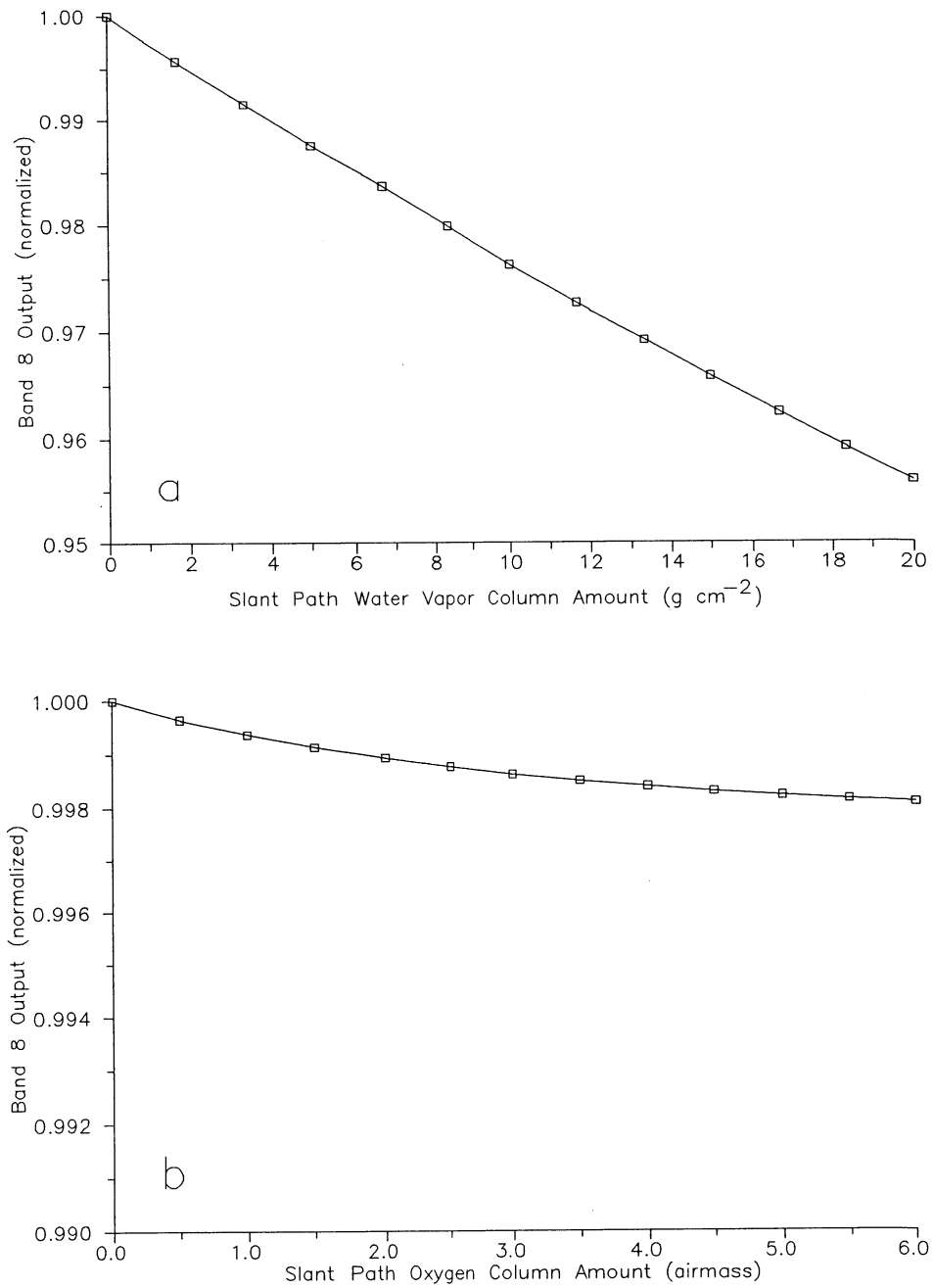
Fig. 8. Relative changes in band 8 (865 nm) total band output (R_T) versus water vapor and oxygen slant path column amount are shown here. The response of the band has been normalized to unity at slant path amounts of zero; **a)** changes with water vapor; and **b)** changes with oxygen.

Table 8. These are the total band (R_T) and in-band (R_{IB}) responses for SeaWiFS bands 1–6 versus slant path oxygen column amounts. There is essentially no effect on these bands for air masses of 6 or more. The responses are the calculated currents from the band's photodiode for each column amount.

Slant Path Oxygen Column [airmass]	R_T [pA]	R_{IB} [pA]	Ratio (R_{IB}/R_T)	R_T [pA]	R_{IB} [pA]	Ratio (R_{IB}/R_T)
	Band 1 (412 nm)			Band 2 (443 nm)		
0.0	2136.222	2125.825	0.99513	3452.778	3438.153	0.99576
6.0	2136.222	2125.825	0.99513	3452.778	3438.153	0.99576
	Band 3 (490 nm)			Band 4 (510 nm)		
0.0	4276.129	4250.652	0.99404	4540.688	4509.905	0.99322
6.0	4276.128	4250.652	0.99404	4540.687	4509.905	0.99322
	Band 5 (555 nm)			Band 6 (670 nm)		
0.0	3904.549	3788.240	0.97021	2125.703	2087.479	0.98202
6.0	3904.548	3788.240	0.97021	2125.693	2087.479	0.98202

Table 9. These are the total band (R_T) and in-band (R_{IB}) responses for SeaWiFS bands 7 and 8 for several slant path oxygen column amounts. The responses are the calculated currents from the band's photodiode for each column amount. The responses for band 7, however, require the use of data with higher spectral resolution than those used here. Those responses, therefore, are shown in their entirety in Table 16 of Barnes (1997b).

Slant Path Oxygen Column [airmass]	Band 7 (765 nm)			Band 8 (865 nm)		
	R_T [pA]	R_{IB} [pA]	Ratio (R_{IB}/R_T)	R_T [pA]	R_{IB} [pA]	Ratio (R_{IB}/R_T)
0.0	2863.650	2820.899	0.98507	2348.277	2190.479	0.93280
0.5				2347.448	2190.479	0.93313
1.0				2346.794	2190.479	0.93339
1.5				2346.243	2190.479	0.93361
2.0				2345.777	2190.479	0.93380
2.5				2345.381	2190.479	0.93395
3.0	*See Table 16 of Barnes (1997b)*			2345.044	2190.479	0.93409
3.5	*for the responses of band 7*			2344.756	2190.479	0.93420
4.0				2344.509	2190.479	0.93430
4.5				2344.296	2190.479	0.93439
5.0				2344.111	2190.479	0.93446
5.5				2343.950	2190.479	0.93452
6.0				2343.810	2190.479	0.93458

Table 10. These are the out-of-band correction factors for the 12,000 K Planck function and the nominal TOA spectrum. The correction factor, k_b, in Barnes and Yeh (1996) is the ratio R_{IB}/R_T. The correction factor, $k_{b'}$, is a replacement value based on the nominal TOA spectrum.

Band Number	Nominal Center Wavelength [nm]	k_b for 12,000 K Planck Function	$k_{b'}$ for Nominal TOA Spectrum
1	412	0.9943	0.9951
2	443	0.9949	0.9958
3	490	0.9930	0.9940
4	510	0.9934	0.9932
5	555	0.9734	0.9702
6	670	0.9856	0.9820
7	765	0.9862	0.9851
8	865	0.9417	0.9328

differences are 0.33% and 0.37%. It is estimated that the correction scheme of Barnes and Yeh (1996), using a set of on-orbit measurements from three SeaWiFS bands, will remove at least half of any residual difference, giving an uncertainty of 0.3% in the final out-of-band correction factor for these bands. For band 8, the differences between the two correction factors is 0.9%; however, the correction factor in Table 10 is the starting point for an on-orbit calculation that uses values from six SeaWiFS bands. It is estimated that this computation will remove 75% or more of the uncertainty in the initial value, giving a residual uncertainty of 0.3% in the final out-of-band correction factor for band 8.

Table 11. These are the out-of-band correction factors for a 2,850 K Planck function curve. This is the correction factor for the measurements in the laboratory. The correction factor is the ratio R_{IB}/R_T.

Band Number	Nominal Center Wavelength [nm]	Correction for 2,850 K Planck Function
1	412	0.9963
2	443	0.9948
3	490	0.9850
4	510	0.9936
5	555	0.9685
6	670	0.9924
7	765	0.9816
8	865	0.9775

The out-of-band correction is, itself, a two step process. The removal of the out-of-band response in the on-orbit measurements must be accompanied by a similar removal of the out-of-band response in the laboratory data. First, this process transforms the conversion of the total band response from the laboratory value to the value on orbit

Second, is the conversion of the in-band response from the laboratory response to the response on orbit. For the laboratory measurements, the source spectral shape is fixed, as is the out-of-band factor for each SeaWiFS band. These correction factors (for a 12,000 K Planck function) were calculated by Barnes and Yeh (1996); the correction factors are also listed in Table 10. The uncertainties in the correction factors in Table 10 are estimated to be 0.1% for all eight SeaWiFS bands. The laboratory correction factors, i.e., those for a 2,850 K blackbody, are listed in Table 11.

2.5 CONCLUDING REMARKS

The conversion process described here for each SeaWiFS band is performed in three steps. First, the total band response is converted from that for a 2,850 K Planck function (the spectral shape of the Santa Barbara Remote Sensing [SBRS] laboratory SIS) to that for the nominal TOA spectrum. Second, the effects of atmospheric absorption by water vapor and oxygen are removed. Finally, the out-of-band response is removed. For five of the SeaWiFS bands, the out-of-band response is a constant fraction of the total band response. For the other bands (bands 5, 6, and 8), the out-of-band response varies with the source spectral shape on-orbit (Barnes and Yeh 1996).

Step one in the conversion process, however, assumes the nominal TOA spectrum of Barnes and Esaias (1997). The out-of-band response of these bands to the nominal TOA spectrum is part of that conversion step. For bands 5, 6, and 8, that out-of-band value is the starting point for a recalculated out-of-band response. For these bands, the new out-of-band value should be used in a second iteration to revise the correction factor in step one. The effect of this iteration on the results from bands 5, 6, and 8 is assumed to be on the order of 1% or less of the total band response.

R.A. Barnes, R.E. Eplee, Jr., E-n. Yeh, and W.E. Esaias

Chapter 3

The Effect of Atmospheric Absorption
on the Output of SeaWiFS Band 7

ROBERT A. BARNES

General Sciences Corporation
Laurel, Maryland

ABSTRACT

Oxygen A-band absorption in SeaWiFS band 7 (765 nm) has been investigated twice previously. Fraser (1995) calculated the ozone equivalent bandwidth for two pathlengths through the atmosphere, and Ding and Gordon (1995) provided an analysis in which ozone absorption was imbedded in their radiative transfer model. Here, ozone absorption is presented using the relative spectral responses from Barnes (1994), the nominal TOA spectrum from Barnes and Esaias (1997), and the ozone absorption spectrum from `MODTRAN7`. The study presented here is compared with the previous studies. The `MODTRAN7` spectrum has much higher wavelength resolution than the `LOWTRAN` spectrum used by Barnes et al. (1997), and Table 16 in this paper completes Table 9 in Barnes et al. (1997). The uncertainty in the correction for oxygen absorption in SeaWiFS band 7 is estimated to be 0.8%.

3.1 INTRODUCTION

SeaWiFS was designed with near-infrared bands at 765 and 865 nm. These bands will provide the basis for the atmospheric correction algorithm used in the procedure to deduce water-leaving radiances from the SeaWiFS data (Gordon and Wang 1994). The band edges for the two bands, that is, the half-maximum response points, are located at 744.7 and 785.0 nm for the nominal 765 nm band, and at 845.7 and 887.0 nm for the nominal 865 nm band (Barnes et al. 1994a). The bandwidths, or the wavelength intervals between the half-maximum response points, for these bands were specified to be 40 nm to allow measurements from the instrument with sufficiently large signal-to-noise ratios. In addition, the two bands have been placed in spectral regions that are relatively free of atmospheric water vapor absorption; however, the 765 nm band encompasses a region of atmospheric oxygen absorption, the oxygen A-band, that extends from approximately 758–771 nm.

Atmospheric oxygen A-band absorption was a consideration in the design of SeaWiFS. The original specification for the 765 nm band included a notch in the spectral response for the band. The design specification called for a bimodal response from the interference filter, with near zero transmission in the wavelength region for the oxygen absorption. Studies by the instrument manufacturer showed that such a feature would make the filter nearly impossible to fabricate, because of the narrowness of the notch and the sharp changes in transmission on either side.

In addition, any filter that could be made would have low overall transmission, creating a major reduction in the optical throughput for the band. The reduction in radiance at the detectors for band 7 would have required a greatly increased electronic gain for the band, reducing the band's signal-to-noise ratio and compromising other design specifications. As a result, the SeaWiFS Project decided that SeaWiFS band 7 would have a *standard shaped* spectral response and that the effects of the oxygen A-band would be included in the processing of the on-orbit data.

3.2 OZONE BANDWIDTH

Fraser (1995) used the concept of ozone equivalent bandwidth to calculate the effects of oxygen A-band absorption on SeaWiFS band 7. In that analysis, the relative spectral response for the band, $R(\lambda)$, normalized to unity, is integrated to give the bandwidth

$$B = \int_{\lambda_1}^{\lambda_2} R(\lambda)d\lambda, \tag{3}$$

where B is the bandwidth (in nanometers), λ_1 is 380 nm, and λ_2 is 1,150 nm. These integration limits encompass the wavelength region over which the SeaWiFS photodiodes have a significant quantum efficiency. Using the relative spectral response values from Barnes (1994), the bandwidth for SeaWiFS band 7 is 40.99 nm. This bandwidth corresponds to that for the total band response (R_T), described in Barnes et al. (1997), where changes to R_T for

Table 12. These are the bandwidths for the SeaWiFS bands. The bandwidths are calculated in three ways. The first is the integral of the relative spectral response over the wavelength region for which the detector has a significant quantum efficiency, that is, from 380–1,150 nm. For this calculation, the RSR is normalized to unity at its maximum value. In the second method, the RSR is integrated over its in-band response region with this region defined as that for a spectrally flat source in Table 13 of Barnes et al. (1994b). The third is the calculation of the FWHM, also taken from Table 13 of Barnes et al. (1994b).

Band Number	Nominal Center Wavelength [nm]	Bandwidth $\int R(\lambda)d\lambda$ 380–1,150 [nm]	Bandwidth $\int R(\lambda)d\lambda$ In-Band [nm]	Bandwidth FWHM [nm]
1	412	19.7	19.6	20.2
2	443	19.3	19.2	19.6
3	490	21.3	21.2	20.6
4	510	23.0	22.8	22.4
5	555	19.1	18.6	18.3
6	670	20.7	20.5	19.9
7	765	41.0	40.3	40.3
8	865	42.2	41.0	41.3

various amounts of atmospheric water vapor and oxygen were calculated.

It is also possible to calculate the bandwidth for the in-band response region. This is the wavelength range where the relative spectral response is 1% or more of the maximum response. For SeaWiFS band 7 (and for a spectrally flat source) the in-band wavelength region lies between 728–815 nm. Using these values for integration limits, the bandwidth calculated using (3) is 40.31 nm. The bandwidth used in Fraser (1995) is 40.5 nm. To maintain consistency with the analysis of Barnes et al. (1997), a bandwidth of 40.99 nm is used here.

The bandwidths for the eight SeaWiFS bands are listed in Table 12. The bandwidths in this table are calculated in three ways. The first calculation is the solution to the integral in (3) with integration limits of 380 and 1,150 nm. The second is the solution to (3) using the 1% response wavelengths (extended band edges) from Table 13 of Barnes et al. (1994b) as the limits of integration. The extended band edges in this calculation are those for a spectrally flat source. The third is the calculation of the FWHM, also given in Table 13 of Barnes et al. (1994b). The choice of the most appropriate bandwidth depends on the need of the user.

The ozone equivalent bandwidth is calculated from the ozone absorption coefficient and the airmass

$$W = \int_{\lambda_1}^{\lambda_2} \left[1 - e^{-\alpha(\lambda)\mu} \right] d\lambda, \qquad (4)$$

where W is the ozone equivalent bandwidth (in nanometers), $\alpha(\lambda)$ is the ozone absorption coefficient per unit airmass at wavelength λ, and μ is the airmass. The lower and upper limits for the integration are 758 and 771 nm, covering the wavelengths over which oxygen A-band absorption occurs. The value, $e^{-\alpha(\lambda)\mu}$, in the integrand is the fractional transmittance through an atmosphere of airmass μ

at wavelength λ for an absorbance of $\alpha(\lambda)$. The entire integrand, $1 - e^{-\alpha(\lambda)\mu}$, is the absorption at wavelength λ. When integrated, (4) gives the total oxygen A-band absorption for an airmass of μ. Since the integrand in (4) is dimensionless, the solved integral has units of nanometers, and the solution is called the ozone equivalent bandwidth. This analysis can be applied because all of the ozone absorption is in-band, that is, because B overlaps W.

Using (3) and (4), it is possible to define the fractional absorption (W/B) and the fractional transmittance $(1 - B/W)$ for the band. Fractional transmittance is the product used by Barnes et al. (1997) to correct for the effects of atmospheric absorption on the SeaWiFS bands. Figure 8 of Barnes et al. (1997) shows plots of fractional transmittance for SeaWiFS band 8 for atmospheric water vapor and atmospheric oxygen.

The techniques of Fraser (1995) and Barnes et al. (1997) lead to nearly identical results; however, the technique of Fraser (1995) has no provision for the spectral shape of the source. In addition, the absorption spectrum used by Fraser (1995) differs from the MODTRAN7 absorption spectrum used by Barnes and Esaias (1997) and tabulated in Barnes (1997a).

The ozone absorption data used in Fraser (1995) are no longer available, but a plot of those data are shown in Fig. 9a, which is a copy of Fig. 9 in Fraser (1995). Figure 9a gives the atmospheric absorption for an airmass of 2. Using the units of (4), the ordinate of Fig. 9a has the units $\alpha(\lambda) \times 2$.

Figure 9b is a transcription of Fig. 9a. The data from Fig. 9a were taken manually at 0.2 nm intervals. Figures 9a and 9b are presented with the same dimensions so that the fidelity of the transcription can be evaluated by eye. For use in the analysis below, the data points in Fig. 9b were interpolated to give values at 0.1 nm intervals, and the absorptions were divided by 2 to give absorbances for an airmass of unity.
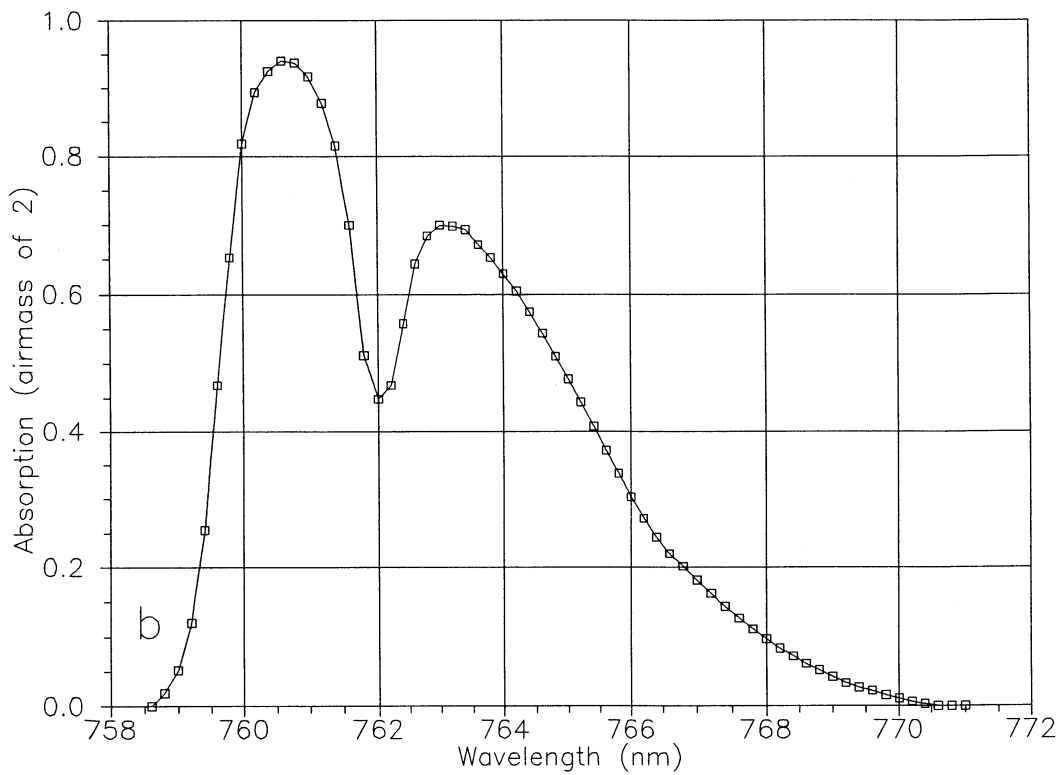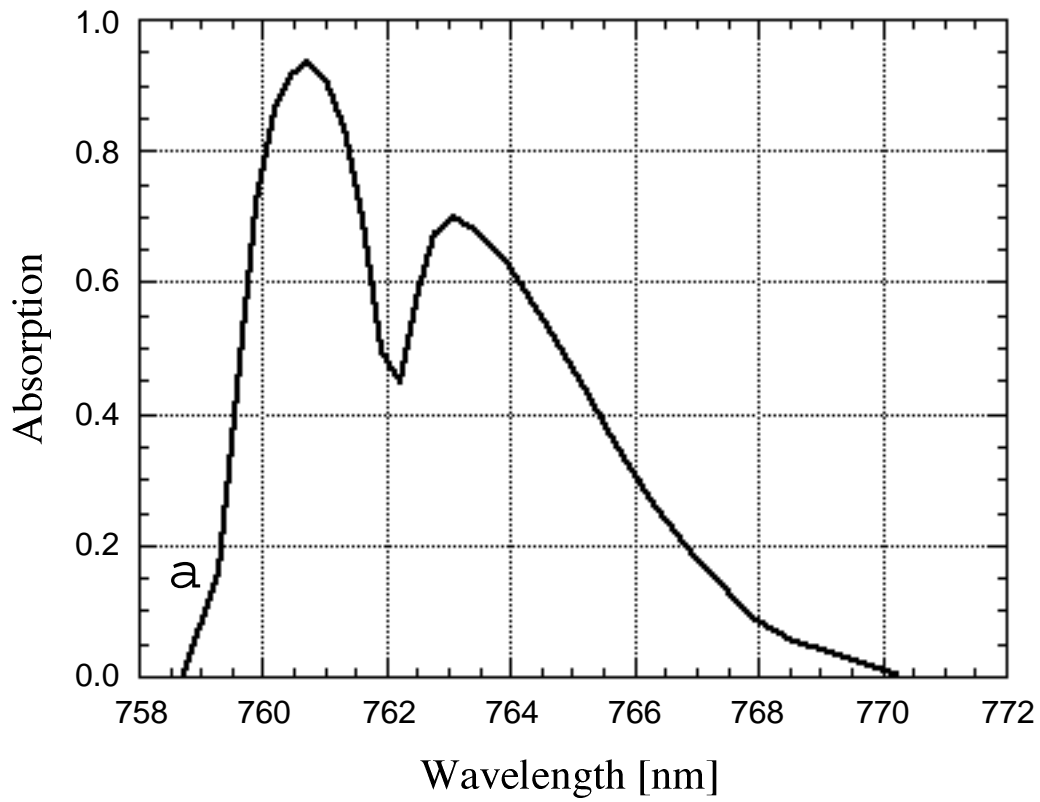
Fig. 9. This figure has two versions of the oxygen absorption spectrum from Fraser (1995). **a)** This is the plot as shown in Fraser (1995). **b)** This is a transcription, by hand, of the plot in **a)** at 2 nm intervals. It is the basis for the Fraser (1995) absorption values used in this study.

This transcription created an absorbance data set that can be compared directly with the MODTRAN7 data tabulated in Barnes (1997a). A comparison of these absorbance data is given in Fig. 10. For the MODTRAN7 data, there is substantially more absorbance in the peak at 761 nm; however, there is more absorbance in the wing of the Fraser spectrum from 763–770 nm.

The effect of the large absorbance centered at 761 nm in MODTRAN7 occurs at airmasses up to about unity. At this airmass, the transmittance at 761 nm is close to zero. For increasing pathlengths through the atmosphere, the transmittance at 761 nm changes little—it is just slightly closer to zero. This effect is called self-absorption. For airmasses greater than unity, the calculated transmission using the MODTRAN7 absorbance spectrum is greater than the transmission using the Fraser absorbance spectrum. This can be seen in Fig. 11, which shows the transmittance, $e^{-\alpha(\lambda)\mu}$, for the two absorbance spectra at an airmass of 6. A large airmass was chosen to give a better visual presentation of this effect.

Table 13 lists the ozone equivalent bandwidths, fractional absorptions, and fractional transmittances for SeaWiFS band 7 using the Fraser absorbance spectrum and airmasses from 0–6 in 0.2 airmass increments. The typical viewing geometries for SeaWiFS will have airmasses that range from around 2 to around 5. The nonlinearity in the calculated bandwidths and transmittances versus airmass is due to self-absorption. Table 14 lists the same values as Table 13, except that the MODTRAN7 oxygen absorption spectrum is used.

The fractional transmittances, values of $1 - W/B$, from the MODTRAN7 and Fraser absorption data are shown in Fig. 12a. The differences versus airmass of the Fraser-based fractional transmittances from those of MODTRAN7 are shown in Fig. 12b. The data for Fig. 12 are listed in Table 15. At an airmass of 2, the fractional transmittance from the Fraser-based calculations is 0.003 (0.3%) less than that for the MODTRAN7-based calculations. At an airmass of 3, the difference is 0.006 (0.6%). As discussed below, this 0.6% difference is a principal component in the estimated uncertainty for the oxygen A-band correction for SeaWiFS band 7.

The calculations in this section are given to show the differences in transmittance that derive from the MODTRAN7 and Fraser oxygen absorption spectra. The calculations to produce results for SeaWiFS data reduction, that is, to produce a replacement for the incomplete Table 9 of Barnes et al. (1997), are presented in Sect. 3.3.

3.3 INTEGRATED RESPONSES

Barnes et al. (1997), calculated the SeaWiFS band responses using knowledge of the relative spectral response of the bands plus the spectral shape of the radiance that SeaWiFS views. The spectral radiance and spectral response at each wavelength are integrated to give

$$R = \int_{\lambda_1}^{\lambda_2} L_e(\lambda) R(\lambda) d\lambda, \qquad (5)$$

where R is the response of the band (in picoamperes), $L_e(\lambda)$ is the spectral radiance from the source at wavelength λ (in mW cm$^{-2}\mu$m^{-1} sr$^{-1)}$), and $R(\lambda)$ is the response of the SeaWiFS band at wavelength λ (in picoamperes mW^{-1} cm$^2\mu$m^1 sr^1). The lower and upper limits for the integration are λ_1 and λ_2, respectively. If the integration covers the range over which the band's detector has a significant quantum efficiency (380–1,150 nm), then the integration yields the total band response, R_T. If the integration limits cover the range where the relative spectral response is equal to or greater than 1% of the maximum response, then the result is called the in-band response, R_{IB}.

In (5), the relative spectral response, $R(\lambda)$, has units of picoamperes per unit spectral radiance. It is not normalized to unity as in (3). The data for the RSRs used here come from the file SPECTRA4 in Barnes (1997a). These data are listed at 0.1 nm intervals from 720–820 nm. For the calculations here, the lower and upper integration limits are 728.0 and 814.5 nm. These are the extended band edges (or 1% response points) for band 7 (see Table 13 of Barnes et al. 1994b). The spectral radiances, $L_e(\lambda)$, also come from SPECTRA4, which gives the nominal Earth-exiting radiance spectrum of Barnes and Esaias (1997); hence, the designation $L_e(\lambda)$. The values of $L_e(\lambda)$ have been normalized to 3.0 mW cm$^{-2}\mu$m^{-1} sr^{-1} at 765 nm to give conformity with the calculations of Barnes et al. (1997).

The effects of oxygen A-band absorption are calculated using the absorbance table in SPECTRA4 and the airmass. The A-band absorbances in SPECTRA4, $\alpha(\lambda)$, are per unit airmass. The absorbance is combined with the airmass to calculate the transmittance, $e^{-\alpha(\lambda)\mu}$, and this term is combined with the calculation in (5). In the actual calculation, the integral is modified to a summation with an interval, $\Delta\lambda$, of 0.1 nm.

$$R_{IB} = \sum_{\lambda=728.0}^{\lambda=814.5} L_e(\lambda) \left[e^{-\alpha(\lambda)\mu} \right] R(\lambda) \Delta\lambda, \qquad (6)$$

The components of (6) are shown in Fig. 13. Figure 13a shows the oxygen A-band transmission spectrum using the Fraser (1995) absorbance and an airmass of 2. Figure 13b shows the nominal TOA spectrum, and Fig. 13c shows the relative spectral response for SeaWiFS band 7.

The calculated values of R_{IB} from (6) for airmasses from zero to 6 are listed in Table 16. Since there is no oxygen A-band absorption outside the 1% response points for band 7, there is no effect on the out-of-band response; thus, the difference between the in-band and total band responses must be a constant. That constant is given in Table 9 of Barnes et al. (1997) as 2863.650 pA$-$2820.899 pA.
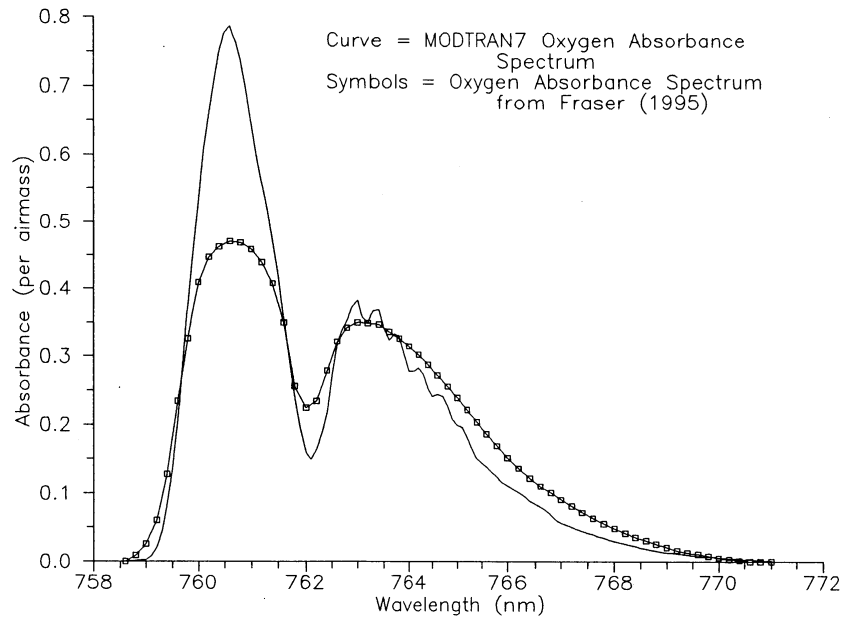
Fig. 10. This is a comparison of the absorbance spectra from `MODTRAN7` and from Fraser (1995).
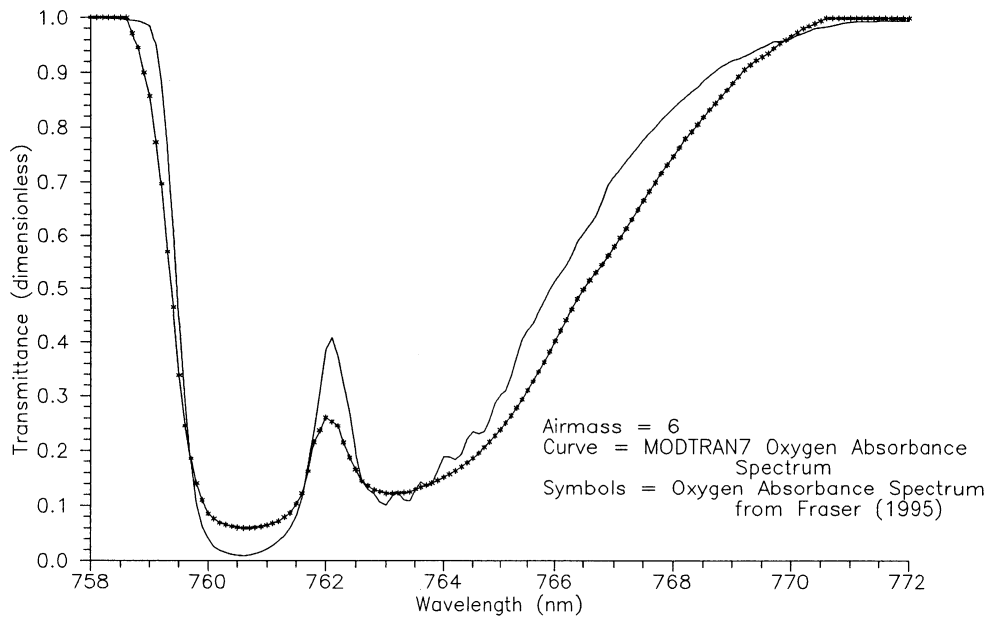
Fig. 11. Here is a comparison of the transmittance spectra at an airmass of 6 using the absorbances from `MODTRAN7` and from Fraser (1995). At this airmass, the total transmittance using the Fraser absorption is less than that using `MODTRAN7`.
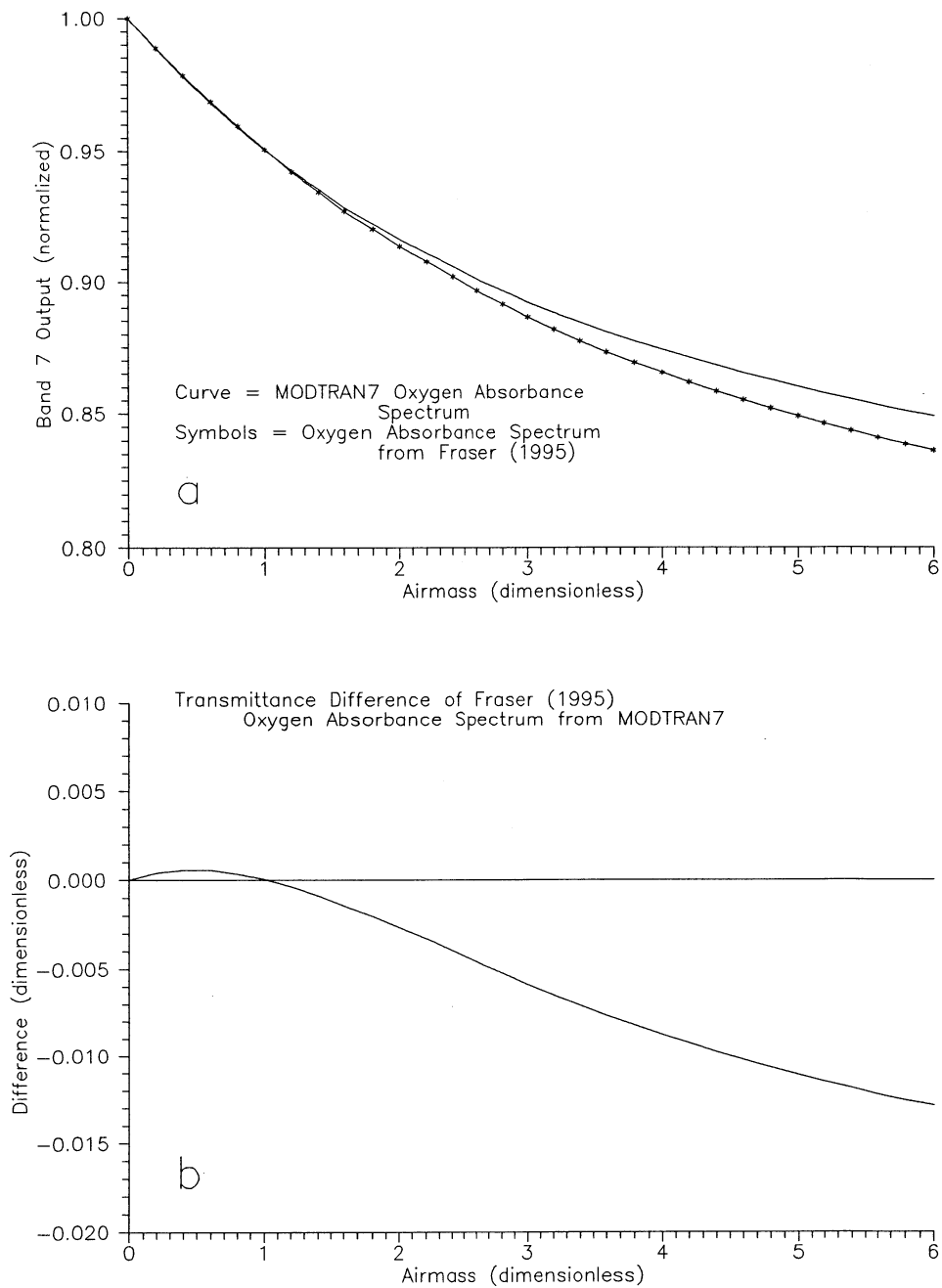
Fig. 12. This is a comparison of the relative output of SeaWiFS band 7 versus airmass for the `MODTRAN7` and Fraser oxygen absorbances. **a)** These are the system level transmittances for the two absorbances from Table 18. **b)** This is the difference of the Fraser-based transmittances from the `MODTRAN7` ones. At an airmass of 6, the Fraser based transmittances are smaller by about 1.5%.

Table 13. These are the ozone equivalent bandwidths using the absorbance spectrum of Fraser. The ozone equivalent bandwidth, W, is calculated using (4). The fractional absorption is calculated using a bandwidth, B, of 40.99 nm. The fractional transmittance is calculated as the difference between unity and the fractional absorption.

Airmass	Ozone Equivalent Bandwidth [nm]	Fractional Absorption	Fractional Transmittance
0.0	0.00000	0.00000	1.00000
0.2	0.45571	0.01112	0.98888
0.4	0.88402	0.02157	0.97843
0.6	1.28681	0.03139	0.96861
0.8	1.66581	0.04064	0.95936
1.0	2.02264	0.04934	0.95066
1.2	2.35877	0.05755	0.94245
1.4	2.67560	0.06527	0.93473
1.6	2.97442	0.07256	0.92744
1.8	3.25640	0.07944	0.92056
2.0	3.52267	0.08594	0.91406
2.2	3.77424	0.09208	0.90792
2.4	4.01209	0.09788	0.90212
2.6	4.23708	0.10337	0.89663
2.8	4.45006	0.10856	0.89144
3.0	4.65179	0.11349	0.88651
3.2	4.84298	0.11815	0.88185
3.4	5.02430	0.12257	0.87743
3.6	5.19636	0.12677	0.87323
3.8	5.35976	0.13076	0.86924
4.0	5.51501	0.13455	0.86545
4.2	5.66263	0.13815	0.86185
4.4	5.80308	0.14157	0.85843
4.6	5.93679	0.14484	0.85516
4.8	6.06417	0.14794	0.85206
5.0	6.18560	0.15091	0.84909
5.2	6.30144	0.15373	0.84627
5.4	6.41201	0.15643	0.84357
5.6	6.51762	0.15901	0.84099
5.8	6.61856	0.16147	0.83853
6.0	6.71510	0.16382	0.83618

Table 14. These are the ozone equivalent bandwidths using the absorbance spectrum from `MODTRAN7`. The ozone equivalent bandwidth, W, is calculated using (4). The fractional absorption is calculated using a bandwidth, B, of 40.99 nm. The fractional transmittance is calculated as the difference between unity and the fractional absorption.

Airmass	Ozone Equivalent Bandwidth [nm]	Fractional Absorption	Fractional Transmittance
0.0	0.00000	0.00000	1.00000
0.2	0.47283	0.01154	0.98846
0.4	0.90812	0.02215	0.97785
0.6	1.30965	0.03195	0.96805
0.8	1.68077	0.04100	0.95900
1.0	2.02444	0.04939	0.95061
1.2	2.34330	0.05717	0.94283
1.4	2.63969	0.06440	0.93560
1.6	2.91571	0.07113	0.92887
1.8	3.17322	0.07741	0.92259
2.0	3.41387	0.08329	0.91671
2.2	3.63915	0.08878	0.91122
2.4	3.85040	0.09394	0.90606
2.6	4.04881	0.09878	0.90122
2.8	4.23545	0.10333	0.89667
3.0	4.41128	0.10762	0.89238
3.2	4.57718	0.11167	0.88833
3.4	4.73393	0.11549	0.88451
3.6	4.88224	0.11911	0.88089
3.8	5.02275	0.12254	0.87746
4.0	5.15605	0.12579	0.87421
4.2	5.28266	0.12888	0.87112
4.4	5.40306	0.13181	0.86819
4.6	5.51769	0.13461	0.86539
4.8	5.62695	0.13728	0.86272
5.0	5.73120	0.13982	0.86018
5.2	5.83078	0.14225	0.85775
5.4	5.92600	0.14457	0.85543
5.6	6.01714	0.14680	0.85320
5.8	6.10444	0.14893	0.85107
6.0	6.18816	0.15097	0.84903

Table 15. This is a comparison of fractional transmittances using the absorbance spectra from `MODTRAN7` and Fraser (1995). The `MODTRAN7`-based fractional transmittances come from Table 14. The Fraser-based values come from Table 13. The difference at an airmass of 3 (0.587%) gives an estimate of a portion of the uncertainty for the oxygen A-band correction.

Airmass	$1 - W/B$ (MODTRAN)	$1 - W/B$ (Fraser)	Difference
0.0	1.00000	1.00000	0.00000
0.2	0.98846	0.98888	0.00042
0.4	0.97785	0.97843	0.00058
0.6	0.96805	0.96861	0.00056
0.8	0.95900	0.95936	0.00036
1.0	0.95061	0.95066	0.00005
1.2	0.94283	0.94245	−0.00038
1.4	0.93560	0.93473	−0.00087
1.6	0.92887	0.92744	−0.00143
1.8	0.92259	0.92056	−0.00203
2.0	0.91671	0.91406	−0.00265
2.2	0.91122	0.90792	−0.00330
2.4	0.90606	0.90212	−0.00394
2.6	0.90122	0.89663	−0.00459
2.8	0.89667	0.89144	−0.00523
3.0	0.89238	0.88651	−0.00587
3.2	0.88833	0.88185	−0.00648
3.4	0.88451	0.87743	−0.00708
3.6	0.88089	0.87323	−0.00766
3.8	0.87746	0.86924	−0.00822
4.0	0.87421	0.86545	−0.00876
4.2	0.87112	0.86185	−0.00927
4.4	0.86819	0.85843	−0.00976
4.6	0.86539	0.85516	−0.01023
4.8	0.86272	0.85206	−0.01066
5.0	0.86018	0.84909	−0.01109
5.2	0.85775	0.84627	−0.01148
5.4	0.85543	0.84357	−0.01186
5.6	0.85320	0.84099	−0.01221
5.8	0.85107	0.83853	−0.01254
6.0	0.84903	0.83618	−0.01285
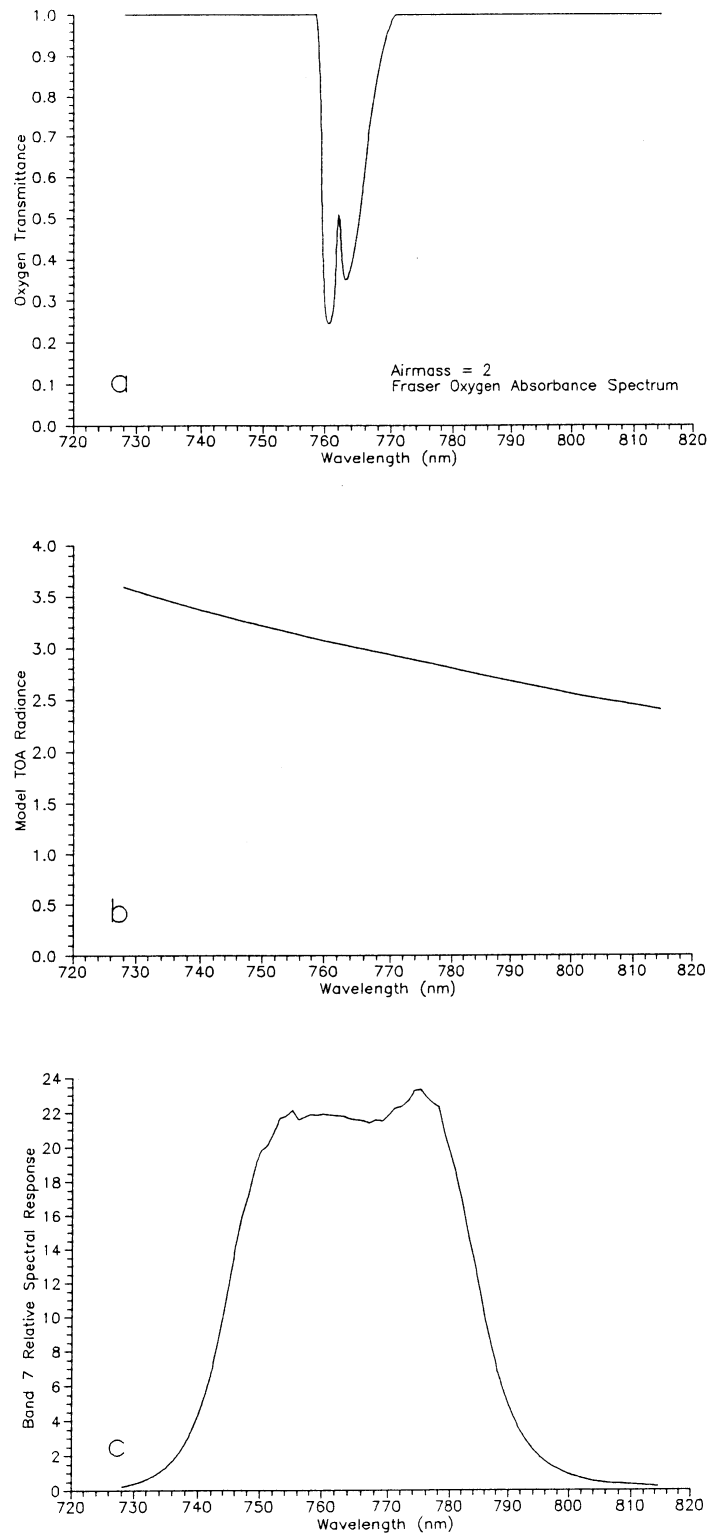
Fig. 13. These are the components for the response of SeaWiFS band 7 in (6), in this case for the Fraser (1995) absorbance and an airmass of 2. **a)** This is the atmospheric transmission spectrum for these conditions; the transmittance is dimensionless. **b)** This is the baseline TOA spectrum from Barnes and Esaias (1997); at each wavelength the spectral radiance has units of $mW\,cm^{-2}\,\mu m^{-1}\,sr^{-1}$. **c)** This is the RSR for SeaWiFS band 7 from Barnes (1994); it is the response of the band to a radiance source with a spectrally constant value of unity. At each wavelength the RSR has units of $pA\,mW^{-1}\,cm^2\,\mu m\,sr$.

Table 16. These are total band (R_T) and in-band (R_{IB}) responses for SeaWiFS band 7 (765 nm) for several slant path oxygen column amounts. The responses are the calculated currents from the band's photodiodes for each column amount. The calculations are based on the `MODTRAN7` absorption spectrum tabulated in Barnes (1997a). This table completes Table 9 in Barnes et al. (1997).

Slant Path Oxygen Column [airmass]	R_T [pA]	R_{IB} [pA]	Ratio R_{IB}/R_T
0.0	2863.650	2820.899	0.98507
0.2	2832.359	2789.608	0.98491
0.4	2803.568	2760.817	0.98475
0.6	2777.025	2734.274	0.98461
0.8	2752.504	2709.753	0.98447
1.0	2729.810	2687.059	0.98434
1.2	2708.764	2666.013	0.98422
1.4	2689.212	2646.461	0.98410
1.6	2671.014	2628.263	0.98399
1.8	2654.045	2611.294	0.98389
2.0	2638.195	2595.444	0.98380
2.2	2623.365	2580.614	0.98370
2.4	2609.465	2566.714	0.98362
2.6	2596.417	2553.666	0.98353
2.8	2584.149	2541.398	0.98346
3.0	2572.597	2529.846	0.98338
3.2	2561.702	2518.951	0.98331
3.4	2551.413	2508.662	0.98324
3.6	2541.682	2498.931	0.98318
3.8	2532.468	2489.717	0.98312
4.0	2523.730	2480.979	0.98306
4.2	2515.434	2472.683	0.98300
4.4	2507.549	2464.798	0.98295
4.6	2500.044	2457.293	0.98290
4.8	2492.894	2450.143	0.98285
5.0	2486.074	2443.323	0.98280
5.2	2479.562	2436.811	0.98276
5.4	2473.338	2430.587	0.98272
5.6	2467.383	2424.632	0.98267
5.8	2461.681	2418.930	0.98263
6.0	2456.214	2413.463	0.98259

This constant is added to each R_{IB} value in Table 16 to give the total band response, R_T. From these data, the ratio R_{IB}/R_T is calculated for each airmass.

Barnes et al. (1997) used `LOWTRAN` absorption spectra to calculate the effects of atmospheric water vapor and oxygen on the on-orbit responses of the SeaWiFS bands. Table 9 of Barnes et al. (1997) was left incomplete, since `LOWTRAN` is inadequate to calculate the effect of oxygen A-band absorption on SeaWiFS band 7. Table 16 completes Table 9 in Barnes et al. (1997) and has been given the same format.

It is possible to create a table similar to Table 16 based on results calculated using the absorbances from Fraser (1995) in place of those from `MODTRAN7`. Table 17 shows the Fraser-based results. Table 18 takes the total band responses from Tables 16 and 17 and converts them into fractional transmittances. They are the system responses at airmass, μ, divided by the response at zero airmass. These fractional transmittances are equivalent to the $1 - W/B$ values in Table 15. In Table 15 for an airmass of 3, the Fraser-based fractional transmittance is 0.0059 (0.6%) lower than that for the `MODTRAN7`-based calculation. In Table 18 for an airmass of 3, the difference is 0.0053 (0.5%). If SeaWiFS measurements are made at nominal airmasses between 3 and 3.5, then the difference in the calculated fractional transmittance using the Fraser and `MODTRAN7` absorption spectra is about 0.6%. As discussed below, this 0.6% difference, which derives from the differences in the $\alpha(\lambda)$ values of Fraser (1995) and `MODTRAN7`, is a principal component in the estimated uncertainty for the oxygen A-band correction for SeaWiFS band 7.

3.4 SURFACE PRESSURE

An airmass of unity assumes a surface pressure of 1013.25 mb (760 torr, or 1 atm). For SeaWiFS measurements, the surface pressure of an ocean scene is provided by ancillary measurements from other satellite instruments. When the solar zenith angle and the viewing angle of the instrument are included and a plane-parallel atmosphere is assumed, the airmass can be calculated as

$$\mu = \frac{P_s}{1013.25}\left(\frac{1}{\cos(\theta_0)} + \frac{1}{\cos(\theta_v)}\right), \qquad (7)$$

where P_s is the surface pressure (in millibars), θ_0 is the solar zenith angle, and θ_v is the viewing angle of the instrument.

For large angles from vertical, the airmass can be determined using the Chapman function (Chapman 1931 and Swider and Gardner 1967), which accounts for the curvature of the Earth. The Chapman function is applied to atmosphere constituents that have concentrations which decrease exponentially with altitude at a known rate. The function is ideal for calculating the airmass of the atmosphere and of well mixed constituents, such as oxygen, at

large angles from the vertical. A discussion of airmass corrections for ocean color measurements is given in Ding and Gordon (1994).

It is estimated that the ancillary pressure values are accurate to about 10 mb, which is 1% of standard pressure (1013.25 mb). It is also assumed that the uncertainty in surface pressure is not the same at all positions on the Earth. For the waters of the North Atlantic and the Mediterranean, for example, *in situ* surface pressure measurements are common, allowing the correction of systematic errors in satellite-based pressure measurements. In the Southern Ocean, on the other hand, such ground truth measurements are much more sparse. The uncertainty estimate presented here, or its improved successors, must be combined with the uncertainty in the ozone absorption coefficient; however, the uncertainty in the absorption coefficient is expected to dominate the total uncertainty.

3.5 AIRMASS AND AEROSOLS

For SeaWiFS band 7, it is assumed that the ocean absorbs all photons that penetrate its surface; thus, all of the radiance viewed by SeaWiFS for this band is generated by the atmosphere. In the lower atmosphere, multiple scattering by air molecules increases the effective air mass slightly, when compared with a purely geometric formulation. The same is true for the presence of marine aerosols near the surface of the ocean. On the other hand, the presence of stratospheric aerosols or of high altitude cirrus clouds will decrease the effective air mass. For large concentrations of these high altitude aerosols, a correction to the SeaWiFS atmospheric radiative transfer equations may be necessary (Ding and Gordon 1995). For SeaWiFS measurements without these upper tropospheric and stratospheric aerosols, it is estimated that the geometric airmass calculation underestimates the actual pathlength through the atmosphere by 0–1%. As shown below, this uncertainty is also small compared to the uncertainty in the ozone absorption coefficient.

3.6 DING AND GORDON (1995)

In a recent study of the effects of oxygen absorption on SeaWiFS band 7, Ding and Gordon (1995) approached this problem from a different point of view. In that study, oxygen absorption was placed within their atmospheric radiative transfer model, rather than treated individually. Also, Ding and Gordon (1995) used a square wave shape for the relative spectral response of band 7. In essence, that relative spectral response was unity within the nominal bandwidth (745–785 nm) and zero at all other wavelengths. In addition, the upwelling Earth radiance viewed by SeaWiFS was assumed to be constant with wavelength.

In addition, Ding and Gordon (1995) used the Air Force Geophysics Laboratory (AFGL) atmospheric absorption line parameters (described in Rothman et al. 1983) as the

Table 17. These are total band (R_T) and in-band (R_{IB}) responses for SeaWiFS band 7 (765 nm) for several slant path oxygen column amounts. The responses are the calculated currents from the band's photodiodes for each column amount. The calculations are based on the absorption spectrum calculated from Fraser (1995).

Slant Path Oxygen Column [airmass]	R_T [pA]	R_{IB} [pA]	Ratio R_{IB}/R_T
0.0	2863.650	2820.899	0.98507
0.2	2833.589	2790.838	0.98491
0.4	2805.343	2762.592	0.98476
0.6	2778.788	2736.037	0.98462
0.8	2753.809	2711.058	0.98448
1.0	2730.299	2687.548	0.98434
1.2	2708.159	2665.408	0.98421
1.4	2687.297	2644.546	0.98409
1.6	2667.627	2624.876	0.98397
1.8	2649.071	2606.320	0.98386
2.0	2631.555	2588.804	0.98375
2.2	2615.011	2572.260	0.98365
2.4	2599.375	2556.624	0.98355
2.6	2584.588	2541.837	0.98346
2.8	2570.596	2527.845	0.98337
3.0	2557.347	2514.596	0.98328
3.2	2544.794	2502.043	0.98320
3.4	2532.894	2490.143	0.98312
3.6	2521.604	2478.853	0.98305
3.8	2510.887	2468.136	0.98297
4.0	2500.708	2457.957	0.98290
4.2	2491.032	2448.281	0.98284
4.4	2481.830	2439.079	0.98277
4.6	2473.071	2430.320	0.98271
4.8	2464.731	2421.980	0.98265
5.0	2456.782	2414.031	0.98260
5.2	2449.203	2406.452	0.98254
5.4	2441.970	2399.219	0.98249
5.6	2435.064	2392.313	0.98244
5.8	2428.466	2385.715	0.98240
6.0	2422.157	2379.406	0.98235

Table 18. Shown here are fractional transmittances calculated from the data in Table 16, based on the MODTRAN7 absorption spectrum from Barnes (1997a), and in Table 17, based on the absorption spectrum from Fraser (1995). The fractional transmittances are given the symbols T_M and T_F for MODTRAN7 and Fraser, respectively.

Airmass	T_M	T_F	$(T_F - T_M)/T_M$
0.0	1.00000	1.00000	0.00000
0.2	0.98907	0.98950	0.00043
0.4	0.97902	0.97964	0.00063
0.6	0.96975	0.97037	0.00064
0.8	0.96119	0.96164	0.00047
1.0	0.95326	0.95343	0.00018
1.2	0.94591	0.94570	−0.00022
1.4	0.93909	0.93842	−0.00071
1.6	0.93273	0.93155	−0.00127
1.8	0.92680	0.92507	−0.00187
2.0	0.92127	0.91895	−0.00252
2.2	0.91609	0.91317	−0.00319
2.4	0.91124	0.90771	−0.00387
2.6	0.90668	0.90255	−0.00456
2.8	0.90240	0.89766	−0.00525
3.0	0.89836	0.89304	−0.00592
3.2	0.89456	0.88865	−0.00661
3.4	0.89097	0.88450	−0.00726
3.6	0.88757	0.88056	−0.00790
3.8	0.88435	0.87681	−0.00853
4.0	0.88130	0.87326	−0.00912
4.2	0.87840	0.86988	−0.00970
4.4	0.87565	0.86667	−0.01026
4.6	0.87303	0.86361	−0.01079
4.8	0.87053	0.86070	−0.01129
5.0	0.86815	0.85792	−0.01178
5.2	0.86587	0.85527	−0.01224
5.4	0.86370	0.85275	−0.01268
5.6	0.86162	0.85034	−0.01309
5.8	0.85963	0.84803	−0.01349
6.0	0.85772	0.84583	−0.01386

basis for their oxygen absorption spectrum. With assumptions that include Lorentz-broadening by collisions with other atmospheric gas molecules (Mitchell and Zemansky 1961), the ozone absorption spectrum of Ding and Gordon (1995) is a set of over 200 individual absorption lines. For Barnes and Esaias (1997), the high resolution oxygen absorption spectrum was derived from MODTRAN7, after smoothing by a $10\,\mathrm{cm}^{-1}$ triangular slit function.

The effect of this difference in the form of the ozone absorption spectrum is beyond the scope of this paper, as is the extraction of ozone absorption from the radiative transfer model of Ding and Gordon (1995). However, Ding and Gordon (1995) described a decrease in upwelling radiance, defined in terms of reflectance, of about 7% at an airmass of 2, and about 11% at an airmass of 5.

3.7 CONCLUDING REMARKS

A simplified instrument-atmosphere system level response for SeaWiFS band 7 (765 nm) is calculated in (6). It is a simplified version of the CZCS *system calibration* in Evans and Gordon (1994), particularly with respect to the atmospheric radiative transfer calculations. The components of (6) are shown in Fig. 13. The first component is the spectral response of band 7 to a source with a constant spectral radiance of unity; the second is an absorption-free TOA radiance; and the third is the transmission of oxygen in the atmosphere. For the analysis of Fraser (1995), the TOA radiance in Fig. 13b was considered to have a constant value of unity. That analysis has been modified here, and the components from that modified analysis (for an airmass of 2) is also shown in Fig. 13. This modification allows for an internally consistent comparison of the

Table 19. This is a summary of the fractional transmittances from three sources: calculations using the oxygen spectrum from MODTRAN7, T_M; calculations using the oxygen spectrum from Fraser (1995), T_F; and the fractional transmittances from Ding and Gordon (1995), T_{DG}.

Airmass	T_M	T_F	T_{DG}	$(T_F - T_M)/T_M$	$(T_{DG} - T_M)/T_M$
2	0.92127	0.91895	0.93000	−0.0025	0.0095
3	0.89836	0.89304	–	−0.0059	–
4	0.88130	0.87326	–	−0.0091	–
5	0.86815	0.85792	0.89000	−0.0118	0.0252
			Average	−0.0073	0.0173

Table 20. This is a summary of the effective ozone absorptions from three sources: calculations using the oxygen spectrum from MODTRAN7, α_M; calculations using the oxygen spectrum from Fraser (1995), α_F; and the fractional transmittances from Ding and Gordon (1995), α_{DG}.

Airmass	α_M	α_F	α_{DG}	$(\alpha_F - \alpha_M)/\alpha_M$	$(\alpha_{DG} - \alpha_M)/\alpha_M$
2	0.04100	0.04226	0.03629	0.0307	−0.1150
3	0.03573	0.03771	–	0.0555	–
4	0.03159	0.03388	–	0.0725	–
5	0.02828	0.03065	0.02331	0.0838	−0.1758
			Average	0.0606	−0.1454

MODTRAN7 and Fraser results.

For Ding and Gordon (1995), the TOA radiance in Fig. 13b was also considered to have a constant value of unity, and the relative spectral response in Fig. 13a was replaced with a square wave function with a value of unity for wavelengths from 745–785 nm and a value of zero at all other wavelengths. In addition, Ding and Gordon (1995) used a high resolution oxygen absorption spectrum, consisting of a series of rotational lines and imbedded oxygen absorption in their radiative transfer model. Consequently, a comparison of the results from MODTRAN7 and from Ding and Gordon (1995) is difficult to make.

A comparison of the system level transmittances from the three analyses is presented in Table 19. The system level transmittances for MODTRAN7 (T_M) are the total band responses from Table 16 divided by the response at zero airmass. For the absorption spectrum of Fraser (1995), the system level transmittances (T_F) are calculated similarly using the data in Table 17. The average difference between the MODTRAN7 and Fraser transmittances for the four airmasses in Table 19 is 0.0073, with the Fraser transmittances lower at each airmass. For the MODTRAN7 and the Ding and Gordon (1995) results, the average difference is 0.0173, with the MODTRAN7 transmittances lower at both airmasses.

A comparison of the effective absorption coefficients from the three analyses is presented in Table 20, where the effective absorption coefficient (using the example of the MODTRAN7 calculation) is obtained from Beer's Law as

$$\alpha_M = \frac{-\ln(T_M)}{\mu} \tag{8}$$

where α_M is the effective ozone absorption coefficient per unit airmass. This is a system level coefficient over the response of the band and should not be confused with the absorbance for an individual wavelength, $\alpha(\lambda)$. Because of self absorption, α_M is not a linear function of μ. The average difference between the MODTRAN7 and Fraser effective absorption coefficients is 0.0606. This is about 8.3 times greater than the average difference in system level transmittances in Table 19. In other words, on the average, a 1% change in transmittance is caused by an 8.3% difference in the effective absorption coefficient.

For the MODTRAN7 and Ding and Gordon (1995) results, the average difference in the effective ozone absorption coefficients is 0.1454. This difference is approximately the same as the 15% estimate of the accuracy of the recent additions to the AFGL compilation (Rothman et al. 1983) upon which the absorption spectrum of Ding and Gordon is based. However, the accuracy uncertainty in the line strengths in Rothman et al. (1983) does not explain the change in the transmittance difference with airmass in Table 19. This dependency may lie in the added self-absorption resulting from the line structure in the oxygen absorption spectrum of Ding and Gordon (1995). It may also derive from other aspects of their radiative transfer model. At present, the differences between the results from Sect. 3.3, based on the MODTRAN7 spectrum smoothed with a 10 cm^{-1} triangular slit function and the results of Ding and Gordon (1995), remain unresolved.

If necessary, there is a means of adjusting the MODTRAN7 transmittances to those of Ding and Gordon (1995). The differences between the two transmittances is 0.0095 at an airmass of 2, and 0.0252 at an airmass of 5. Because both data sets must agree at an airmass of zero, a linear

correction factor with a slope of 0.0050 per airmass can force an agreement between the two data sets. Such a correction is not suggested here; however, the correction might be addressed by an expert panel on atmospheric radiative transfer within the SeaWiFS Project.

A simple uncertainty estimate for T_M can be derived using the difference in the average values for α_M and α_F in Table 20 (6.06%), plus the uncertainties in the airmass. This gives the total uncertainty for an airmass of approximately 3.5. As discussed above, there is a 1% estimated uncertainty in μ from the surface pressure and a 1% estimated uncertainty in μ from aerosol scattering. The root square sum (RSS) sum of these three uncertainties is 6.22%. When the factor of 8.3 between the transmittance and effective ozone absorption coefficient is applied, the uncertainty in T_M becomes 0.75%, rounded up to 0.8%. It is assumed here that the uncertainty in T_M will remain unchanged if the correction to the values of Ding and Gordon (1995) are applied.

As shown in (6), the response of band 7 also contains the term, $\sum L_e(\lambda)R(\lambda)\Delta\lambda$, which has no dependence on airmass. The uncertainty in this term is directly related to the uncertainty in the laboratory calibration of the instrument. From the SeaWiFS specifications, this uncertainty is given as 5% in absolute terms and as 2% in relative (band-to-band) terms.

R.A. Barnes, R.E. Eplee, Jr., E-n. Yeh, and W.E. Esaias

Chapter 4

The 1993 SeaWiFS Calibration Using Band-Averaged Spectral Radiances

Robert A. Barnes
Robert E. Eplee, Jr.
General Sciences Corporation, Laurel, Maryland

Abstract

The radiometric calibration of SeaWiFS in November 1993 used a calibration technique that paired the digital counts from the instrument bands, with the spectral radiances from the laboratory SIS at the nominal center wavelengths for those bands. Using the spectral shape of the output of the laboratory radiance source, as provided by the manufacturer, it is possible to provide a radiometric calibration of SeaWiFS in terms of band-averaged spectral radiances. That calibration is presented here. It is given for three wavelength ranges, 380–940 nm, 380–1,150 nm, and for the in-band response ranges for the SeaWiFS bands.

4.1 INTRODUCTION

The data for the 1993 calibration of SeaWiFS at SBRS were provided by the instrument's manufacturer in terms of the digital counts from the instrument bands versus the spectral radiances at the nominal center wavelengths for the bands. Those data can be found in Table 8 of Barnes et al. (1994b). A series of instrument modelling studies (Barnes and Yeh 1996 and Barnes et al. 1997) examined the effects of this calibration method. When an instrument with finite bandwidths, such as SeaWiFS, is calibrated at one fixed wavelength, the relationship between the instrument output and the spectral radiance at that wavelength changes with the spectral shape of the source that is measured. This effect has been included in the current Sea-WiFS radiometric calibration (Barnes et al. 1994b), where the laboratory calibration, for a source with the spectral shape of a 2,850 K blackbody, was transferred into an on-orbit calibration, for a source with the spectral shape of a 5,900 K blackbody, by revising the calibration coefficients.

There is an alternate calibration method, in which the band-averaged (or band-weighted) spectral radiance is calculated. This requires knowledge of the radiance from the laboratory source over the wavelength region at which the instrument responds. For SeaWiFS, the spectral responses of the bands were measured from 380–1,150 nm (Barnes 1994 and Barnes et al. 1994b). The band-averaged (or band-weighted) spectral radiance is calculated using

$$L_B(\lambda_B) \;=\; \frac{\int_{\lambda_1}^{\lambda_2} L_s(\lambda)R(\lambda)d\lambda}{\int_{\lambda_1}^{\lambda_2} R(\lambda)d\lambda}, \tag{9}$$

and

$$\lambda_B \;=\; \frac{\int_{\lambda_1}^{\lambda_2} \lambda L_s(\lambda)R(\lambda)d\lambda}{\int_{\lambda_1}^{\lambda_2} L_s(\lambda)R(\lambda)d\lambda}, \tag{10}$$

where $L_B(\lambda_B)$ is the band-averaged spectral radiance for the band at wavelength, λ_B; λ_1 and λ_2 are the lower and upper integration wavelengths (380 nm and 1,150 nm for SeaWiFS); $L_s(\lambda)$ is the spectral radiance from the source at wavelength λ; and $R(\lambda)$ is the response of the band at wavelength λ.

In (9), the spectral response of the band, $R(\lambda)$, is the weighting function. For SeaWiFS, $R(\lambda)$ is given as the current of the band's photodiode (in picoamperes) at each nanometer from 380–1,150. This current is amplified and quantized to give a digital output. It is possible to normalize this spectral response to an integral value of unity, where unity represents the entire output from the photodiode. This normalization shows the link between the spectral response and the digital output from the band. The integral of the relative spectral response is transformed to the total number of digital counts from the band; however, $R(\lambda)$ appears in both the numerator and denominator of (9), so any normalizing constant for $R(\lambda)$ falls out of the calculation.

The band-averaged spectral radiance and the band-averaged center wavelength are tied together. Once calibrated using the laboratory source, the output from each band will give the band-averaged spectral radiance for any other source spectral shape. However, the band-averaged center wavelength (that is, the wavelength associated with the band-averaged spectral radiance) will vary with source spectral shape.

4.2 SPHERE SPECTRAL SHAPE

The laboratory calibration data from SBRS were listed in Table 8 of Barnes et al. (1994b). They are being reprinted for completeness in this chapter as Table 21. In addition, the output from the SBRS SIS for six lamp configurations were provided by the manufacturer in an appendix to the SeaWiFS Calibration and Data Package (SCADP which is an internal SBRS report).

The spectral radiances from the sphere, given at 20 nm intervals from 380–940 nm, are listed in Table 22. The SBRS SIS uses three types of lamps: 5 W, 45 W, and 200 W. The lamp configurations in Table 22 give the number of each type of lamp illuminated. For the 0-7-10 configuration, zero 5 W, seven 45 W, and ten 200 W lamps are illuminated. For the 0-1-0 configuration, only one 45 W lamp is illuminated. None of the lamp configurations of Table 22 use 5 W lamps. Although not explained in the SCADP, the spectral radiances in Table 21 can be derived from the spectral radiances in Table 22 via linear interpolation.

The data in Table 22 have neither the wavelength resolution nor the wavelength range of the relative spectral response measurements for the SeaWiFS bands, which cover wavelengths from 380–1,150 nm in 1 nm increments. There are several methods for estimating the sphere radiances at wavelengths between those in Table 22. In addition to the linear interpolation performed by the manufacturer, it is possible to use a fitting routine that creates a Planck-like (or blackbody-like) curve using

$$L(\lambda) = \frac{(a_0 + a_1\lambda)e^{(b_1/\lambda)}}{\lambda^5}, \qquad (11)$$

where the coefficients a_0, a_1, and b_1 are determined from a least squares fit of the data points in Table 22. Such a fitting routine is used to interpolate between the calibration wavelengths of standard lamps, such as those available from the National Institute of Standards and Technology (NIST). The results of such a curve fit are shown in Fig. 14. The figure shows measurements of the output of a standard lamp taken by the SXR during the Fifth SeaWiFS Intercalibration Round-Robin Experiment (SIRREX-5). The fitted curve in Fig. 14, given at 1 nm intervals from 380–1,150 nm, varies smoothly with wavelength and shows no structure; structure is not possible with only three fitted coefficients (a_0, a_1, and b_1).

The data from the SBRS sphere in Table 22, on the other hand, do show a structure in the spectral shape curves. The structure shows a nearly identical pattern for all of the lamp settings in the table. The output from the 0-7-10 lamp setting is shown in Fig. 15 as a typical example. A fitted curve, using (11), cannot reproduce the structure in this shape.

As part of the analysis for this paper, there was an attempt to use the spectral shape of the radiance from the GSFC sphere (Barnes et al. 1996) as a basis for interpolating between the measurement wavelengths in the characterization of the SBRS sphere. Both spheres have output with similar shapes, and using the shape of the GSFC sphere would add a curvature to the interpolated results for the SBRS sphere. These interpolations, however, formed loops between the measured points (similar to the shape of telephone lines between telephone pole). This effect was particularly true in the portion of the SBRS sphere output near 420 nm. The cause of this effect can be seen in Fig. 16a.

Figure 16a shows the spectral radiances from the SBRS sphere (with a 0-7-10 lamp configuration) at wavelengths from 380–440 nm. The curve is an exponential fit using the spectral radiances at 380, 400, and 440 nm. Using the shape of this exponential fit to interpolate between wavelengths creates the looping effect. Figure 16b shows a spline fit interpolation between the four radiances. This type of fitting was used in this analysis to interpolate between the measurement wavelengths in the characterization of the SBRS sphere.

The choice of an appropriate interpolation scheme for the sphere output will be an important factor in the recalibration of SeaWiFS that follows the integration and thermal vacuum testing of the instrument and spacecraft by the spacecraft manufacturer. This recalibration will use the SXR as the spectral radiance standard and the GSFC SIS as the radiance source (Barnes et al. 1996). The quality of the interpolation scheme is an important component of the uncertainty estimate for the absolute and the relative (band-to-band) calibration of SeaWiFS. No such uncertainty analysis is made here for the SBRS sphere, and a simple spline interpolation is used. (A spline fit freezes the noise in the measurements into the result along with any wavelength structure.)

The SBRS sphere was characterized at wavelengths from 380–940 nm, and the relative spectral responses of the SeaWiFS bands extend from 380–1,150 nm. In this analysis, the shape of the GSFC sphere was used to extend the radiance curve for the SBRS sphere from 940–1,150 nm. The output from the GSFC sphere was normalized to the measured spectral radiance at 940 nm. For the eight SeaWiFS bands, the radiance in the 940–1,150 nm wavelength range causes a negligible change in the band-averaged spectral radiances and the band-averaged center wavelengths. The radiance spectrum for the SBRS sphere with a lamp configuration of 0-7-10 is shown in Fig. 17. The curve shown in the figure gives the spectral radiances at 1 nm intervals from 380–1,150 nm.

4.3 BAND-AVERAGED RESULTS

As shown in Table 21, each SeaWiFS band has three high sensitivity channels and one low sensitivity channel. For bands 1–5, the same spectral radiance (that is, the

Table 21. These are the input values and calculated sensitivities for the eight SeaWiFS bands from Table 8 of Barnes et al. (1994b). The spectral radiances for each band are the values at that band's nominal center wavelength. The spectral radiances, the measurement counts, and the offset counts come from the laboratory data. The sensitivities are calculated from the spectral radiances and the net counts. The values are given for Science Gain 1, the standard gain for SeaWiFS ocean color measurements. The spectral radiances are given as $mW\,cm^{-2}\,sr^{-1}\,\mu m^{-1}$. The sensitivities are units of spectral radiance per count.

Band Number	Channel	Spectral Radiance	Measurement [counts]	Offset [counts]	Net [counts]	Sensitivity
1	1	9.246	175	21	154	0.060039
	2	9.246	871	23	848	0.010903
	3	9.246	859	18	841	0.010994
	4	9.246	871	21	850	0.010878
2	1	9.122	883	18	865	0.010546
	2	9.122	887	21	866	0.010533
	3	9.122	878	16	862	0.010582
	4	9.122	153	18	135	0.067570
3	1	7.216	127	21	106	0.068075
	2	7.216	899	22	877	0.008228
	3	7.216	905	21	884	0.008163
	4	7.216	903	19	884	0.008163
4	1	5.970	856	21	835	0.007150
	2	5.970	855	20	835	0.007150
	3	5.970	856	19	837	0.007133
	4	5.970	111	21	90	0.066333
5	1	4.692	98	26	72	0.065167
	2	4.692	840	22	818	0.005736
	3	4.692	837	22	815	0.005757
	4	4.692	828	17	811	0.005785
6	1	1.682	540	21	519	0.003241
	2	1.682	538	17	521	0.003228
	3	1.682	544	33	511	0.003292
	4	8.058	168	21	147	0.054816
7	1	9.885	253	23	230	0.042978
	2	2.057	915	20	895	0.002298
	3	2.057	913	21	892	0.002306
	4	2.057	922	27	895	0.002298
8	1	1.063	671	20	651	0.001633
	2	1.063	670	24	646	0.001646
	3	1.063	671	18	653	0.001628
	4	10.283	320	20	300	0.034277

Table 22. These are the measured spectral radiances (in mW cm^{-2} sr^{-1} μm^{-1}) from the SBRS sphere for six lamp configurations. These measurements were made just prior to the November 1993 radiometric calibration of SeaWiFS. For the 0-7-10 configuration, zero 5 W, seven 45 W, and ten 200 W lamps are illuminated. For the 0-1-0 configuration, only one 45 W lamp is illuminated. None of these configurations use 5 W lamps.

| Wavelength [nm]	Lamp Settings					
	0-7-10	0-0-7	0-5-2	0-9-0	0-5-0	0-1-0
380	4.660	2.844	1.275	0.869	0.479	0.105
400	7.109	4.303	1.950	1.331	0.735	0.159
420	10.670	6.499	2.924	1.996	1.107	0.238
440	14.390	8.736	3.945	2.696	1.491	0.320
460	18.720	11.310	5.115	3.497	1.935	0.413
480	23.770	14.370	6.503	4.443	2.461	0.524
500	28.950	17.480	7.929	5.423	3.003	0.637
520	34.740	20.980	9.508	6.516	3.611	0.765
540	40.280	24.520	11.130	7.621	4.223	0.893
560	46.170	28.110	12.740	8.735	4.848	1.023
580	52.330	31.760	14.410	9.887	5.480	1.155
600	58.360	35.410	16.070	11.030	6.129	1.290
620	63.710	38.660	17.540	12.060	6.703	1.405
640	68.910	41.840	19.010	13.085	7.267	1.521
660	74.060	44.940	20.440	14.060	7.806	1.632
680	78.700	47.720	21.720	14.940	8.309	1.732
700	83.390	50.590	23.020	15.850	8.810	1.837
720	87.250	52.770	23.980	16.565	9.194	1.916
740	90.680	54.860	24.980	17.215	9.573	1.995
760	93.110	56.300	25.640	17.670	9.826	2.045
780	95.330	57.600	26.240	18.090	10.060	2.091
800	96.760	58.460	26.690	18.350	10.220	2.121
820	96.740	58.410	26.650	18.340	10.210	2.115
840	96.950	58.520	26.710	18.405	10.230	2.123
860	97.150	58.650	26.820	18.455	10.270	2.126
880	97.830	59.010	26.980	18.570	10.320	2.141
900	98.250	59.250	27.100	18.667	10.390	2.148
920	97.920	59.050	27.010	18.635	10.340	2.143
940	96.260	58.050	26.550	18.305	10.180	2.105
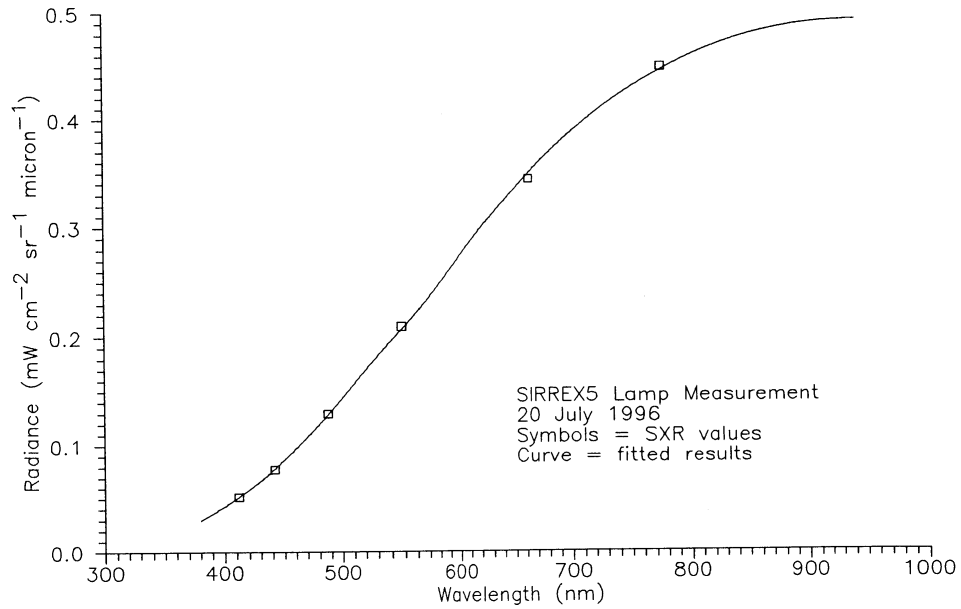
Fig. 14. These are the results of measurements of the radiance from a standard lamp using the SXR. The fitted results use three statistically derived coefficients. The resulting curve varies smoothly with wavelength and shows no structure.
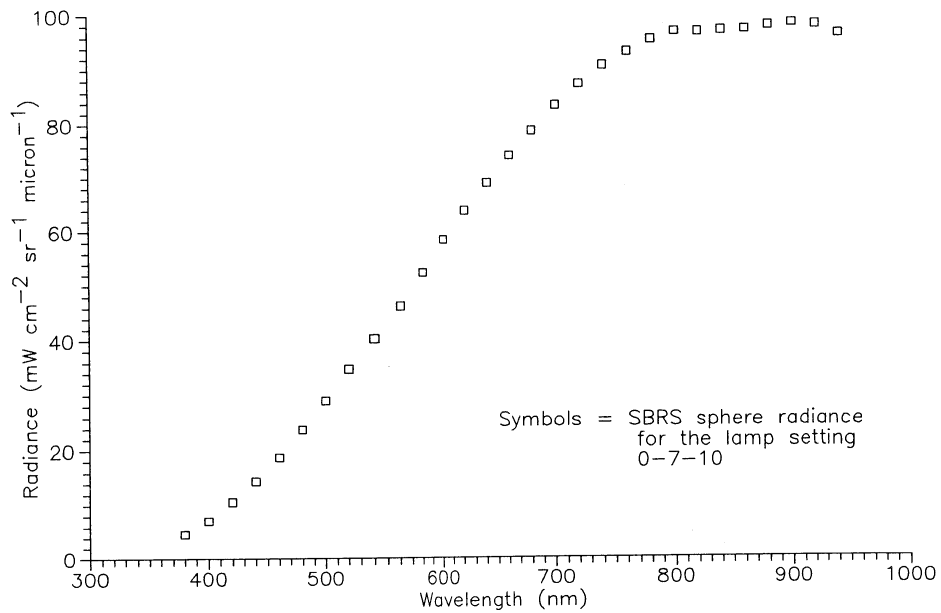

Fig. 15. This is a plot of the output from the SBRS sphere for a lamp configuration of 0-7-10. For this configuration, there are zero 5 W, seven 45 W, and ten 200 W lamps illuminated.
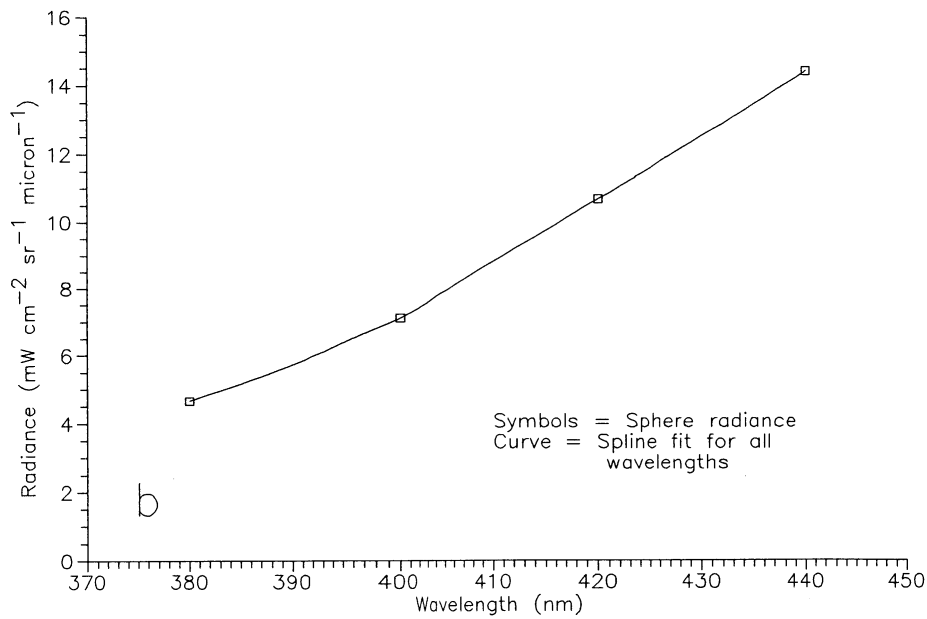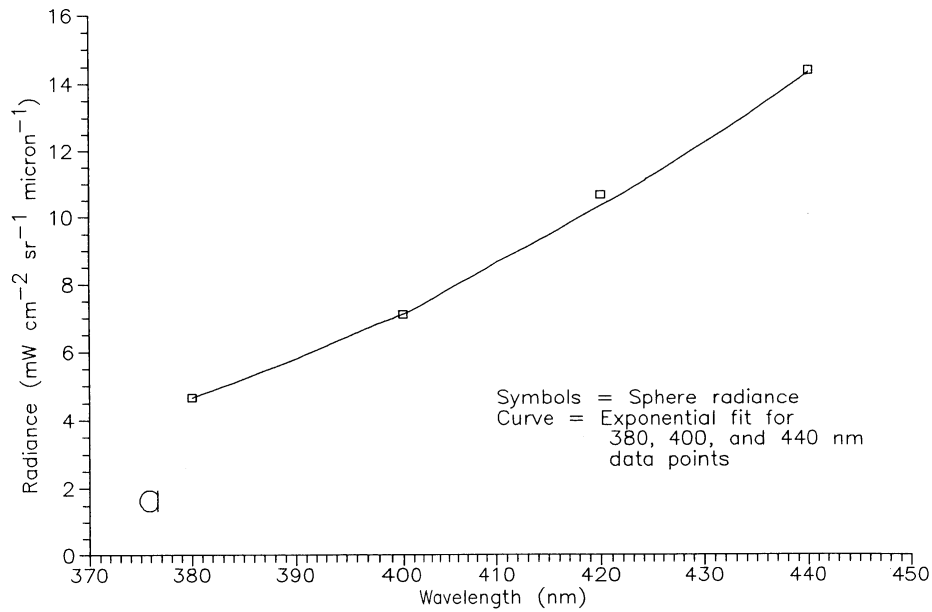
Fig. 16. These are the SBRS sphere spectral radiances. The measured values are for the 0-7-10 lamp configuration. **a)** These are the sphere spectral radiances with an exponential fit of the 380, 400, and 440 nm data points. Such a curve fit cannot adequately incorporate the 420 nm data point. **b)** These are the sphere spectral radiances with a spline fit. The curvature of the interpolation between the 380 and 400 nm data points is similar to that in part **a)**.
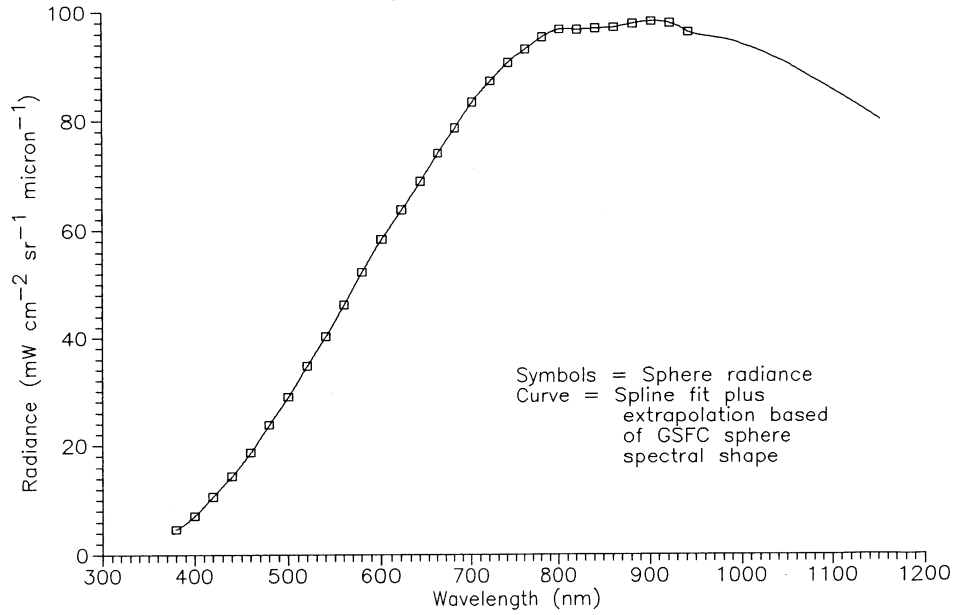
Fig. 17. These are the SBRS sphere spectral radiances. The measured values are for the 0-7-10 lamp configuration. The curve from 380–940 nm is a spline fit to the measured values. The curve from 940–1,150 nm uses the spectral shape of the GSFC sphere, normalized to the measured value at 940 nm.

Table 23. These are the band-averaged spectral radiances and center wavelengths from the 1993 calibration of SeaWiFS. The results are calculated over two wavelength ranges, 380–940 nm and 380–1,150 nm.

Band Number	Sphere Setting	Band-Averaged Measurements			
		Spectral Radiance[1]	Center Wavelength[1]	Spectral Radiance[2]	Center Wavelength[2]
1	0-7-10	9.5607	415.46	9.5610	415.48
2	0-7-0	9.2350	444.71	9.2351	444.72
3	0-5-2	7.3232	492.60	7.3275	493.00
4	0-9-0	5.9640	510.71	5.9665	510.99
5	0-5-0	4.7048	557.66	4.7073	558.17
6	0-5-0	8.0039	668.66	8.0044	668.79
7	0-5-0	9.8834	766.55	9.8837	767.47
8	0-5-0	10.2369	864.15	10.2345	864.97
6	0-1-0	1.6711	668.65	1.6712	668.77
7	0-1-0	2.0561	766.53	2.0562	767.45
8	0-1-0	2.1217	864.13	2.1212	864.95

1) $\lambda_1 = 380$ nm and $\lambda_2 = 940$ nm
2) $\lambda_1 = 380$ nm and $\lambda_2 = 1,150$ nm

Table 24. These are the band-averaged spectral radiances and center wavelengths from the 1993 calibration of SeaWiFS. The results are calculated over the in-band response ranges for each band.

Band Number	Sphere Setting	λ_1 [nm]	λ_2 [nm]	Band-Averaged Spectral Radiance	Band-Averaged Center Wavelength [nm]
1	0-7-10	395	433	9.4978	414.49
2	0-7-0	424	464	9.2334	444.58
3	0-5-2	471	511	7.2892	491.57
4	0-9-0	489	530	5.9667	510.53
5	0-5-0	537	577	4.6885	555.18
6	0-5-0	647	692	8.0207	668.69
7	0-5-0	728	814	9.8873	765.70
8	0-5-0	827	908	10.2874	866.29
6	0-1-0	647	692	1.6746	668.68
7	0-1-0	728	814	2.0570	765.69
8	0-1-0	827	908	2.1319	866.29

same lamp configuration in the SIS) is used in the laboratory calibration for both the high and low sensitivity channels. For bands 6–8, the spectral radiances used for the high and low sensitivity channels are different. This leads to a total of 11 combinations of lamp configurations and SeaWiFS bands (Table 23).

Table 23 shows the band-averaged spectral radiance and the band-averaged center wavelength for each combination. The results have been calculated using (9) and (10). They have also been calculated for two wavelength ranges, 380–940 nm and 380–1,150 nm. The differences between the calculations using these two limits of integration are small, particularly for the band-averaged spectral radiances. For calculations of the band-averaged center wavelengths using the 380–1,150 nm integration limits, the center wavelengths occur at wavelengths that are longer than those for calculations using the 380–1,150 nm integration limits. These differences in the center wavelengths range from near zero to about 1 nm.

It is also possible to integrate (9) and (10) over the in-band response range of the SeaWiFS bands. The results of these calculations are given in Table 24. The lower and upper integration wavelengths in Table 24 come from Table 13 of Barnes et al. (1994b). They are the lower and upper extended band edges (lower and upper 1% response points) for a spectrally flat source. The band-averaged spectral radiances in Table 24 agree with the corresponding values in Table 23 to 0.5% or better, and the band-averaged center wavelengths agree to 2 nm or better.

The results from Table 23, *integrated over the wavelength range from 380–1,150 nm,* have been chosen as the band-averaged spectral radiances for the November 1993 calibration of SeaWiFS at SBRS. The results, integrated from 380–940 nm, are essentially the same, and the integration from 380–1,150 nm gives the band-averaged spectral

radiances over the entire wavelength ranges of the SeaWiFS relative spectral responses. The sensitivities of the 32 SeaWiFS channels using band-averaged spectral radiances are listed in Table 25. These values can be substituted for those in Table 21 to provide a prelaunch radiometric calibration for SeaWiFS in terms of band-averaged spectral radiances.

4.4 CONCLUDING REMARKS

It is anticipated that the band-averaged spectral radiances in Table 25 will never be used in the calibration of SeaWiFS. After more than three years, the November 1993 calibration of the instrument is outdated. A second radiometric calibration of the instrument was performed in the first quarter of 1997 after thermal vacuum testing of the instrument and spacecraft system. The results presented here will be used to check for changes in the radiometric sensitivity between the two calibrations.

The relationship between band-averaged spectral radiances and the counts from the SeaWiFS bands in Table 25 can be applied to measurements of the TOA spectral shapes that SeaWiFS will view on orbit. No corrections to the relationships in Table 25 for source spectral shape are required; however, the band-averaged center wavelengths associated with these spectral radiances do depend on the on-orbit source spectral shapes. For SeaWiFS band 8 (865 nm), which has a significant out-of-band response at wavelengths shorter than 820 nm, the on-orbit band-averaged center wavelength can be as short as 850 nm (Barnes 1997c). With the out-of-band response removed, the band-averaged center wavelength for band 8 on orbit has an estimated uncertainty of 0.9 nm.

The modelling studies in Barnes et al. (1996) and in this technical memorandum have been made in an effort to

Table 25. These are the results of the 1993 SeaWiFS calibration using band- averaged spectral radiances. This table duplicates Table 23, except that band-averaged spectral radiances are used. The band-averaged spectral radiances are given as $mW\,cm^{-2}\,sr^{-1}\,\mu m^{-1}$. The sensitivities are given as units of band-averaged spectral radiance per count.

Band Number	Channel	Band-Weighted Spectral Radiance	Measurement [counts]	Offset [counts]	Net [counts]	Sensitivity
1	1	9.561	175	21	154	0.062084
	2	9.561	871	23	848	0.011275
	3	9.561	859	18	841	0.011369
	4	9.561	871	21	850	0.011248
2	1	9.235	883	18	865	0.010676
	2	9.235	887	21	866	0.010664
	3	9.235	878	16	862	0.010713
	4	9.235	153	18	135	0.068407
3	1	7.328	127	21	106	0.069132
	2	7.328	899	22	877	0.008356
	3	7.328	905	21	884	0.008290
	4	7.328	903	19	884	0.008290
4	1	5.966	856	21	835	0.007145
	2	5.966	855	20	835	0.007145
	3	5.966	856	19	837	0.007128
	4	5.966	111	21	90	0.066289
5	1	4.707	98	26	72	0.065375
	2	4.707	840	22	818	0.005754
	3	4.707	837	22	815	0.005775
	4	4.707	828	17	811	0.005804
6	1	1.671	540	21	519	0.003220
	2	1.671	538	17	521	0.003207
	3	1.671	544	33	511	0.003270
	4	8.004	168	21	147	0.054449
7	1	9.884	253	23	230	0.042974
	2	2.056	915	20	895	0.002297
	3	2.056	913	21	892	0.002305
	4	2.056	922	27	895	0.002297
8	1	1.058	671	20	651	0.001626
	2	1.058	670	24	646	0.001638
	3	1.058	671	18	653	0.001621
	4	10.234	320	20	300	0.034113

understand the relationships between the on-orbit source spectral shapes, the SeaWiFS measured spectral radiances, and the center wavelengths for these measurements. An understanding of these relationships is particularly impor- tant for SeaWiFS band 8 (865 nm), which has a large out-of-band response from 380–820 nm and which is the cornerstone for the SeaWiFS atmospheric correction (Gordon and Wang 1994).

Chapter 5

SeaWiFS Measurements in Orbit: Band-Averaged Spectral Radiances

ROBERT A. BARNES

General Sciences Corporation, Laurel, Maryland

ABSTRACT

This paper presents the culmination of the source spectra shape studies in Barnes et al. (1996) and in this technical memorandum. The SeaWiFS band-averaged spectral radiances are independent of the spectral shape of the source that the instrument measures; however, the band-averaged center wavelengths associated with them do have such a dependence. The current radiometric calibration (Barnes et al. 1994b) does not use band-averaged measurements. The adoption of band-averaged spectral radiances awaits analysis of the radiometric recalibration of SeaWiFS at the spacecraft manufacturer, which was done during the first quarter of 1997. For measurements of on-orbit band-averaged spectral radiances, it is recommended that the in-band results be used. A modification of the technique of Barnes and Yeh (1996), for use with band-averaged measurements, is presented. Since band-averaged center wavelengths are not part of the SeaWiFS level-1b processing, the best estimates for these wavelengths are given here. In addition, estimates are provided of the uncertainties in the on-orbit band-averaged spectral radiances and center wavelengths that derive from the lack of information on the spectral shape of the Earth-exiting radiance.

5.1 INTRODUCTION

The band-averaged spectral radiance and center wavelength for SeaWiFS measurements of the Earth-exiting radiance are defined as

$$L_{\mathrm{B}}(\lambda_{\mathrm{B}}) \;=\; \frac{\int_{\lambda_1}^{\lambda_2} L_e(\lambda)R(\lambda)d\lambda}{\int_{\lambda_1}^{\lambda_2} R(\lambda)d\lambda}, \qquad (12)$$

and

$$\lambda_{\mathrm{B}} \;=\; \frac{\int_{\lambda_1}^{\lambda_2} \lambda L_e(\lambda)R(\lambda)d\lambda}{\int_{\lambda_1}^{\lambda_2} L_e(\lambda)R(\lambda)d\lambda}, \qquad (13)$$

where $L_{\mathrm{B}}(\lambda_{\mathrm{B}})$ is the band-averaged spectral radiance for the band at wavelength, λ_{B}; λ_1 and λ_2 are the lower and upper integration wavelengths (380 nm and 1,150 nm for SeaWiFS); $L_e(\lambda)$ is the spectral radiance from the source at wavelength λ; and $R(\lambda)$ is the response of the band at wavelength λ.

In (12), the integral in the numerator is the total band response. In Barnes et al. (1997), the total band response was calculated as the total current from the photodiode (in picoamperes). With electronic amplification and digitization within the instrument, this current is converted into digital counts. There is no spectral dependence in this amplification, and it can be treated as a constant multiplier

in the term $R(\lambda)$. Since $R(\lambda)$ is found in the numerators and denominators for (12) and (13), the amplification and digitization constant falls out of both equations.

In (12), the relative spectral response in the denominator has been calculated for each SeaWiFS band as the response to a source with a constant spectral radiance of $1\,\mathrm{mW\,cm^{-2}\,sr^{-1}\,\mu m^{-1}}$ (Barnes et al. 1994b). For solutions to (12), the denominator is a constant for each SeaWiFS band. As a result, the sensitivity studies of total band response (R_T) in Barnes et al. (1997) can be directly applied to the band-averaged spectral responses, as calculated using (12). This applies both to the effects of source spectral shape and atmospheric absorption.

For the sensitivity studies in Barnes et al. (1997), the wavelengths for the SeaWiFS bands were the nominal center wavelengths as given in the performance specification for the instrument (Barnes et al. 1994a). In the current calibration of SeaWiFS (November 1993) the digital counts from each band are linked to the spectral radiance at the nominal center wavelength for that band. In this type of calibration, the relationship of counts to spectral radiance also includes a dependence on the spectral shape of the radiance source (Barnes et al. 1994b and Barnes et al. 1996a).

For calculations of the band-averaged spectral response using (12), the numerator of the equation gives the total band output. Since the integral in the numerator of (12)

Table 26. Shown here are the band-averaged spectral radiances and center wavelengths for a 12,000 K Planck function and the nominal TOA spectrum from Barnes and Esaias (1997). The band averages are calculated over wavelengths from 380–1,150 nm. The spectral radiances are given in terms of mW cm^{-2} μm^{-1} sr^{-1}; the wavelengths are given in nanometers. The table also includes the nominal center wavelengths and nominal spectral radiances at those wavelengths from the SeaWiFS Performance Specifications (Barnes et al. 1994a).

Band Number	Nominal Measurements		Total-Band Band-Averaged Measurements			
	Spectral[1] Radiance	Center[1] Wavelength	Spectral[2] Radiance	Center[2] Wavelength	Spectral[3] Radiance	Center[3] Wavelength
1	9.100	412.00	9.020	413.55	8.894	413.55
2	8.410	443.00	8.374	443.68	8.456	444.10
3	6.560	490.00	6.516	491.04	6.628	490.78
4	5.640	510.00	5.647	509.55	5.548	509.20
5	4.570	555.00	4.580	553.64	4.602	552.97
6	2.460	670.00	2.491	666.62	2.508	665.86
7	1.610	765.00	1.605	764.64	1.607	764.40
8	1.090	865.00	1.120	852.87	1.131	849.87

1) From Performance Specifications.

2) For 12,000 K Planck function.

3) For nominal TOA spectrum.

covers the entire wavelength range over which the photodiodes in SeaWiFS have a significant quantum efficiency, the band-averaged spectral radiance for each band is always the total response from that band. There is no dependence on source spectral shape in the band-averaged spectral radiance. There is, however, a source spectral shape dependence in the band-averaged center wavelength, as calculated using (13).

For the in-band responses of the SeaWiFS bands, the band-averaged center wavelengths have been calculated for several source spectral shapes by Barns et al. (1996b). The in-band response covers the wavelength region over which the response of the band is 1% or more of the maximum response of the band. The 1% response points are also called the extended band edges. For these calculations, the wavelengths for the extended band edges are those for a spectrally flat source in Table 13 of Barnes et al. (1994b). For the in-band responses of the SeaWiFS bands, the effects of source spectral shape on the band-averaged center wavelength is very small (Barnes 1996b).

For bands with significant out-of-band responses, such as SeaWiFS band 8 (865 nm nominal center wavelength), source spectral shape can have a significant effect on the calculated band-averaged center wavelength for the total band response. This effect must be understood if SeaWiFS on-orbit measurements are to be interpreted in terms of band-averaged spectral radiances.

5.2 TOA SPECTRA

The TOA spectra in this study are a subset of the spectra used in Barnes et al. (1997). The spectra used here include a 12,000 K Planck function and the nominal TOA spectrum from Barnes and Esaias (1997) as baseline spectra. In addition, the nominal TOA spectrum has been

modified to include the effects of atmospheric water vapor for slant path column amounts of 6.664, 13.328, and 19.992 g cm^{-2} (see Barnes and Esaias 1997).

Oxygen A-band absorption is not included in this study. For all SeaWiFS bands, except band 7, the effects of oxygen absorption are very small (0.2% or less). For band 7, the effects of A-band absorption must be removed to make the band usable, since the absorption occurs in the heart of the in-band response. Thus, for this study, the oxygen notch in band 7 is assumed to be removed (Barnes 1997b).

5.3 BAND-AVERAGED RESPONSES

The results presented here have been divided into the total band and in-band spectral responses.

5.3.1 Total Band Responses

Table 26 gives the band-averaged spectral radiances and center wavelengths for two source spectral shapes that approximate the ones SeaWiFS will measure as it observes ocean scenes. These are the spectral shapes for a 12,000 K Planck function and the nominal TOA spectrum from Barnes and Esaias (1997). Neither spectrum shows the effects of atmospheric absorption. For each band, the two spectra are normalized at the nominal spectral radiance and center wavelength from the SeaWiFS Performance Specifications (Barnes et al. 1994a). The normalization values are also shown in Table 26. The effects of this normalization on the source spectral shapes for SeaWiFS band 1 (412 nm) and band 8 (865 nm) are shown in Fig. 6 of Barnes et al. (1997). This normalization process does not effect the comparison results presented below. Finally, the lower and upper integration limits for the calculations—λ_1

and λ_2 in (12) and (13)—are 380 and 1,150 nm respectively. These are the wavelength limits for the measured relative spectral responses of the SeaWiFS bands.

For band-averaged spectral radiances, no corrections for the spectral shape of the TOA source are required. The band-averaged spectral radiances are directly linked with the counts from the bands on orbit. However, there is a dependence in the band-averaged center wavelengths on the spectral shape of the source that the instrument measures. These center wavelengths are not part of any data reduction scheme for SeaWiFS measurements on orbit. These wavelengths can be estimated using model TOA radiance curves, such as the ones used here, or they can be estimated using actual TOA spectra that are measured on orbit.

For five of the SeaWiFS bands (bands 1, 2, 3, 4, and 7), there is little difference in the band-averaged center wavelengths calculated from the 12,000 K and nominal TOA spectra. For these five bands, Table 26 shows the maximum change in wavelengths to be about 0.4 nm. For SeaWiFS bands 5 and 6, the agreement between the band-averaged center wavelengths for the two source spectral shapes is not as good.

For band 8, the band-averaged center wavelengths for the two source spectral shapes disagree by 3 nm—and the wavelengths differ by up to 15 nm from the nominal center wavelength in the performance specifications. This results directly from the blue leak (the out-of-band response at wavelengths shorter than 825 nm) in the relative spectral response for band 8, as shown in Barnes et al. (1994b), combined with a TOA radiance spectrum (Barnes and Esaias 1997) that has an order of magnitude more radiance near 400 nm than near 865 nm, as shown in Fig. 1 of Barnes et al. (1997).

Table 27 shows the changes in band-averaged spectral radiance and center wavelength that come from different slant path water vapor amounts in the atmosphere. For all eight bands, atmospheric water vapor has little effect on the center wavelength. For bands 1–7, there is very little effect on the band-averaged spectral radiance. For band 8, there is about a 5% decrease in the band-averaged spectral radiance as the water vapor amount increases from zero to 20 g cm^{-2}. This relative change duplicates the change calculated in Barnes et al. (1997). This should be the case since Barnes et al. (1997) use the numerator of (12) and the same water vapor spectra to calculate these changes; this agreement is shown in Fig. 18. For this figure, the total band response values for band 8 in Table 7 of Barnes et al. (1997) were normalized to unity at zero water vapor amount. In the same manner, the values from Table 27 were normalized at zero water vapor slant path amount. The relative changes in the two data sets agree exactly.

5.3.2 In-Band Responses

The calculation of the results in Table 28 duplicates the manner of that for Table 26, except that the band-averaged spectral radiances and center wavelengths have been calculated over the in-band wavelengths for each band. The lower and upper integration limits for the calculations— λ_1 and λ_2 in (12) and (13)—are also given in Table 28. They are the lower and upper extended band edges for a spectrally flat source. Of interest in Table 28 is the agreement of the band-averaged center wavelengths for bands 5, 6, and 8. For band 8, the center wavelengths for the two source spectral shapes are essentially the same, and both agree with the nominal center wavelength (865 nm) to within 0.5 nm.

The results in Table 29 duplicate those in Table 27, except that the band-averaged spectral radiances and center wavelengths have been calculated over the in-band wavelengths for each band. And, as the relative change in the total band response for band 8 in Table 27 agrees with that in Table 7 of Barnes et al. (1997), so does the relative change in in-band response in Table 29 agree with the in-band responses in Table 7 of Barnes et al. (1997).

In more general terms, the changes in band output with water vapor and oxygen slant path column amount in Barnes et al. (1997) and those presented here, when expressed in relative terms, are the same changes that occur in the band-averaged spectral radiances. The corrections for atmospheric absorption in Barnes et al. (1997) can be applied directly to the band-averaged spectral radiances on orbit.

5.4 OUT-OF-BAND RESPONSE

For the SeaWiFS bands, there is little change in the in-band band-averaged center wavelength with source spectral shape (Table 28). The center wavelengths in this table, duplicate those in Table 26 of Barnes (1996b) to within 0.1 nm. That table in Barnes (1996b) gives the in-band band-averaged center wavelengths for Planck function curves with three different temperatures: 10,000 K, 12,000 K, and 14,000 K.

This agreement, however, depends on the ability to remove the out-of-band response accurately. The out-of-band responses for SeaWiFS bands 1, 2, 3, 4, and 7 have very little dependence on the spectral shape of the TOA radiance that the instrument will view. The out-of-band correction factors in Table 10 of Barnes et al. (1997) for bands 1, 2, 3, 4, and 7 agree to within 0.1% for the 12,000 K Planck function and the nominal TOA spectrum. This is the estimated uncertainty in the out-of-band correction for these bands.

It is assumed that a 0.1% uncertainty in the out-of-band correction for SeaWiFS bands 1, 2, 3, 4, and 7 will have a negligible effect on the band-averaged center wavelengths for these bands. As a result, the estimate of the uncertainty in the center wavelength for these bands comes from the differences in the paired center wavelengths in Table 28. That difference is about 0.3 nm. This difference derives from differences in the structure of the TOA radiance over the in-band wavelength ranges for these bands.

Table 27. Shown here are the band-averaged spectral radiances and center wavelengths versus slant path water vapor amount. The baseline spectrum (with no water vapor) is the nominal TOA spectrum from Barnes and Esaias (1997). The band averages are calculated over wavelengths from 380–1,150 nm. The spectral radiances are given in terms of $mW\,cm^{-2}\,\mu m^{-1}\,sr^{-1}$. The wavelengths are given in nanometers. The water vapor slant path amounts (WVSPA) are a subset of those in Barnes et al. (1997).

Band	Total Band Band-Averaged Measurements							
Number	Spectral[1] Radiance	Center[1] Wavelength	Spectral[2] Radiance	Center[2] Wavelength	Spectral[3] Radiance	Center[3] Wavelength	Spectral[4] Radiance	Center[4] Wavelength
1	8.894	413.55	8.894	413.55	8.894	513.55	8.894	413.55
2	8.456	444.10	8.456	444.10	8.456	444.10	8.456	444.10
3	6.628	490.78	6.627	490.77	6.627	490.77	6.627	490.77
4	5.548	509.20	5.548	509.20	5.548	509.19	5.548	509.19
5	4.602	552.97	4.598	552.91	4.595	552.86	4.591	552.82
6	2.508	665.86	2.492	665.86	2.477	665.86	2.462	665.87
7	1.607	764.40	1.593	764.11	1.582	763.98	1.572	763.91
8	1.131	849.87	1.113	849.78	1.091	849.74	1.082	849.73

1) WVSPA $= 0.000\,g\,cm^{-2}$.

2) WVSPA $= 6.664\,g\,cm^{-2}$.

3) WVSPA $= 13.328\,g\,cm^{-2}$.
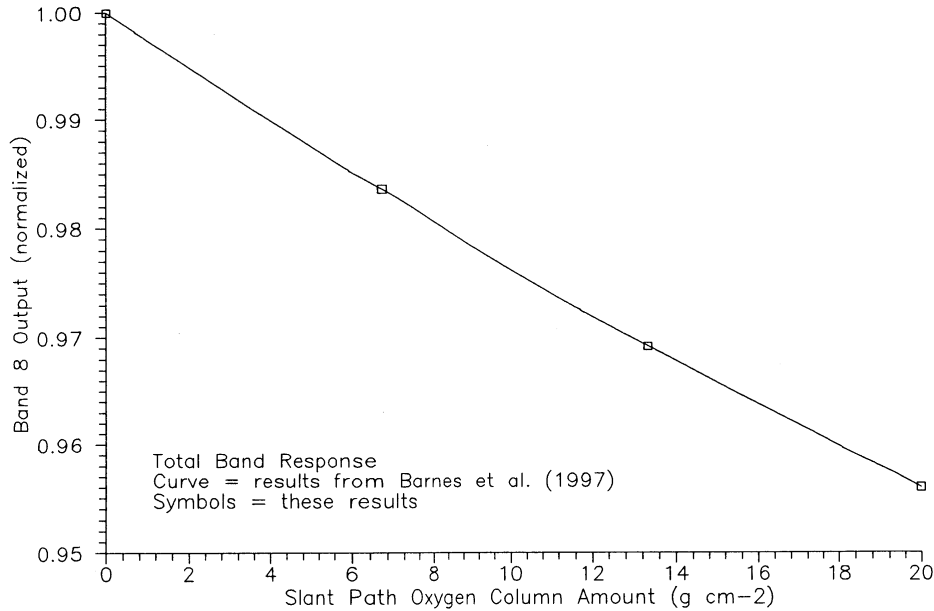
4) WVSPA $= 19.992\,g\,cm^{-2}$.

Fig. 18. The effects of water vapor absorption on the total band output of SeaWiFS band 8 are shown here. The output of the band has been normalized to unity at a water vapor slant path amount of zero. The curve shows the effect as presented in Table 7 of Barnes et al. (1997). The symbols show the effect for the band-averaged spectral radiances from Table 27. The two calculation schemes give identical results.

Table 28. Shown here are the in-band band-averaged spectral radiances and center wavelengths for a 12,000 K Planck function and the nominal TOA spectrum from Barnes and Esaias (1997). The spectral radiances are given in terms of $\mathrm{mW\,cm^{-2}\,\mu m^{-1}\,sr^{-1}}$. The wavelengths are given in nanometers. The table also includes the wavelength limits for the in-band responses.

| Band | Lower | Upper | In-Band Band-Averaged Measurements | | | |
Number	Integration Wavelengths	Integration Wavelengths	Spectral[1] Radiance	Center[1] Wavelength	Spectral[2] Radiance	Center[2] Wavelength
1	395	433	9.030	413.39	8.910	413.39
2	424	464	8.372	443.74	8.462	444.12
3	471	511	6.527	490.85	6.646	490.62
4	489	530	5.643	509.75	5.544	509.40
5	537	577	4.575	554.70	4.581	554.57
6	647	692	2.479	668.31	2.486	668.26
7	728	814	1.610	764.63	1.610	764.61
8	827	908	1.086	865.48	1.087	865.49

1) For 12,000 K Planck function.

2) For nominal TOA spectrum.

Table 29. Shown here are the in-band band-averaged spectral radiances and center wavelengths versus slant path water vapor amount. The baseline spectrum (with no water vapor) is the nominal TOA spectrum from Barnes and Esaias (1997). The band averages for each band are calculated over the wavelengths in Table 28. The spectral radiances are given in terms of $\mathrm{mW\,cm^{-2}\,\mu m^{-1}\,sr^{-1}}$. The wavelengths are given in nanometers.

| Band | In-Band Band-Averaged Measurements | | | | | | | |
Number	Spectral[1] Radiance	Center[1] Wavelength	Spectral[2] Radiance	Center[2] Wavelength	Spectral[3] Radiance	Center[3] Wavelength	Spectral[4] Radiance	Center[4] Wavelength
1	8.910	413.39	8.910	413.39	8.910	413.39	8.910	413.39
2	8.462	444.12	8.462	444.12	8.462	444.12	8.462	444.12
3	6.646	490.62	6.646	490.62	6.646	490.62	6.646	490.62
4	5.544	509.40	5.544	509.40	5.544	509.40	5.544	509.40
5	4.581	554.57	4.579	554.57	4.577	554.56	4.575	554.55
6	2.486	668.26	2.471	668.29	2.457	668.32	2.443	668.35
7	1.610	764.61	1.600	764.61	1.591	764.62	1.582	764.62
8	1.087	865.49	1.071	865.51	1.057	865.54	1.044	865.59

1) WVSPA $= 0.000\,\mathrm{g\,cm^{-2}}$.

2) WVSPA $= 6.664\,\mathrm{g\,cm^{-2}}$.

3) WVSPA $= 13.328\,\mathrm{g\,cm^{-2}}$.

4) WVSPA $= 19.992\,\mathrm{g\,cm^{-2}}$.

Table 30. These are the integrated relative spectral responses ($\int R(\lambda)d\lambda$) for the SeaWiFS bands. These values are the denominators for (12) and (13). For each band, the wavelengths λ_a and λ_b mark the limits of the in-band response, and for each band, the wavelengths 380 and 1150 nm mark the limits of the total band response. The integrated responses are given in picoamperes and the wavelengths are given in nanometers. For each band, k_c is the ratio of the in-band response to the total band response.

Band Number	Integrated Response[1]	λ_a	λ_b	Integrated Response[2]	Ratio (k_c)
1	160.3505	395	433	159.3574	0.9938
2	259.1614	424	464	258.1423	0.9961
3	403.0866	471	511	399.5793	0.9913
4	508.3871	489	530	505.3296	0.9940
5	500.9510	537	577	488.2154	0.9746
6	496.5061	647	692	491.8024	0.9905
7	956.5129	728	814	940.6170	0.9834
8	1062.1624	827	908	1031.8517	0.9715

1) $\lambda_1 = 380$ and $\lambda_2 = 1{,}150$

2) $\lambda_1 = \lambda_a$ and $\lambda_2 = \lambda_b$

The out-of-band correction for bands 1, 2, 3, 4, and 7 are based strictly on models of the TOA spectra that Sea-WiFS will view. For bands 5, 6, and 8, Barnes and Yeh (1996) developed a technique for calculating the out-of-band response that uses the measured spectral radiances from several SeaWiFS bands. For SeaWiFS, this is the closest approximation to the actual TOA spectra on orbit, closer than any single model. For bands 5, 6, and 8, the uncertainty in the removal of the out-of-band response has been estimated at 0.3% (Barnes et al. 1997). The transfer of this uncertainty to that for the band-averaged center wavelengths for these bands is a matter of judgement. It is assumed that the 3 nm uncertainty in the center wavelength for band 8 will be decreased by about a factor of 4, using the out-of-band removal technique of Barnes and Yeh (1996). This would give an estimated uncertainty of 0.8 nm for the center wavelength for band 8. This estimate can also be applied to the band-averaged center wavelengths for bands 5 and 6.

The out-of-band correction of Barnes and Yeh (1996), however, cannot be directly applied to band-averaged spectral radiances and center wavelengths. That correction involves only the numerators of (12) and (13). The change in the limits of integration in these equations from 380–1,150 nm to the in-band response wavelengths for these bands also changes the value of the normalizing factor in the denominators of these equations.

Table 30 gives the integrated relative spectral responses for the SeaWiFS bands. The RSRs have been calculated as the response of the band to a source with a constant spectral radiance of $1 \, \mathrm{mW \, cm^{-2} \, \mu m^{-1} \, sr^{-1}}$ over the wavelength range from 380–1,150 nm (Barnes et al. 1994b). The response at each 1 nm interval is given as picoamperes of current from the photodiode. The response is integrated over the wavelength range for the total band response, 380–1,150 nm, and over the range for the in-band response. The wavelength limits for the in-band integration are also listed in the table. Table 30 also gives the correction factor, k_c, which is the ratio of the integrated in-band response to the integrated total band response.

The application of the out-of-band response requires a modification of the equations in Barnes and Yeh (1996). For SeaWiFS band 1 (412 nm) as an example, the out-of-band correction for the band-averaged spectral radiance has the form

$$L_{IB}(\lambda_{IB}) = \frac{k_{b'}(412)L_B(\lambda_B)}{k_c(412)}, \qquad (14)$$

where $L_{IB}(\lambda_{IB})$ is the in-band averaged spectral radiance with its associated center wavelength, $k_{b'}(412)$ is the correction factor from Table 10 of Barnes et al. (1997), $L_B(\lambda_B)$ is the total band-averaged spectral radiance with its associated center wavelength, and $k_c(412)$ is the correction factor from Table 30.

$L_B(\lambda_B)$, the input to this correction scheme, has been represented mathematically in (12). For SeaWiFS band 1 (412 nm), $k_{b'}(412)$ acts as a correction to the numerator of (12), and $k_c(412)$ acts as a correction to the denominator. The values of $k_{b'}(412)$ and $k_c(412)$ have been calculated using the band 1 (412 nm) RSR and the nominal TOA spectrum from Barnes and Esaias (1997), which is assumed to be the best model of the actual TOA radiance.

For SeaWiFS bands 5, 6, and 8, the values of $k_{b'}$ are intended as initial values for the corrections in Sect. 2.5.3 and 2.5.4 of Barnes and Yeh (1996). The corrections in those sections are based on SeaWiFS measurements on orbit, rather than a TOA radiance model. The values of k_c come from the laboratory measurements of the RSRs of the SeaWiFS bands and are unrelated to the source spectral shape.

It is possible to perform a consistency check of the out-of-band removal scheme using the total band and in-band spectral radiances in Tables 26 and 28, plus the values of

Table 31. Listed here are the SeaWiFS in-band band-averaged center wavelengths on orbit. It is a general procedure to refer to each band by its nominal center wavelength. The band-averaged center wavelengths come from Table 28. The laboratory uncertainty comes from an estimate of the spectral shape uncertainty (Sect. 4).

Band Number	Nominal Center Wavelength [nm]	Band-Averaged Center Wavelength [nm]	Uncertainty From Laboratory Calibration [nm]	Uncertainty From On-Orbit Source Spectral Shape [nm]	RSS Wavelength Uncertainty [nm]
1	412	413.4	0.5	0.3	0.6
2	443	444.1	0.5	0.3	0.6
3	490	490.6	0.5	0.3	0.6
4	510	509.4	0.5	0.3	0.6
5	555	554.6	0.5	0.8	0.9
6	670	668.3	0.5	0.8	0.9
7	765	764.6	0.5	0.3	0.6
8	865	865.5	0.5	0.8	0.9

Table 32. Listed here are the uncertainties in the SeaWiFS in-band band-averaged spectral radiances from TOA spectral factors. The uncertainties include only those in the corrections to remove atmospheric absorbers and out-of-band response. This does not include uncertainties from the laboratory calibration of the instrument, which may be as high as 5% (absolute) and 2% (band-to-band), nor does it include any uncertainties in the transfer of the laboratory calibration to orbit.

Band Number	Water Vapor Correction [%]	Oxygen A-Band Correction [%]	Out-of-Band Correction [%]	RSS Spectral Radiance Uncertainty [%]
1	0.0	0.0	0.1	0.1
2	0.0	0.0	0.1	0.1
3	0.0	0.0	0.1	0.1
4	0.0	0.0	0.1	0.1
5	0.0	0.0	0.3	0.3
6	0.0	0.0	0.3	0.3
7	0.0	0.8	0.1	0.8
8	0.3	0.0	0.3	0.4

$k_{b'}(412)$ in Table 10 of Barnes et al. (1997) and the values of k_c from Table 30. The following calculation is made for band 1 (412 nm) in units of $mW\,cm^{-2}\,\mu m^{-1}\,sr^{-1}$. It is a solution to (14).

$$L_{IB}(413.4) = \frac{0.9951(8.894)}{0.9938} \tag{15}$$
$$= 8.906.$$

This calculated spectral radiance is about 0.05% lower than the value of 8.910 $mW\,cm^{-2}\,\mu m^{-1}\,sr^{-1}$ in Table 28. For the eight SeaWiFS bands, the calculated spectral radiances average 0.03% lower than the corresponding values in Table 28. In all cases, the agreement is better than 0.1%.

5.5 CONCLUDING REMARKS

Based on the analysis presented here, it is recommended that band-averaged spectral radiances be used in the analysis of on-orbit measurements by SeaWiFS. It is also recommended that the measured spectral radiances from orbit be corrected for absorption by water vapor and oxygen in the atmosphere and for out-of-band response. In particular, the out-of-band correction can decrease the uncertainty in the center wavelength for band 8 (865 nm) from about 3 nm (for the total band response) to about 0.8 nm (for the in-band response).

The on-orbit in-band band-averaged center wavelengths and their uncertainties are listed in Table 31. These include the uncertainties derived from the source spectral shape on orbit, as well as estimates in the uncertainty of the wavelength characterization of the bands in the laboratory. The estimate of the laboratory uncertainty comes from a superficial review of the wavelength characterization of the monochromatic light source at SBRS, which was characterized using mercury emission lines. It is important to note that SeaWiFS does not include a mechanism to determine shifts in the center wavelengths of the bands since their characterization by SBRS in 1993. The characterization of wavelength shifts, if that is possible at all, must come from the analysis of flight measurements from the instrument.

Listed in Table 32 are the uncertainties in the on-orbit in-band band-averaged spectral radiances from SeaWiFS due to TOA spectral factors; these uncertainties are small. For band 7 (765 nm), the uncertainty due to oxygen A-band absorption is more substantial, deriving from the 10–15% attenuation of the upwelling radiance in the in-band portion of the band's response. The uncertainties in Table 32 do not include the uncertainties in the radiometric calibration of the instrument. These uncertainties may be as high as 5% in the absolute calibration of the bands and as high as 2% in the band-to-band calibration of the instrument. Finally, the uncertainties in Table 32 do not include the uncertainty in the transfer of the laboratory calibration of the instrument to orbit.

Chapter 6

The SeaWiFS Temperature Calibration

ROBERT E. EPLEE, JR.
ROBERT A. BARNES
General Sciences Corporation, Laurel, Maryland

ABSTRACT

The radiometric calibration of SeaWiFS data includes a correction for the temperature dependence of the individual detector sensitivities. The detector temperatures are measured by temperature sensors mounted on the instrument focal planes. Processing of the temperature sensor output by an onboard instrument computer introduces a nonlinear response into the temperature data. This chapter describes the calibration of the temperature sensor output and the computation of the temperature corrections for the radiometric calibration of the instrument.

6.1 INTRODUCTION

The radiometric calibration equation for SeaWiFS data includes a correction for the temperature dependence of the sensitivity of the individual detectors. This multiplicative correction to the calibration has the form (Barnes et al. 1994b):

$$F(T) = 1.0 + K_3(T - T_{\text{ref}}), \qquad (16)$$

where K_3 is the temperature dependency coefficient for the detector, T is the detector temperature, and T_{ref} is the reference temperature for the detector (Table 33).

Table 33. These temperature parameters are detector-specific. The data are from the SeaWiFS Calibration and Acceptance Data Package.

Band Number	K_3 $[(°\text{C})^{-1}]$	T_{ref} $[°\text{C}]$
1	0.000901	20.0
2	0.000585	20.0
3	0.000420	20.0
4	0.000390	20.0
5	0.000391	20.0
6	0.000151	20.0
7	0.000106	20.0
8	0.000078	20.0

The detector temperatures are measured by temperature sensors mounted on the instrument focal planes. Since two detectors are located on each focal plane, the detector temperatures for bands 1 and 2 are the same, as are those for bands 3 and 4, 5 and 6, and 7 and 8. The SeaWiFS temperature calibration entails deriving the focal plane temperatures from the temperature sensors and computing the temperature corrections for the radiometric calibration of the data.

6.2 TEMPERATURES

A SeaWiFS focal plane temperature sensor is composed of a precision negative temperature coefficient thermistor, in parallel with a load resistor, which is driven by a current source diode and buffered by a noninverting unity-gain operational amplifier. The output of the sensor is the voltage across the thermistor–resistor pair and has a range of 0.0–5.1 V. The SeaWiFS Interface Unit (SIU), an onboard instrument computer, uses an analog-to-digital converter (ADC) to change the analog temperature sensor voltages into 8-bit digital telemetry data.

The sensor calibration data provided by SBRS, the instrument builder, in the SeaWiFS Calibration and Acceptance Data Package (an SBRS internal document) shows that there should be a linear relationship between the focal plane temperatures and the temperature sensor voltages output from the SIU. The temperature sensor voltage is defined by:

$$V_T = K_5 C_T + K_6, \qquad (17)$$

where K_5 is the ADC conversion factor for temperature sensors, K_6 is the ADC offset for the temperature sensors (Table 34), and C_T is the 8-bit temperature sensor voltage in counts.

V_T runs from 0.0–5.1 V as C_T runs from 0–255 counts. An approximate relationship between the temperature sensor voltages and the corresponding focal plane temperatures, in degrees Celsius, is given by:

$$T_C = (5.0 - V_T)\frac{40.0}{3.0}. \qquad (18)$$

Table 34. These temperature parameters are focal-plane specific. The data are from the SeaWiFS Calibration and Acceptance Data Package.

Focal Plane	K_5 [V/count]	K_6 [V]	K_7 [mA]	R_L [$k\Omega$]
1/2	0.020	0.0	0.493	16.2
3/4	0.020	0.0	0.492	16.2
5/6	0.020	0.0	0.491	16.2
7/8	0.020	0.0	0.486	16.2
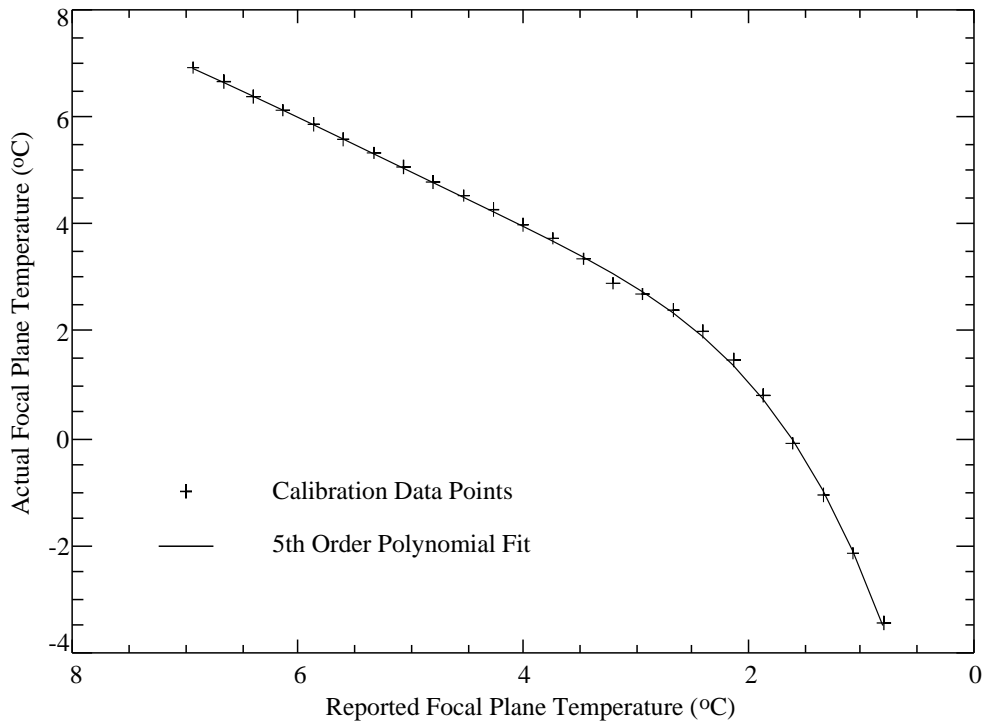
Fig. 19. Actual focal plane temperatures measured by OSC during the SIU calibration are plotted as a function of reported temperatures. A 5th order polynomial has been fit to the temperatures to reduce the noise in the data.

Table 35. These data provide the SIU temperature calibration. The reported and actual temperature data were provided by J. McCarthy of OSC.

C_T [counts]	Reported Temp. [°C]	Actual Temp. [°C]	Fitted Temp. [°C]
224	6.933	6.933	6.923
225	6.667	6.667	6.667
226	6.400	6.400	6.407
227	6.133	6.133	6.143
228	5.867	5.867	5.875
229	5.600	5.600	5.605
230	5.333	5.333	5.333
231	5.067	5.067	5.060
232	4.800	4.800	4.788
233	4.533	4.533	4.516
234	4.267	4.267	4.244
235	4.000	4.000	3.969
236	3.733	3.733	3.689
237	3.467	3.350	3.396
238	3.200	2.900	3.083
239	2.933	2.700	2.740
240	2.667	2.400	2.352
241	2.400	2.000	1.903
242	2.133	1.450	1.373
243	1.867	0.800	0.737
244	1.600	−0.100	−0.033
245	1.333	−1.050	−0.971
246	1.067	−2.150	−2.114
247	0.800	−3.450	−3.506
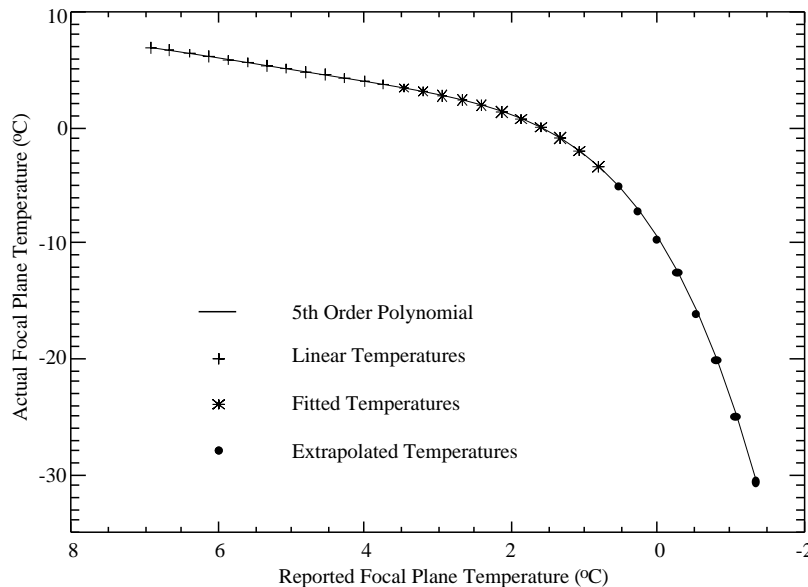
Fig. 20. The 5th order polynomial was used to extrapolate the focal plane temperatures over the full range of temperature sensor voltages (224–255 counts). The data points indicated by (+) are where the reported and actual temperatures are in agreement. The data points indicated by (✷) are the polynomial fit to the calibration data. The data points indicated by (•) are the extrapolated temperatures.
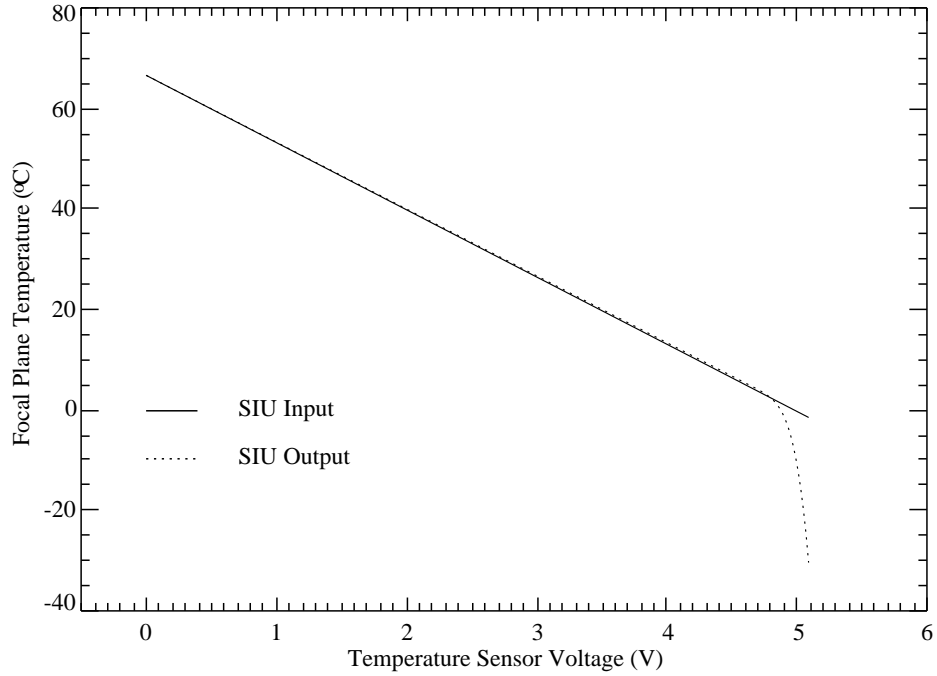
Fig. 21. Focal plane temperatures are plotted as a function of temperature sensor voltage. The data given by the solid line are the linear temperature sensor input to the SIU. The data given by the dotted line are the nonlinear response of the SIU at low temperatures.
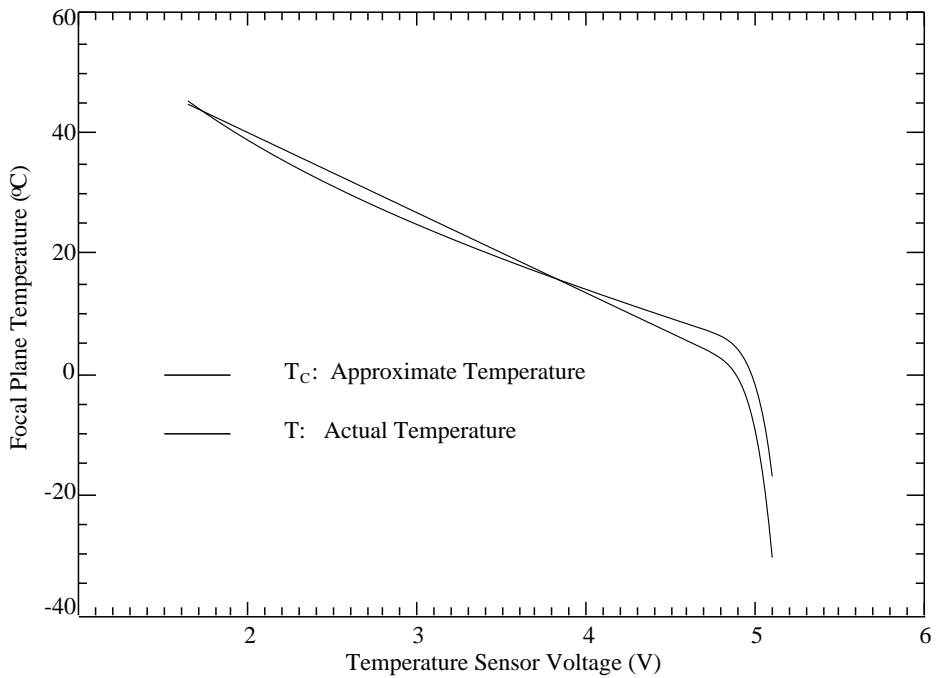

Fig. 22. Focal plane temperatures are plotted as a function of temperature sensor voltage. The data given by the solid line are the approximate temperatures, T_C. The data given by the dotted line are the actual temperatures computed from (22).
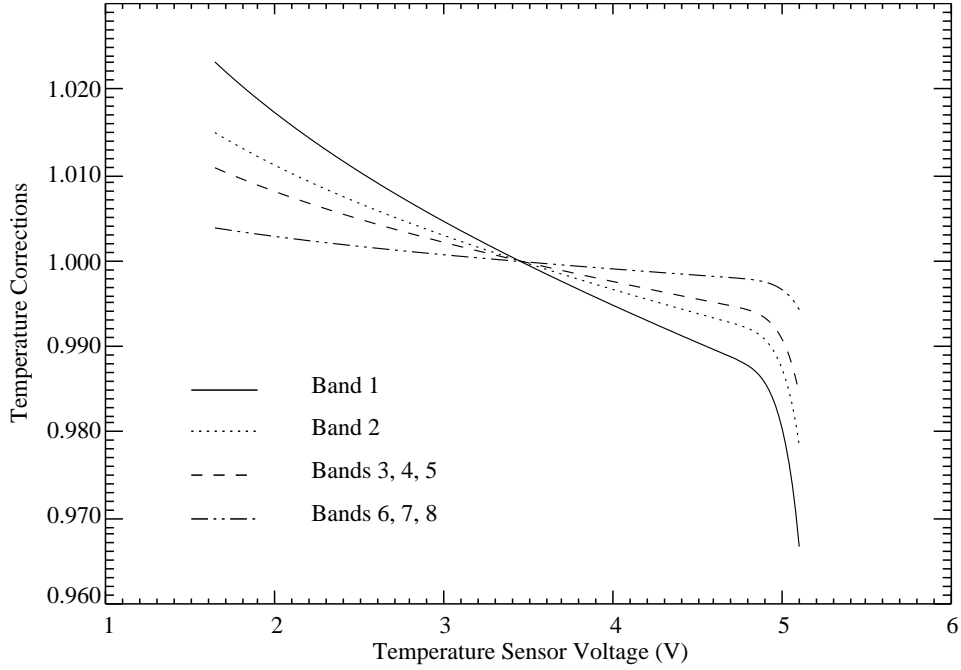
Fig. 23. The temperature corrections for all 8 bands are plotted over the full range of temperature sensor voltages. On this scale, the corrections for bands 3, 4, and 5 and for bands 6, 7, and 8 overlap. Note that $V_T = 3.5$ V at $T_{\text{ref}} = 20.0°$C, where the corrections are unity.
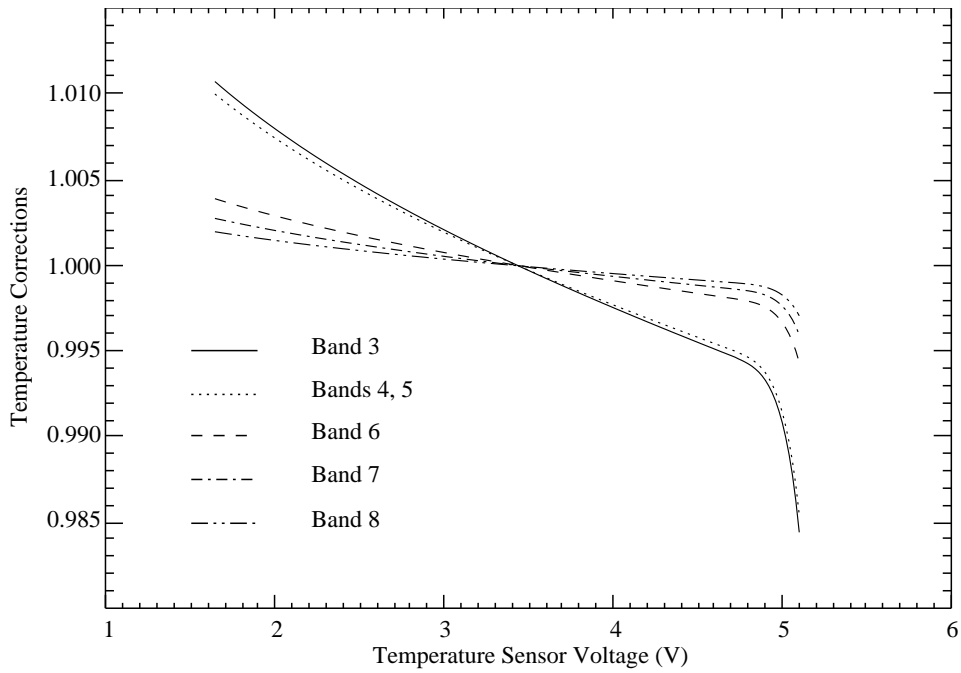
Fig. 24. Temperature corrections for bands 3–8 are plotted over the full range of temperature sensor voltages. Note that $V_T = 3.5$ V at $T_{\text{ref}} = 20.0°$C, where the corrections are unity.
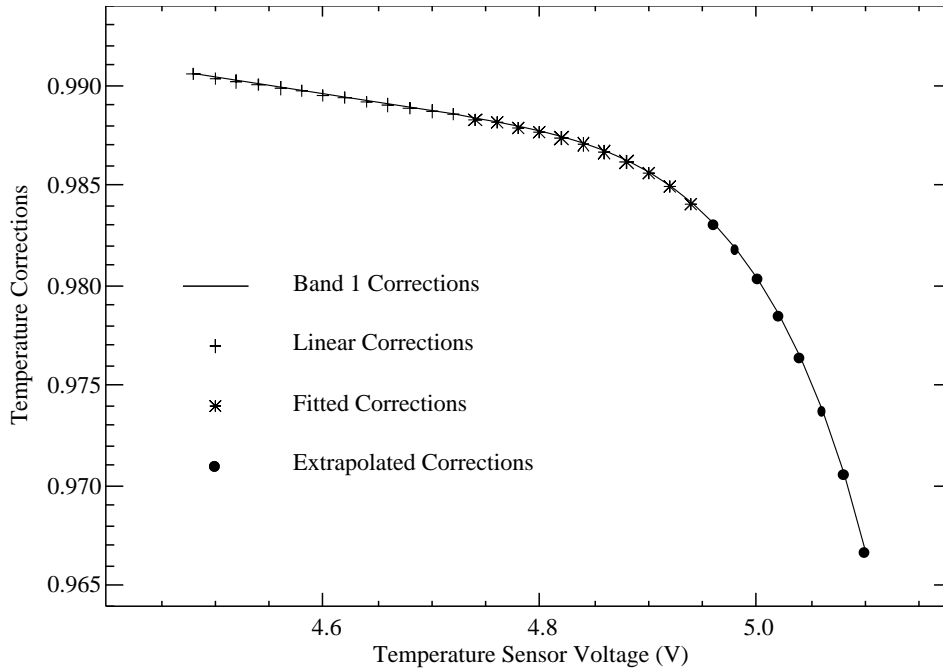
Fig. 25. Band 1 temperature corrections for fitted and extrapolated data are plotted over the range of the fitted and extrapolated SIU data. The data points indicated by (+) are where the reported and actual focal plane temperature are in agreement. The data points indicated by (✳) are where the polynomial was fit to the calibration data. The data points indicated by (●) are where the polynomial was extrapolated to the full range of temperature sensor voltages.

6.3 NONLINEARITIES

There is a clamping circuit in the SIU that prevents saturation of the ADC. This circuit introduces a nonlinear response into the temperature sensors at temperatures below approximately 7°C. OSC calibrated the nonlinear response of the SIU by applying known voltages (corresponding to specific focal plane temperatures) to the input of the SIU while heating the SIU to these simulated temperatures. The calibration data are shown in Table 35 and are plotted in Fig. 19. The digital voltage output of the SIU was converted to the reported temperatures using (17) and (18) and was compared to the actual measured temperature of the SIU. The calibration was performed for 24 temperatures over a range of 7°C to −4°C (C_T over a range of 224–247). The measured temperatures started to diverge from the reported temperatures below 3.7°C (when $C_T > 236$).

6.4 REVISED TEMPERATURES

The SeaWiFS Project's Calibration and Validation Team used the SIU calibration data in Table 35 to generate an array of actual focal plane temperatures for the temperature sensor voltages output by the SIU. A 5th-order polynomial was fit to the measured temperatures in order to reduce the noise in the data (Fig. 19). An order of 5 was necessary to minimize the deviations of the fitted temperatures from the reported temperatures over the range of 7°C to 3.7°C, where the reported temperatures agreed with the measured temperatures. The polynomial was used to extrapolate the temperature response of the SIU out to $C_T = 255$ (Fig. 20). An array of focal plane temperatures, T_C, was generated based on (18), where the extant temperatures were replaced by the fitted or extrapolated temperatures from the calibration for temperatures below 3.7°C (for C_T over the range 237–255). Then, (17) was used to generate a set of corresponding temperature sensor voltages (Fig. 21).

6.5 TEMPERATURE CORRECTION

Using the algorithm specified in Barnes et al. (1994b), a new lookup table of temperature corrections was generated for the SeaWiFS sensor calibration model, based on the values of T_C and V_T, which incorporate the nonlinear response of the SIU. There is an entry in the lookup table for all eight detectors over the full range of C_T (0–255).

The temperatures of the focal planes are computed from the temperature sensors as follows. The current from the current source diode, in milliamperes, is:

$$ICS = K_7 - 0.0013(T_C - T_{\text{ref}}), \tag{19}$$

where K_7 is the current from the diode at T_{ref} (Table 34).

The effective resistance of the thermistor-resistor pair, in $k\Omega$, is:

$$R_E = \frac{V_T}{ICS}. \tag{20}$$

61

The actual resistance of the thermistor, in kΩ, is:

$$R_{\mathrm{Th}} = \frac{R_L R_E}{R_L - R_E}, \tag{21}$$

where R_L is the load resistance (Table 34).

The focal plane temperature, in degrees Celsius, is:

$$T = -341.0 + \frac{5398.94}{\ln(254898.0 \ R_{\mathrm{Th}})}. \tag{22}$$

The temperature correction term is computed from (16). The resulting lookup table of temperature correction terms was incorporated into the SeaWiFS calibration table. Fig-

ure 22 shows plots of T_C and T as functions of V_T computed during this process. Figures 23 and 24 show the temperature corrections computed for all eight bands over the full range of C_T. Note that $V_T = 3.5\,\mathrm{V}$ at $T_{\mathrm{ref}} = 20.0°\mathrm{C}$. Figure 25 shows the temperature corrections for band 1 (the band with the largest temperature dependence) over the range of the fitted and extrapolated data from the SIU calibration. OSC reports that the coldest the focal planes should get before the focal plane heaters turn on is $-8°\mathrm{C}$. This temperature is encompassed within the first three extrapolated data points plotted in Fig. 25. The correction for band 1 at the third extrapolated data point ($-9.691°\mathrm{C}$) is 0.980309; in this extreme case, the temperature correction to the radiometric calibration is only 2%.

R.A. Barnes, R.E. Eplee, Jr., E-n. Yeh, and W.E. Esaias

Glossary

ADC	Analog-to-Digital Converter
AFGL	Air Force Geophysics Laboratory
FWHM	Full-Width at Half-Maximum
GSFC	Goddard Space Flight Center
NASA	National Aeronautics and Space Administration
NIST	National Institute of Standards and Technology
OSC	Orbital Sciences Corporation
RSR	Relative Spectral Response
RSS	Root Square Sum
SBRS	(Hughes) Santa Barbara Research Sensing
SCADP	SeaWiFS Calibration and Data Package (SBRS internal report)
SeaWiFS	Sea-viewing Wide Field-of-View Sensor
SIRREX-5	Fifth SeaWiFS Intercalibration Round-Robin Experiment
SIS	Spherical Integrating Source
SIU	SeaWiFS Interface Unit
SXR	SeaWiFS Transfer Radiometer
TOA	Top-of-the-Atmosphere

Symbols

$a(\lambda)$ The absorption cross section as a function of wavelength.

a_0 Fitted coefficient.

a_1 Fitted coefficient.

b The pathlength in centimeters.

b_1 Fitted coefficient.

B Bandwidth (in nanometers).

c The concentration of the absorber in per cubic centimeters.

C_T Temperature sensor voltage in counts.

$e^{-\alpha(\lambda)\mu}$ The fractional transmittance through an atmosphere of airmass μ at wavelength λ for an absorbance of $\alpha(\lambda)$.

$F(T)$ Temperature correction to the radiometric calibration.

$I(\lambda)$ The intensity of light with absorption as a function of wavelength.

ICS Current source diode current.

$I_0(\lambda)$ The intensity of light in the absence of absorption as a function of wavelength.

k_b Out-of-band correction factor.

$k_{b'}(412)$ Correction factor (from Table 10 of Barnes et al. 1997).

$k_c(412)$ Correction factor (from Table 30).

K_3 Temperature dependency coefficient for the detectors.

K_5 ADC conversion factor for the temperature sensors.

K_6 ADC offset for the temperature sensors.

K_7 Current source diode current at T_{ref}.

$L_B(\lambda_B)$ Band-averaged spectral radiance with its associated center wavelength.

L_e Spectral radiance from the source.

$L_e(\lambda)$ Spectral radiance from the source at a given wavelength.

$L_{IB}(\lambda_{IB})$ In-band averaged spectral radiance with its associated center wavelength.

L_s Sphere spectral radiance integrated over the SeaWiFS spectral response.

$L_s(\lambda)$ Spectral radiance from the source at a given wavelength.

$L_{typical}$ Typical radiances from the SeaWiFS specifications.

P_s Surface pressure (in millibars).

R Spectral response.

$R(\lambda)$ Spectral response of the band at a given wavelength.

R_{IB} In-band response.

R_L Load resistance.

R_{Th} Actual thermistor resistance.

R_T Total band response.

T Detector temperature.

T_C Focal plane temperature.

T_{DG} Fractional transmittances from Ding and Gordon (1995),

T_F The system level transmittances from the absorption spectrum of Fraser (1995).

T_M System level transmittances for `MODTRAN7`.

T_{ref} Detector reference temperature.

V_T Temperature sensor voltage.

W Ozone equivalent bandwidth (in nanometers).

W/B Fractional absorption.

α Absorption coefficient in per units of airmass.

$\alpha(\lambda)$ The ozone absorption coefficient per unit airmass at a given wavelength.

α_{DG} Effective ozone absorptions from calculations using fractional transmittances from Ding and Gordon (1995).

α_F Effective ozone absorptions from calculations using the oxygen spectrum from Fraser (1995).

α_M Effective ozone absorption from calculations using the oxygen spectrum from `MODTRAN7`.

λ Wavelength.

λ_B Band-weighted center wavelength.

λ_{eff} Effective center wavelength, that is, the wavelength where $L_s(\lambda)$ equals $L_B(\lambda_B)$.

λ_m Wavelength for maximum radiance.

λ_1 Lower limits of integration.

λ_2 Upper limits of integration.

μ The airmass.

σ Rayleigh scattering cross section per molecule.

θ_v Viewing angle of the instrument.

θ_0 Solar zenith angle.

References

Barnes, R.A., 1994: *SeaWiFS Data: Actual and Simulated.* [World Wide Web page.] From URLs: `http://seawifs .gsfc.nasa.gov/SEAWIFS/IMAGES/spectra1.dat` and `/spectra2.dat` NASA Goddard Space Flight Center, Greenbelt, Maryland.

——, 1996a: "Calculation of an equivalent blackbody temperature for the GSFC sphere." In Barnes, R.A., E-n. Yeh, and R.E. Eplee, 1996: SeaWiFS Calibration Studies, Part 1. *NASA Tech. Memo. 104566, Vol. 39,* S.B. Hooker and E.R. Firestone, Eds., NASA Goddard Space Flight Center, Greenbelt, Maryland, 5–17.

——, 1996b: "A comparison of the spectral response of Sea-WiFS and the SeaWiFS Transfer Radiometer." In Barnes, R.A., E-n. Yeh, and R.E. Eplee, 1996: SeaWiFS Calibration Topics, Part 1, *NASA Tech. Memo. 104566, Vol. 39,* S.B. Hooker and E.R. Firestone, Eds., NASA Goddard Space Flight Center, Greenbelt, Maryland, 39–48.

——, 1997a: *SeaWiFS Data: Actual and Simulated* [World Wide Web Page.] From URLs: `http//seawifs` `.gsfc.nasa.gov/SEAWIFS/IMAGES/spectra3.dat` and `/spectra4.dat`, NASA Goddard Space Flight Center, Greenbelt, Maryland.

——, 1997b: "The effect of atmospheric absorption on the output of SeaWiFS band 7." In Barnes, R.A., R.E. Eplee, Jr., E-n. Yeh, and W.E. Esaias, 1997b: SeaWiFS Calibration Topics, Part 2, *NASA Tech. Memo. 104566, Vol. 40,* S.B. Hooker and E.R. Firestone, Eds., NASA Goddard Space Flight Center, Greenbelt, Maryland, 23–38.

——, 1997c: "SeaWiFS Measurements in Orbit: Band-Averaged Spectral Radiances." In Barnes, R.A., R.E. Eplee, Jr., E-n. Yeh, and W.E. Esaias, 1997c: SeaWiFS Calibration Topics, Part 2, *NASA Tech. Memo. 104566, Vol. 40,* S.B. Hooker and E.R. Firestone, Eds., NASA Goddard Space Flight Center, Greenbelt, Maryland, 48–55.

——, A.C. Holland, and H.S. Lee, 1986: An improved rocket ozonesonde (ROCOZ-A) 2. Preparation of Stratospheric Ozone Profiles, *J. Geophys. Res.,* **91,** 14,521–14,531.

——, W.L. Barnes, W.E. Esaias, and C.R. McClain, 1994a: Prelaunch Acceptance Report for the SeaWiFS Radiometer. *NASA Tech. Memo. 104566, Vol. 22,* S.B. Hooker and E.R. Firestone, Eds., NASA Goddard Space Flight Center, Greenbelt, Maryland, 32 pp.

——, A.W. Holmes, W.L. Barnes, W.E. Esaias, C.R. McClain, and T. Svitek, 1994b: SeaWiFS Prelaunch Radiometric Calibration and Spectral Characterization. *NASA Tech. Memo. 104566, Vol. 23,* S.B. Hooker and E.R. Firestone, Eds., NASA Goddard Space Flight Center, Greenbelt, Maryland, 55 pp.

——, W.E. Esaias, and C.R. McClain, 1995: "A proposed on-orbit, out-of-band correction scheme for SeaWiFS." In McClain, C.R., K. Arrigo, W.E. Esaias, M. Darzi, F.S. Patt, R.H. Evans, J.W. Brown, C.W. Brown, R.A. Barnes, and L. Kumar, 1995: SeaWiFS Algorithms, Part 1, *NASA Tech. Memo. 104566, Vol. 28,* S.B. Hooker and E.R. Firestone, Eds., NASA Goddard Space Flight Center, Greenbelt, Maryland, 20–25.

——, R.E. Eplee, and E-n. Yeh, 1996: SeaWiFS Calibration Topics, Part 1, *NASA Tech. Memo. 104566, Vol. 39,* S.B. Hooker and E.R. Firestone, Eds., NASA Goddard Space Flight Center, Greenbelt, Maryland, 66 pp.

——, and E-n. Yeh, 1996: "The effects of source spectral shape on SeaWiFS radiance measurements." In Barnes, R.A., E-n. Yeh, and R.E. Eplee, 1996: SeaWiFS Calibration Topics, Part 1. *NASA Tech. Memo. 104566, Vol. 39,* S.B. Hooker and E.R. Firestone, Eds., NASA Goddard Space Flight Center, Greenbelt, Maryland, 18–38.

——, and W.E. Esaias, 1997: "A nominal top-of-the-atmosphere spectrum for SeaWiFS." In Barnes, R.A., R.E. Eplee, Jr., E-n. Yeh, and W.E. Esaias, 1997c: SeaWiFS Calibration Topics, Part 2, *NASA Tech. Memo. 104566, Vol. 40,* S.B. Hooker and E.R. Firestone, Eds., NASA Goddard Space Flight Center, Greenbelt, Maryland, 3–11.

——, R.E. Eplee, Jr., and E-n. Yeh, 1997: "SeaWiFS measurements in orbit: spectral radiances at the nominal center wavelengths." In Barnes, R.A., R.E. Eplee, Jr., E-n. Yeh, and W.E. Esaias, 1997c: SeaWiFS Calibration Topics, Part 2, *NASA Tech. Memo. 104566, Vol. 40,* S.B. Hooker and E.R. Firestone, Eds., NASA Goddard Space Flight Center, Greenbelt, Maryland, 12–22.

Brasseur, G., and S. Solomon, 1986: *Aeronomy of the Middle Atmosphere: Chemistry and Physics of the Stratosphere and Mesosphere, Second Edition.* D. Reidel Publishing Co., Hingham, Massachusetts, 452 pp.

Chamberlain, J.W., and D.M. Hunten, 1987: *Theory of Planetary Atmo- spheres, 2nd edition,* Academic Press, New York, 481 pp.

Chapman, S., 1931: The absorption and dissociative or ionizing effect of monochromatic radiation in an atmosphere on a rotating Earth. 2. Grazing incidence, *Proc. Phys. Soc. London,* **43**, 483–501.

Ding, K., and H.R. Gordon, 1994: Analysis of the influence of O_2 "A" band absorption on atmospheric correction of ocean color imagery. *Appl. Opt.,* **34,** 2,068–2,080.

——, and H.R. Gordon, 1995: Analysis of the influence of O_2 A-band absorption on atmospheric correction of ocean-color imagery. *Appl. Opt.,* **34,** 2,068–2,080.

Evans, R.H., and H.R. Gordon, 1994: Coastal Zone Color Scanner "system calibration:" a retrospective examination. *J. Geophys. Res.,* **99,** 7,293–7,307.

Fraser, R.S., 1995: "The effect of oxygen absorption on Sea-WiFS band 7 radiance." In Mueller, J.L., R.S. Fraser, S.F. Biggar, K.J. Thome, P.N. Slater, A.W. Holmes, R.A. Barnes, C.T. Weir, D.A. Siegel, D.W. Menzies, A.F. Michaels, and G. Podesta, 1995: Case Studies for SeaWiFS Calibration and Validation, Part 3. *NASA Tech. Memo. 104566, Vol. 27,* S.B. Hooker and E.R. Firestone, Eds., NASA Goddard Space Flight Center, Greenbelt, Maryland, 16–19.

Gordon, H.R., 1995: Remote sensing of ocean color: a methodology for dealing with broad spectral bands and significant out-of-band response. *Appl. Opt.,* **34,** 8,363–8,374.

——, and M. Wang, 1994: Retrieval of water-leaving radiance and aerosol optical thickness over the oceans with Sea-WiFS: a preliminary algorithm. *Appl. Opt.,* **33,** 443–452.

Hooker, S.B., W.E. Esaias, G.C. Feldman, W.W. Gregg, and C.R. McClain, 1992: An Overview of SeaWiFS and Ocean Color. *NASA Tech. Memo. 104566, Vol. 1,* S.B. Hooker and E.R. Firestone, Eds., NASA Goddard Space Flight Center, Greenbelt, Maryland, 24 pp., plus color plates.

Kidder, S.Q., and T.H. Vonder Haar, 1995: *Satellite Meteorology,* Academic Press, New York, 466 pp.

Mitchell, A.C.G., and M.W. Zemansky, 1961: *Resonance Radiation and Excited Atoms,* Cambridge University Press, London, 481 pp.

Okabe, H., 1978: *Photochemistry of Small Molecules,* Wiley Interscience, New York, 431 pp.

Rothman, L.S., R.R. Gamache, A. Barbe, A. Goldman, J.R. Gillis, L.R. Brown, R.A. Toth, J-M. Flaud, and C. Carny-Peyret, 1983: AFGL Atmospheric Absorption Line Parameters: 1982 Edition. *Appl. Opt.,* **22,** 2,247–2,256.

Swider, W., and M.E. Gardner, 1967: On the Accuracy of Certain Approximations for the Chapman Function, *Environmental Research Papers No. 272,* Air Force Cambridge Research, Bedford, Massachusetts.

The SeaWiFS Technical Report Series

Vol. 1

Hooker, S.B., W.E. Esaias, G.C. Feldman, W.W. Gregg, and C.R. McClain, 1992: An Overview of SeaWiFS and Ocean Color. *NASA Tech. Memo. 104566, Vol. 1,* S.B. Hooker and E.R. Firestone, Eds., NASA Goddard Space Flight Center, Greenbelt, Maryland, 24 pp., plus color plates.

Vol. 2

Gregg, W.W., 1992: Analysis of Orbit Selection for SeaWiFS: Ascending vs. Descending Node. *NASA Tech. Memo. 104566, Vol. 2,* S.B. Hooker and E.R. Firestone, Eds., NASA Goddard Space Flight Center, Greenbelt, Maryland, 16 pp.

Vol. 3

McClain, C.R., W.E. Esaias, W. Barnes, B. Guenther, D. Endres, S.B. Hooker, G. Mitchell, and R. Barnes, 1992: Calibration and Validation Plan for SeaWiFS. *NASA Tech. Memo. 104566, Vol. 3,* S.B. Hooker and E.R. Firestone, Eds., NASA Goddard Space Flight Center, Greenbelt, Maryland, 41 pp.

Vol. 4

McClain, C.R., E. Yeh, and G. Fu, 1992: An Analysis of GAC Sampling Algorithms: A Case Study. *NASA Tech. Memo. 104566, Vol. 4,* S.B. Hooker and E.R. Firestone, Eds., NASA Goddard Space Flight Center, Greenbelt, Maryland, 22 pp., plus color plates.

Vol. 5

Mueller, J.L., and R.W. Austin, 1992: Ocean Optics Protocols for SeaWiFS Validation. *NASA Tech. Memo. 104566, Vol. 5,* S.B. Hooker and E.R. Firestone, Eds., NASA Goddard Space Flight Center, Greenbelt, Maryland, 43 pp.

Vol. 6

Firestone, E.R., and S.B. Hooker, 1992: SeaWiFS Technical Report Series Cumulative Index: Volumes 1–5. *NASA Tech. Memo. 104566, Vol. 6,* S.B. Hooker and E.R. Firestone, Eds., NASA Goddard Space Flight Center, Greenbelt, Maryland, 9 pp.

Vol. 7

Darzi, M., 1992: Cloud Screening for Polar Orbiting Visible and IR Satellite Sensors. *NASA Tech. Memo. 104566, Vol. 7,* S.B. Hooker and E.R. Firestone, Eds., NASA Goddard Space Flight Center, Greenbelt, Maryland, 7 pp.

Vol. 8

Hooker, S.B., W.E. Esaias, and L.A. Rexrode, 1993: Proceedings of the First SeaWiFS Science Team Meeting. *NASA Tech. Memo. 104566, Vol. 8,* S.B. Hooker and E.R. Firestone, Eds., NASA Goddard Space Flight Center, Greenbelt, Maryland, 61 pp.

Vol. 9

Gregg, W.W., F.C. Chen, A.L. Mezaache, J.D. Chen, J.A. Whiting, 1993: The Simulated SeaWiFS Data Set, Version 1. *NASA Tech. Memo. 104566, Vol. 9,* S.B. Hooker, E.R. Firestone, and A.W. Indest, Eds., NASA Goddard Space Flight Center, Greenbelt, Maryland, 17 pp.

Vol. 10

Woodward, R.H., R.A. Barnes, C.R. McClain, W.E. Esaias, W.L. Barnes, and A.T. Mecherikunnel, 1993: Modeling of the SeaWiFS Solar and Lunar Observations. *NASA Tech. Memo. 104566, Vol. 10,* S.B. Hooker and E.R. Firestone, Eds., NASA Goddard Space Flight Center, Greenbelt, Maryland, 26 pp.

Vol. 11

Patt, F.S., C.M. Hoisington, W.W. Gregg, and P.L. Coronado, 1993: Analysis of Selected Orbit Propagation Models for the SeaWiFS Mission. *NASA Tech. Memo. 104566, Vol. 11,* S.B. Hooker, E.R. Firestone, and A.W. Indest, Eds., NASA Goddard Space Flight Center, Greenbelt, Maryland, 16 pp.

Vol. 12

Firestone, E.R., and S.B. Hooker, 1993: SeaWiFS Technical Report Series Cumulative Index: Volumes 1–11. *NASA Tech. Memo. 104566, Vol. 12,* S.B. Hooker and E.R. Firestone, Eds., NASA Goddard Space Flight Center, Greenbelt, Maryland, 28 pp.

Vol. 13

McClain, C.R., K.R. Arrigo, J. Comiso, R. Fraser, M. Darzi, J.K. Firestone, B. Schieber, E-n. Yeh, and C.W. Sullivan, 1994: Case Studies for SeaWiFS Calibration and Validation, Part 1. *NASA Tech. Memo. 104566, Vol. 13,* S.B. Hooker and E.R. Firestone, Eds., NASA Goddard Space Flight Center, Greenbelt, Maryland, 52 pp., plus color plates.

Vol. 14

Mueller, J.L., 1993: The First SeaWiFS Intercalibration Round-Robin Experiment, SIRREX-1, July 1992. *NASA Tech. Memo. 104566, Vol. 14,* S.B. Hooker and E.R. Firestone, Eds., NASA Goddard Space Flight Center, Greenbelt, Maryland, 60 pp.

65

Vol. 15

Gregg, W.W., F.S. Patt, and R.H. Woodward, 1994: The Simulated SeaWiFS Data Set, Version 2. *NASA Tech. Memo. 104566, Vol. 15,* S.B. Hooker and E.R. Firestone, Eds., NASA Goddard Space Flight Center, Greenbelt, Maryland, 42 pp., plus color plates.

Vol. 16

Mueller, J.L., B.C. Johnson, C.L. Cromer, J.W. Cooper, J.T. McLean, S.B. Hooker, and T.L. Westphal, 1994: The Second SeaWiFS Intercalibration Round-Robin Experiment, SIRREX-2, June 1993. *NASA Tech. Memo. 104566, Vol. 16,* S.B. Hooker and E.R. Firestone, Eds., NASA Goddard Space Flight Center, Greenbelt, Maryland, 121 pp.

Vol. 17

Abbott, M.R., O.B. Brown, H.R. Gordon, K.L. Carder, R.E. Evans, F.E. Muller-Karger, and W.E. Esaias, 1994: Ocean Color in the 21st Century: A Strategy for a 20-Year Time Series. *NASA Tech. Memo. 104566, Vol. 17,* S.B. Hooker and E.R. Firestone, Eds., NASA Goddard Space Flight Center, Greenbelt, Maryland, 20 pp.

Vol. 18

Firestone, E.R., and S.B. Hooker, 1995: SeaWiFS Technical Report Series Cumulative Index: Volumes 1–17. *NASA Tech. Memo. 104566, Vol. 18,* S.B. Hooker and E.R. Firestone, Eds., NASA Goddard Space Flight Center, Greenbelt, Maryland, 47 pp.

Vol. 19

McClain, C.R., R.S. Fraser, J.T. McLean, M. Darzi, J.K. Firestone, F.S. Patt, B.D. Schieber, R.H. Woodward, E-n. Yeh, S. Mattoo, S.F. Biggar, P.N. Slater, K.J. Thome, A.W. Holmes, R.A. Barnes, and K.J. Voss, 1994: Case Studies for SeaWiFS Calibration and Validation, Part 2. *NASA Tech. Memo. 104566, Vol. 19,* S.B. Hooker, E.R. Firestone, and J.G. Acker, Eds., NASA Goddard Space Flight Center, Greenbelt, Maryland, 73 pp.

Vol. 20

Hooker, S.B., C.R. McClain, J.K. Firestone, T.L. Westphal, E-n. Yeh, and Y. Ge, 1994: The SeaWiFS Bio-Optical Archive and Storage System (SeaBASS), Part 1. *NASA Tech. Memo. 104566, Vol. 20,* S.B. Hooker and E.R. Firestone, Eds., NASA Goddard Space Flight Center, Greenbelt, Maryland, 40 pp.

Vol. 21

Acker, J.G., 1994: The Heritage of SeaWiFS: A Retrospective on the CZCS NIMBUS Experiment Team (NET) Program. *NASA Tech. Memo. 104566, Vol. 21,* S.B. Hooker and E.R. Firestone, Eds., NASA Goddard Space Flight Center, Greenbelt, Maryland, 43 pp.

Vol. 22

Barnes, R.A., W.L. Barnes, W.E. Esaias, and C.R. McClain, 1994: Prelaunch Acceptance Report for the SeaWiFS Radiometer. *NASA Tech. Memo. 104566, Vol. 22,* S.B. Hooker, E.R. Firestone, and J.G. Acker, Eds., NASA Goddard Space Flight Center, Greenbelt, Maryland, 32 pp.

Vol. 23

Barnes, R.A., A.W. Holmes, W.L. Barnes, W.E. Esaias, C.R. McClain, and T. Svitek, 1994: SeaWiFS Prelaunch Radiometric Calibration and Spectral Characterization. *NASA Tech. Memo. 104566, Vol. 23,* S.B. Hooker, E.R. Firestone, and J.G. Acker, Eds., NASA Goddard Space Flight Center, Greenbelt, Maryland, 55 pp.

Vol. 24

Firestone, E.R., and S.B. Hooker, 1995: SeaWiFS Technical Report Series Cumulative Index: Volumes 1–23. *NASA Tech. Memo. 104566, Vol. 24,* S.B. Hooker and E.R. Firestone, Eds., NASA Goddard Space Flight Center, Greenbelt, Maryland, 36 pp.

Vol. 25

Mueller, J.L., and R.W. Austin, 1995: Ocean Optics Protocols for SeaWiFS Validation, Revision 1. *NASA Tech. Memo. 104566, Vol. 25,* S.B. Hooker, E.R. Firestone, and J.G. Acker, Eds., NASA Goddard Space Flight Center, Greenbelt, Maryland, 66 pp.

Vol. 26

Siegel, D.A., M.C. O'Brien, J.C. Sorensen, D.A. Konnoff, E.A. Brody, J.L. Mueller, C.O. Davis, W.J. Rhea, and S.B. Hooker, 1995: Results of the SeaWiFS Data Analysis Round-Robin (DARR-94), July 1994. *NASA Tech. Memo. 104566, Vol. 26,* S.B. Hooker and E.R. Firestone, Eds., NASA Goddard Space Flight Center, Greenbelt, Maryland, 58 pp.

Vol. 27

Mueller, J.L., R.S. Fraser, S.F. Biggar, K.J. Thome, P.N. Slater, A.W. Holmes, R.A. Barnes, C.T. Weir, D.A. Siegel, D.W. Menzies, A.F. Michaels, and G. Podesta, 1995: Case Studies for SeaWiFS Calibration and Validation, Part 3. *NASA Tech. Memo. 104566, Vol. 27,* S.B. Hooker, E.R. Firestone, and J.G. Acker, Eds., NASA Goddard Space Flight Center, Greenbelt, Maryland, 46 pp.

Vol. 28

McClain, C.R., K.R. Arrigo, W.E. Esaias, M. Darzi, F.S. Patt, R.H. Evans, J.W. Brown, C.W. Brown, R.A. Barnes, and L. Kumar, 1995: SeaWiFS Algorithms, Part 1. *NASA Tech. Memo. 104566, Vol. 28,* S.B. Hooker, E.R. Firestone, and J.G. Acker, Eds., NASA Goddard Space Flight Center, Greenbelt, Maryland, 38 pp., plus color plates.

Vol. 29

Aiken, J., G.F. Moore, C.C. Trees, S.B. Hooker, and D.K. Clark, 1995: The SeaWiFS CZCS-Type Pigment Algorithm. *NASA Tech. Memo. 104566, Vol. 29,* S.B. Hooker and E.R. Firestone, Eds., NASA Goddard Space Flight Center, Greenbelt, Maryland, 34 pp.

Vol. 30

Firestone, E.R., and S.B. Hooker, 1996: SeaWiFS Technical Report Series Cumulative Index: Volumes 1–29. *NASA Tech. Memo. 104566, Vol. 30,* S.B. Hooker and E.R. Firestone, Eds., NASA Goddard Space Flight Center, Greenbelt, Maryland, 43 pp.

Vol. 31

Barnes, R.A., A.W. Holmes, and W.E. Esaias, 1995: Stray Light in the SeaWiFS Radiometer. *NASA Tech. Memo. 104566, Vol. 31,* S.B. Hooker, E.R. Firestone, and J.G. Acker, Eds., NASA Goddard Space Flight Center, Greenbelt, Maryland, 76 pp.

Vol. 32

Campbell, J.W., J.M. Blaisdell, and M. Darzi, 1995: Level-3 SeaWiFS Data Products: Spatial and Temporal Binning Algorithms. *NASA Tech. Memo. 104566, Vol. 32,* S.B. Hooker, E.R. Firestone, and J.G. Acker, Eds., NASA Goddard Space Flight Center, Greenbelt, Maryland, 73 pp., plus color plates.

Vol. 33

Moore, G.F., and S.B. Hooker, 1996: Proceedings of the First SeaWiFS Exploitation Initiative (SEI) Team Meeting. *NASA Tech. Memo. 104566, Vol. 33,* S.B. Hooker and E.R. Firestone, Eds., NASA Goddard Space Flight Center, Greenbelt, Maryland, 53 pp.

Vol. 34

Mueller, J.L., B.C. Johnson, C.L. Cromer, S.B. Hooker, J.T. McLean, and S.F. Biggar, 1996: The Third SeaWiFS Intercalibration Round-Robin Experiment (SIRREX-3), 19–30 September 1994. *NASA Tech. Memo. 104566, Vol. 34,* S.B. Hooker, E.R. Firestone, and J.G. Acker, Eds., NASA Goddard Space Flight Center, Greenbelt, Maryland, 78 pp.

Vol. 35

Robins, D.B., A.J. Bale, G.F. Moore, N.W. Rees, S.B. Hooker, C.P. Gallienne, A.G. Westbrook, E. Marañón, W.H. Spooner, and S.R. Laney, 1996: AMT-1 Cruise Report and Preliminary Results. *NASA Tech. Memo. 104566, Vol. 35,* S.B. Hooker and E.R. Firestone, Eds., NASA Goddard Space Flight Center, Greenbelt, Maryland, 87 pp.

Vol. 36

Firestone, E.R., and S.B. Hooker, 1996: SeaWiFS Technical Report Series Cumulative Index: Volumes 1–35. *NASA Tech. Memo. 104566, Vol. 36,* S.B. Hooker and E.R. Firestone, Eds., NASA Goddard Space Flight Center, Greenbelt, Maryland, 55 pp.

Vol. 37

Johnson, B.C., S.S. Bruce, E.A. Early, J.M. Houston, T.R. O'Brian, A. Thompson, S.B. Hooker, and J.L. Mueller, 1996: The Fourth SeaWiFS Intercalibration Round-Robin Experiment (SIRREX-4), May 1995. *NASA Tech. Memo. 104566, Vol. 37,* S.B. Hooker and E.R. Firestone, Eds., NASA Goddard Space Flight Center, Greenbelt, Maryland, 65 pp.

Vol. 38

McClain, C.R., M. Darzi, R.A. Barnes, R.E. Eplee, J.K. Firestone, F.S. Patt, W.D. Robinson, B.D. Schieber, R.H. Woodward, and E-n. Yeh, 1996: SeaWiFS Calibration and Validation Quality Control Procedures. *NASA Tech. Memo. 104566, Vol. 38,* S.B. Hooker and E.R. Firestone, Eds., NASA Goddard Space Flight Center, Greenbelt, Maryland, 68 pp.

Vol. 39

Barnes, R.A., E-n. Yeh, and R.E. Eplee, 1996: SeaWiFS Calibration Topics, Part 1. *NASA Tech. Memo. 104566, Vol. 39,* S.B. Hooker and E.R. Firestone, Eds., NASA Goddard Space Flight Center, Greenbelt, Maryland, 66 pp.

Vol. 40

Barnes, R.A., R.E. Eplee, Jr., E-n. Yeh, and W.E. Esaias, 1997: SeaWiFS Calibration Topics, Part 2. *NASA Tech. Memo. 104566, Vol. 40,* S.B. Hooker and E.R. Firestone, Eds., NASA Goddard Space Flight Center, Greenbelt, Maryland, 67 pp.

REPORT DOCUMENTATION PAGE

1. AGENCY USE ONLY *(Leave blank)*	2. REPORT DATE June 1997	3. REPORT TYPE AND DATES COVERED Technical Memorandum

4. TITLE AND SUBTITLE
SeaWiFS Technical Report Series
  Volume 40: SeaWiFS Calibration Topics, Part 2

5. FUNDING NUMBERS

  Code 970.2

6. AUTHOR(S)
  Robert A. Barnes, Robert E. Eplee, and Eueng-nan Yeh

   Series Editors: Stanford B. Hooker and Elaine R. Firestone

7. PERFORMING ORGANIZATION NAME(S) AND ADDRESS(ES)

  Laboratory for Hydrospheric Processes
  Goddard Space Flight Center
  Greenbelt, Maryland 20771

8. PERFORMING ORGANIZATION REPORT NUMBER

  97B00059

9. SPONSORING/MONITORING AGENCY NAME(S) AND ADDRESS(ES)

   National Aeronautics and Space Administration
   Washington, D.C. 20546–0001

10. SPONSORING/MONITORING AGENCY REPORT NUMBER

  TM–104566, Vol. 40

11. SUPPLEMENTARY NOTES
   Elaine R. Firestone, Robert A. Barnes, Eueng-nan Yeh, and Robert E. Eplee: General Sciences Corporation, Laurel, Maryland

12a. DISTRIBUTION/AVAILABILITY STATEMENT
  Unclassified–Unlimited
  Subject Category 48
  Report is available from the Center for AeroSpace Information (CASI),
  7121 Standard Drive, Hanover, MD 21076–1320; (301)621-0390

12b. DISTRIBUTION CODE

13. ABSTRACT *(Maximum 200 words)*

For Earth-observing satellite instruments, it was standard to consider each instrument band to have a spectral response that is infinitely narrow, i.e., to have a response from a single wavelength. The SeaWiFS bands, however, have nominal spectral bandwidths of 20 and 40 nm. These bandwidths effect the SeaWiFS measurements on orbit. The effects are also linked to the manner in which the instrument was calibrated and to the spectral shape of the radiance that SeaWiFS views. The spectral shape of that radiance will not be well known on orbit. In this technical memorandum, two source spectra are examined. The first is a 12,000 K Planck function, and the second is based on the modeling results of H. Gordon at the University of Miami. By comparing these spectra, the best available corrections to the SeaWiFS measurements for source spectral shape, plus estimates of the uncertainties in these corrections, can be tabulated.

14. SUBJECT TERMS
  SeaWiFS, Oceanography, Calibration, Validation, Blackbody Temperature
  Spectral Shape, Radiance Measurements, Spectral Responses, Center Wavelengths, Solar Diffuser

15. NUMBER OF PAGES
  67

16. PRICE CODE

17. SECURITY CLASSIFICATION OF REPORT Unclassified	18. SECURITY CLASSIFICATION OF THIS PAGE Unclassified	19. SECURITY CLASSIFICATION OF ABSTRACT Unclassified	20. LIMITATION OF ABSTRACT Unlimited